A Mathematical Model for a Mineral Melting Cupola Furnace

Leth-Miller, Rasmus; Jørgensen, Sten Bay

Publication date:
2002

Document Version
Publisher's PDF, also known as Version of record

A Mathematical Model for a Mineral Producing Cupola Furnace

Ph.D. Dissertation

Rasmus Leth-Miller, EF 766

ROCKWOOL® International A/S, Denmark

and

Department of Chemical Engineering,
Technical University of Denmark

June 13, 2002

Abstract

This Ph.D. project was initiated to increase the knowledge about mineral melting cupola furnaces used for stone wool production. The project aimed at improving operation of existing cupolas.

The project's focuses on development of a first engineering principles mathematical model of a mineral melting cupola furnace used for stone wool production. Results from lab scale measurements were used as input to the model, and full scale measurements were used for calibration and validation of the model.

The coke property measurements ranked seven cokes relevant to stone wool production after reactivity towards CO_2, and correlated the reactivity to the manufacturing process of the coke. It was found that cokes produced with a long baking time were the least reactive.

The raw material property measurements supplied enthalpy as function of temperature for nine raw materials used in stone wool production. An empirical model was developed to predict the enthalpy as function of temperature based on the chemical composition of the raw material.

The full scale measurements include measurements with probes inserted horizontally through the wall in the hot part of the cupola and probes inserted vertically from the top of the cupola. The temperature and gas composition were measured and melt samples were collected with the wall probes. The gas temperature was measured with the top probes. Melt samples from the wall probes, collected through the tuyeres and at the furnace outlet were used to establish where the iron oxides in the raw materials are reduced to metallic iron. An operating cupola was quenched to obtain a picture of the internal structure. E.g. the melt zone was found between 400mm and 750mm above the tuyeres, and the bulk porosity was found not to contradict the expectation of $0.4 - 0.5$.

The mathematical model developed is a static 1-D model that predicts temperatures, gas composition and mass flow rates of each phase as function of vertical position. The model accounts for seven chemical reactions for conversion of coke, O_2, C, CO, CO_2, H_2O, H_2, FeO, Fe_3O_2 and $CaCO_3$. Mass transfer is modelled as convection and heat transfer as convection and radia-

tion. The differential equations were discretised using orthogonal collocation and the algebraic equations solved using Levenberg-Marquardt and Newton-Raphson methods.

The mathematical model uses the measured properties of the coke and raw material. Full scale measurements formed the basis of the calibration, and the subsequent validation. The validation showed that the model has captured the essential phenomena sufficiently detailed for predicting temperatures and gas composition in the cupola as function of the vertical position.

Application of the model show how different operating condition affects process changes, so that a change can be beneficial under some circumstances but not under others. E.g. oxygen enrichment is more beneficial in terms of coke savings when the blast air temperature is 500^oC than 800^oC.

Preface

Cupola furnaces have been used for stone wool production the past 70 years. Many improvements of the operation have been made in this period. However the developments has mainly been done by trial and error. Improvements have been obtained but still the energy efficiency of the cupola is only about 50%. The Ph.D. project described in this dissertation was initiates to improve cupola operation that has not been improved significantly the past 15 years.

The project started with my employment at ROCKWOOL® International A/S February 15th, 1999, but the official starting date was April 1st, 1999. The termination date was thus March 31st, 2002, and apart from minor revisions the Ph.D. project terminated that day.

This dissertation consist of four papers that have been submitted to international journals, and this dissertation is an introduction to the papers and summery and conclusions.

Acknowledgement

This work is part of the research programme of ROCKWOOL® International A/S in cooperation with CAPEC (Computer Aided Process Engineering Centre) and CHEC (Combustion and Harmful Emission Control) at the Department of Chemical Engineering at The Technical University of Denmark. The project is funded by ROCKWOOL® and Erhvervsfremmestyrelsen (The Danish Ministry of Business and Industry).

Several people have helped me throughout the project. Above all my manager in ROCKWOOL® Leif Møller Jensen has been an inspiration and given challenges to move the project forward, and he has provided good working conditions.

My supervisors, Sten Bay Jørgensen, Peter Glarborg and Anker Jensen at The Technical University of Denmark (DTU) have given invaluable scientific support and discussions that helped me clarify my thinking. With their critical review on my papers and this dissertation the meaning was clarified and my English language was corrected.

Discussions with Peter Binderup Hansen (ROCKWOOL® International A/S), Poul V. Larsø (Danish ROCKWOOL®), Roel Moonen and Jos van Appeven (Dutch ROCKWOOL®) and other ROCKWOOL® employees have helped clarifying the objective of the project and continuously keeping it in mind.

Finally Lone (with whom I live) has been the support to turn to when the frustration that seems to be inevitable in a Ph.D. project was getting too much. Her support has truly been invaluable.

Rasmus Leth-Miller
Copenhagen, April 2002

Contents

1

Introduction

This project was initiated with the aimed of improving cupola operation in ROCKWOOL® factories. The energy efficiency of mineral melting cupolas is only approximately 50%. However, only little improvement has been achieved during the past 15 years. Below the background of this dissertation is described through briefly presenting the ROCKWOOL® company and the mineral wool production process. Subsequently the objectives of this dissertation are presented and the applied methodologies given in chapter 2. The experimental investigation and the model developments with results are briefly presented in chapter 3. The results are related to the objectives of this dissertation in the discussion in chapter 4 and the conclusions are drawn in chapter 5. Finally further work to achieve improved insight is suggested.

More complete accounts of the experimental investigations, the model development and application are given in four papers which are included in appendices to this dissertation as follows:

I Experimental Investigation and Modelling of Heat Capacity, Heat of Melting and Melting Interval of Rocks.[1] (submitted to Thermochemica Acta.)

II Comparative Study of Coke reactivity towards CO_2.[2] (submitted to Ironmaking and Steelmaking.)

III Experimental Investigation and Mathematical Modelling of a Mineral Melting Cupola Furnace.[3] (submitted to Industrial and Engineering Chemical Research.)

IV Application of a Mathematical Model of a Mineral Melting Cupola.[4] (submitted to Industrial and Engineering Chemistry Research.)

1.1 Background

ROCKWOOL® International A/S is the holding company of a Danish group with world wide activities (see figure 1.1). The headquarter is located in Hedehusene near Copenhagen in Denmark. The company was founded in 1909 as a company running gravel pits, marl pits and digging brown coal, but the company as we know it today did not start before 1935 when contact was established to the Baldwin-Hill company in New Jersey, USA. Know-how about stone wool production and rights were bought from Baldwin-Hill for 5000$. This was the beginning of a primitive stone wool production in Scandinavia. The production has developed since then through license agreements and purchased know-how in the beginning but in recent years the development has been made in house in the R&D department in Hedehusene. More information about the company can be found on the internet (`http://www.rockwool.com`).

The main product of ROCKWOOL® is insulation materials (see figure 1.2). Stone wool has the advantage over other insulation materials that it is fire resistant.

1.2 The Mineral Wool Production Process

The production process of stone wool is illustrated in figure 1.3. At the beginning of the production line coke and raw materials (rocks, briquettes, slags, lime, etc.) are stored in silos. From the silos charges are added by weight onto a conveyer belt that transports the coke and raw materials to the top of the cupola furnace. In the cupola furnace the coke is combusted and the heat released melts the raw materials. The melt runs out of the cupola and is directed to the spinning machines. The spinning machines spin the melt to wool that is mixed with an organic binder. The wool and binder are collected on a conveyer that transports it through a curing oven. In the curing oven the organic binder is cured and this gives the wool a stable structure. After the curing oven the wool is cut into the final shape of the product, packed and shipped to the costumer.

A more detailed schematic of the cupola furnace is shown in figure 1.4. The cupola is charged with coke and raw materials at the top and air is blasted through a number of tuyeres (nozzles) near the bottom of the cupola. The coke combusts in the region from the tuyeres and approximately 0.5m up. The hot gas from the combustion flows up through the cupola and leaves the top at a temperature of $100 - 200^{o}$C. The upward flowing hot gas transfers its heat to

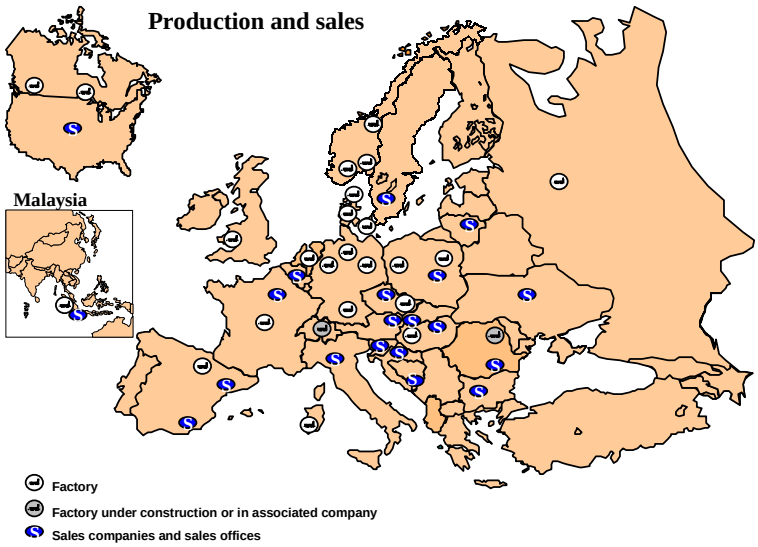

Figure 1.1. Overview of the location of ROCKWOOL®.

the down flowing raw materials that melt and to the coke. The raw materials melt in the region approximately 0.5m to 1m above the tuyeres. The melt runs to the bottom of the cupola and is collected in the melt bath, located below the tuyeres. The level of the melt bath is maintained with a siphon.

In the cupola several chemical reactions take place. The coke reacts with the oxygen near the bottom of the cupola, and all the oxygen has been consumed approximately 0.5m above the tuyeres. The CO_2 formed reacts with the coke forming CO. In addition the water in the blast air reacts with the coke forming CO and H_2. The gasification reactions (coke with CO_2 and H_2O) also occur in the combustion zone, but the formed CO and H_2 is rapidly oxidised as long as oxygen is present. The temperature is decreasing up through the cupola and the gasification virtually stops at some point when the temperature becomes too low. The lime and $CaCO_3$ decomposes due to the heating and iron oxides in the raw materials are reduced to metallic iron on the coke surfaces. Trace elements such as organic binder in recycled wool also react in the cupola.

The raw materials fed to a mineral melting cupola can be rocks, briquettes, slags and limestone. The rocks are typically formed in volcanos and could be diabase, gabbro or basalt. The briquettes are made of various minerals such as olivine, basalt, diabase and gabbro. Waste stone wool can also be recycled in the briquettes. The limestone is mostly added to adjust the viscosity of the melt to the requirements of the spinning process.

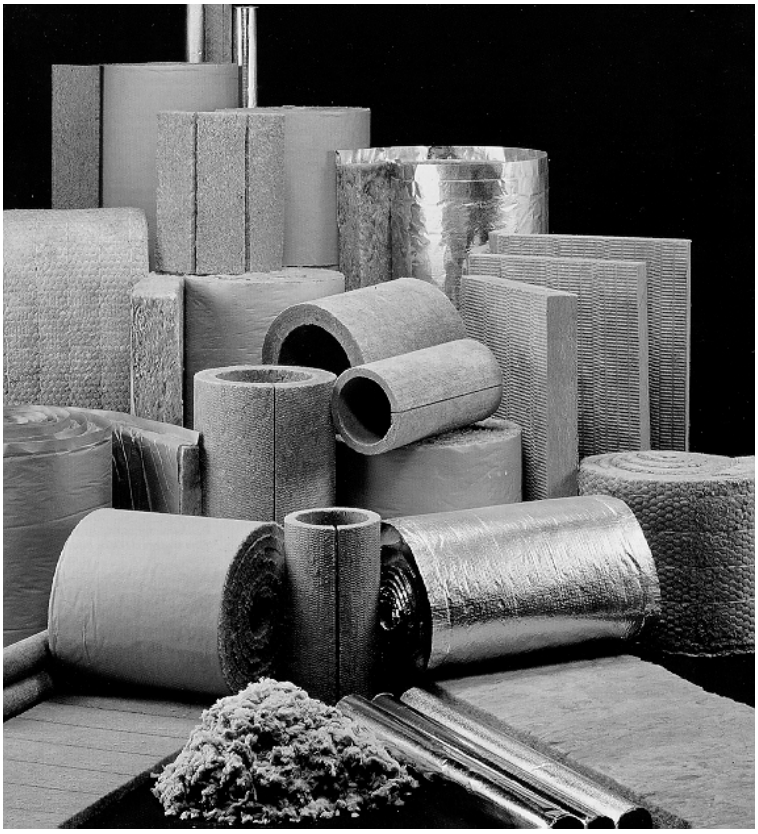

Figure 1.2. Picture of ROCKWOOL® products.

The cupola is made of steel and equipped with a cooling jacket with water that evaporates. The cooling jacket is connected with a tank above the cupola, and as the water evaporates in the jacket more water by the force of gravity runs into the cooling jacket.

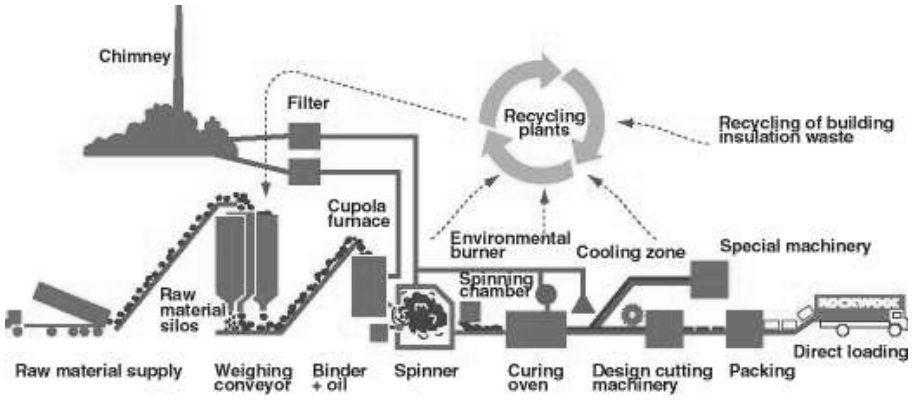

Figure 1.3. Schematic overview of the production process

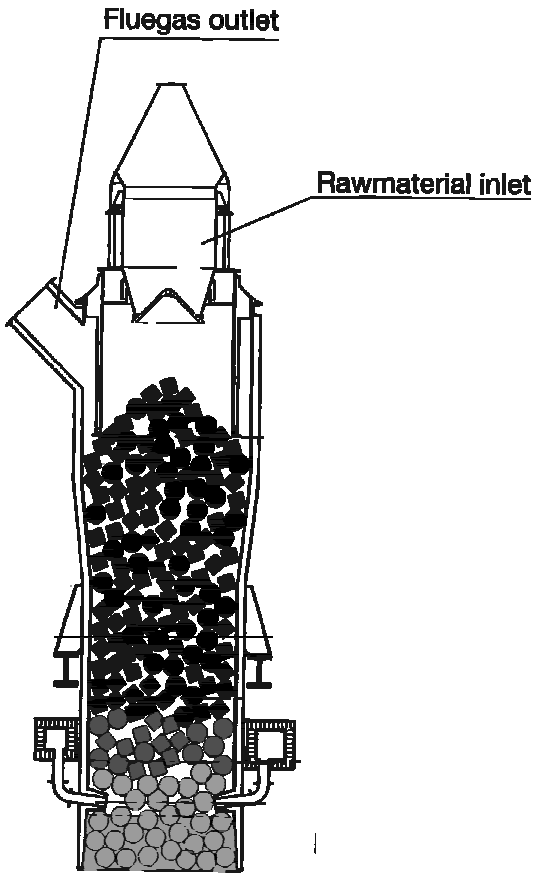

Figure 1.4. Schematic overview of the cupola furnace

2

Objectives

The ultimate goals are to improve the operation of mineral melting cupolas through improved understanding of the process. The methodological approach taken in this dissertation to attempt to achieve these goals is first engineering principles modelling supported by both laboratory and full scale measurements. Thus the subgoals of this dissertation are to understand and explain the complex interaction of the significant phenomena taking place in the furnace. These interactions include:

- Locating the combustion zone and the rates of the combustion and gasification reactions.
  - Describing the heat transfer to and from the coke
  - Describing the mass transfer to and from the coke
  - Describing the reaction mechanisms
- Locating the melting zone.
  - Describing the melting process (melting interval, heat of melting etc)
  - Describing the heat transfer to/from the rocks
- Determining the temperature of the melt
  - Describing the velocity of the melt as it runs down through the furnace to find the residence time available for superheating of the melt.
  - Describing the heat transfer to/from the melt
- Determining the heat loss to the surroundings through the furnace wall

Lab scale experiments have been made to measure the properties of the raw materials and coke used in the cupola (article I and II). Full scale experiments

have been performed to obtain new knowledge about the cupola, which can also be used in the development of the mathematical model (article III).

The mathematical model development should result in a tool that can give insight into how different phenomena in the process constrain the cupola performance under different operation conditions.

3

Results

This chapter presents the key procedures and results of the experiments, model development and model application, which were undertaken to achieve the objectives of this dissertation.

3.1 Experimental Work

During the Ph.D. project a number of different experimental investigations have been conducted. The work includes laboratory measurements and full scale cupola measurements. The laboratory measurements and modelling of coke properties and raw material properties were made to determine supply input information to the model. Full scale measurements on operating cupolas were made to calibrate and validate the model as well as supply information valuable in it self.

Laboratory Tests

The laboratory tests were made to obtain information that is both valuable in it self and that can be used for the cupola model. The lab scale tests include measurements of coke properties and raw material heat capacities and heats of fusion. The experiments are briefly summarised in the following.

Coke Properties

The purpose of the coke property measurements was to determine the reactivity towards CO_2. In addition the porosity, density and surface area were measured

to provide explanations for the results. The measurements are described in article II[2].

The reactivity measurements were made in a thermo gravemetric analyser (TGA). A small sample ($\approx$ 1mg) of small particles ($90 - 105\mu$m) is placed in a crucible in a controlled atmosphere and controlled temperature. The mass of the sample is then registered throughout the experiment, and the signal can afterwards be used to determine reaction rate constants. The reactivity measurements was used to rank seven types of coke relevant to ROCKWOOL® based on reactivity towards CO_2. The cokes were produced in Western Europe, Eastern Europe and China.

The measurements showed that Western European cokes made on American coal in coke batteries are the most reactive. The least reactive cokes were the Chinese that were produced in beehives. An Eastern European coke had intermediate reactivity. The reactivities are illustrated in figure 3.1 and the results are compared to the model used to estimate reactivity parameters in figure 3.2. The reactivity was found to correlate with the baking time of the coke in the production process. The longer baking time the lower reactivity. The porosity and density measurements confirmed that the cokes produced

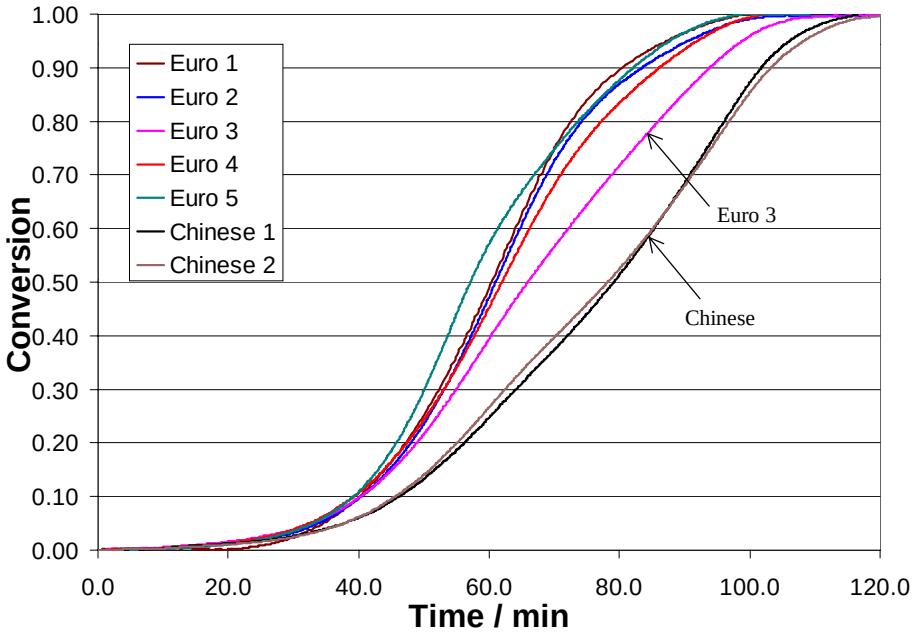

Figure 3.1. Conversion as function of time. The temperature is $T = 1073$K at time $t = 0$. The heating rate is 5K/min

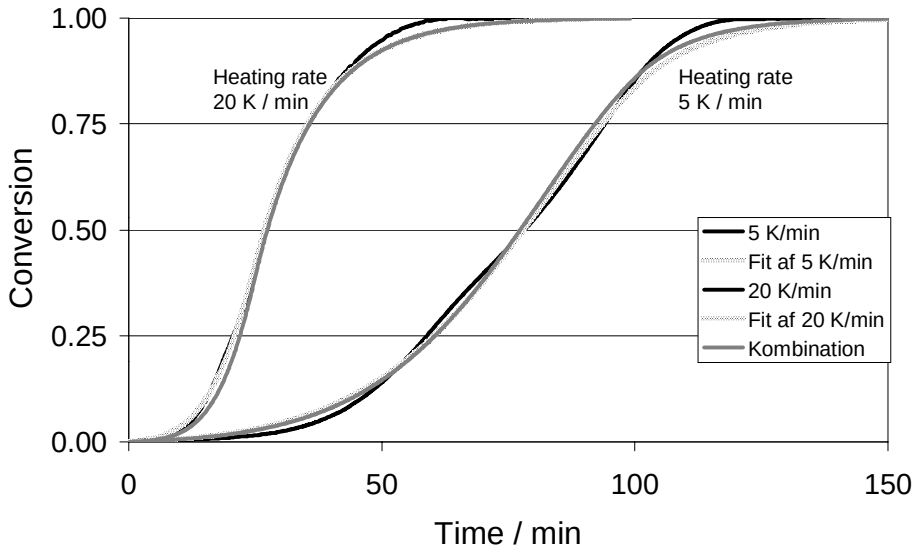

Figure 3.2. Experimental data and fitted model for *Chinese 2* coke at 20% CO_2.

with long baking time are more dense and less porous. The longer baking time of the coke the more the structure is expected to approach that of graphite and thereby lower the reactivity.

Raw Material Properties

The purpose of the measurements of the raw material properties was to determine the heat capacity of the solid and melted raw material and the heat of fusion in the temperature range 25°C to 1500°C. A detailed description of the measurements is given in article I[1].

The thermodynamic properties were measured using differential scanning calorimetry (DSC). A sample ($\approx$ 20mg) is placed in a crucible and a reference material with known properties is placed in another crucible. The crucibles and their content are then heated from 25°C to 1500°C and the temperature difference between the two crucibles is registered as function of temperature. The temperature difference signal can be used to determine the apparent heat capacity. The apparent heat capacity is a mix of the heat capacity of the solid material, the heat of fusion and the heat capacity of the melted material.

The results (see figure 3.3) show some differences between the different materials. The heat of fusion is so low that it can be neglected for some purposes,

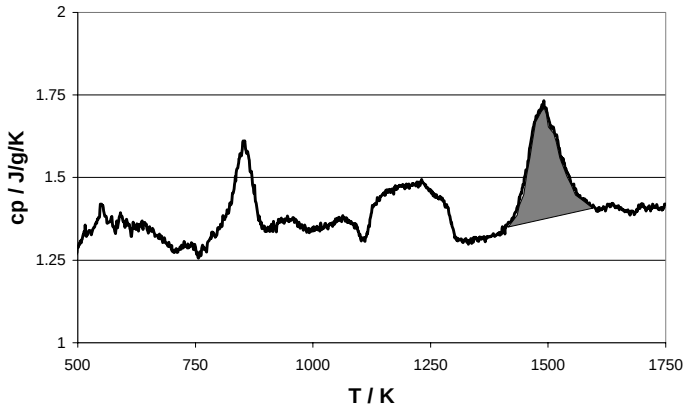

Figure 3.3. The heat capacity (or other transition heats) can be extracted from the resulting heat capacity function as the grey area, assuming that the heat capacity follows the base line of the grey area.

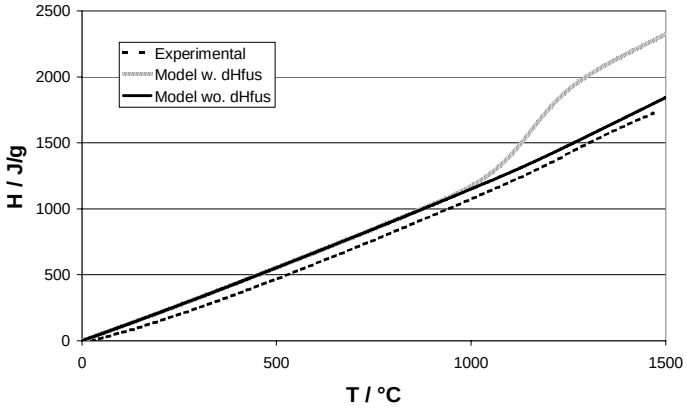

Figure 3.4. The enthalpy, modelled and measured, plotted against temperature. Beyond 1775K the measurements have been extrapolated. The modelled curves is one with and one without the heat of fusion term, i.e. either the heat of fusion was estimated or it was set to zero.

e.g. the melting only takes up a very small fraction of the total energy required for heating, melting and superheating the raw materials from 25°C to 1500°C as it happens in the cupola, see figure 3.4.

Full Scale Tests

Full scale tests were conducted to obtain information about the conditions inside operating cupolas. This information is valuable in itself and is used for development of the cupolas furnace, since it supplies better understanding of the cupola.

Five types of experiments have been performed on full scale operating cupolas. Four of these (wall probing, top probing, collection of melt samples and quenching) involves measurements in or sample collection from the inside of the cupola. The fifth type is measurement of input to and output from an operating cupola. The experiments are described in more detail in article III [3]. The procedures and results are briefly summarised in the following.

Wall Probes

The wall probe equipment was made to measure temperature, gas concentration and melt composition in the hot part of the cupola from the tuyeres and 1m up. This had never been done before on a stone wool cupola.

The wall probe equipment consists of a frame with an electrical motor. The frame is placed outside the cupola and the electrical motor is used to drive the probes horizontally into the cupola. The probes are steel tubes designed for either gas concentration, temperature or melt sample measurements. The openings in the cupola wall that the probes are pushed through are closed with ball valves. Five gates were installed above the tuyeres in the cupola. Measurements were attempted at three radial positions for each gate, i.e. at the wall, in the centre and in between the two positions.

The measurements of th CO concentration indicates that the oxygen is consumed approximately 300mm above the tuyeres and that the CO concentration from that point increases upwards. The CO formation is fastest at the centre of the cupola. The temperature is slightly higher than what was expected, but the temperature decreased up through the cupola as expected. The measured CO concentrations and temperatures are shown in figure 3.5 and 3.6.

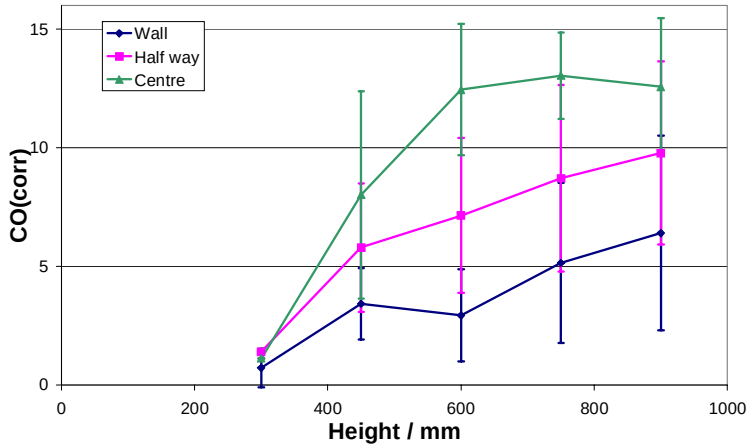

Figure 3.5. CO profile measured with the probes. (Vertical bars indicate the standard deviation of the measurement.)

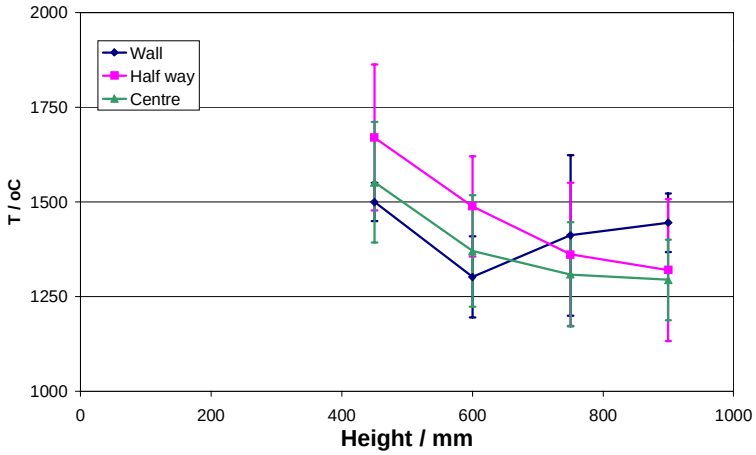

Figure 3.6. Temperature profile measured with the probes. (Vertical bars indicate the standard deviation of the measurement.)

Top Probe

Operating cupolas have been probed from the top to measure the axial temperature profile in the cupola.

A top probe is a steel pipe with a thermocouple inside. The probe is inserted at the top of the cupola and the burden of the coke and raw materials then pulls the probe down through the cupola as the cokes are burned away and the raw materials are melted. The probe can not be pulled back out but is lost and melts in the cupola.

The temperature profiles obtained have been used to validate the cupola model. The measured temperature profile is shown in figure 3.7.

Iron Reduction

In the cupola iron oxides from the raw materials are reduced to metallic iron on the coke. The iron reduction is unwanted since the iron is not miscible with the melt and therefore can not be a part of the product. The metallic iron sinks to the bottom of the melt bath and the iron level is then increasing during the production. When the iron level reaches the siphon outlet the cupola must be tapped and thus the production is stopped for a period of time.

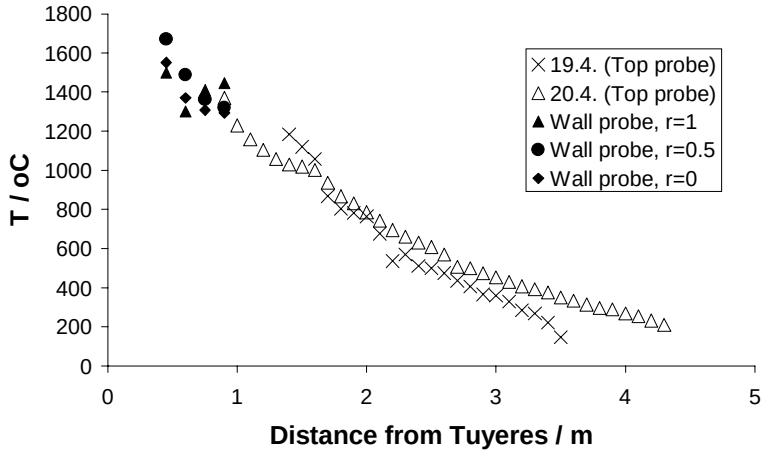

Figure 3.7. Gas temperature profiles measured two different days with the top probe and the temperature profiles obtained with the wall probes.

Melt samples were collected with the wall probes, through the tuyeres and at the siphon outlet. The samples were then analysed for chemical composition to determine the iron content (metallic and oxides). From the results of the analyses the position of the iron reduction could be determined.

The results showed that the iron reduction mainly take place in the region from the tuyeres and 0.5m upwards. This conclusion contradicts the earlier perception that the iron reduction would occur when the oxygen concentration was low, which is higher in the cupola.

The results were used to formulate a simple empirical reaction rate expression for the iron reduction in the cupola model that only depends on the position in the cupola and the initial amount of iron oxides in the raw materials.

Quenching

An operating cupola was quenched to obtain a picture of how the porosity in the cupola varies and to determine the position of the melting zone.

The quenching was done by injecting nitrogen instead of air into the cupola. This quenched the combustion and cooled the coke, raw materials and melt. The injection of nitrogen continued until the temperature in all regions was below the self ignition temperature of the coke, i.e. $500 - 600^{o}$C. Then the quenched cupola was cooled to room temperature during the next weeks. The void of the cupola was then filled with cement, so that the cupola could subsequently be cut to pieces and the structure of the inside of the cupola was revealed.

The vertical cross sections show that the porosity is approximately $0.4 - 0.5$ as expected. The porosity is apparently constant over the entire cupola. The position of the melting zone was established between 400mm and 750mm above the tuyeres, which was found closer to the tuyeres than expected.

Input/Output Measurements

The input and output parameters have been measured on different cupolas at different occasions. The purpose of the measurements has been to analyse the impact a change in input has on the output. In this work, however, the measurements have only been used for calibrating the cupola model, i.e. as basis for parameter estimation.

The inputs measured are the types and amount of raw material and coke and the temperature composition and amount of blast air. The outputs measured are the temperature and composition of the flue gas, the cooling water loss and the melt temperature.

3.2 The Mathematical Cupola Model

A mathematical model was developed to simulate different cupola operation scenarios. A mathematical model has the advantage that simulations are fast and cheap compared to full scale trials. Furthermore a mathematical model can give an overview and insights that empirical observations can not. For instance it is possible to test changes in specific parameters that are not easily tested in reality such as changes in coke reactivity towards CO_2 without changing the reactivity towards O_2. Additionally, it is in practice never possible to change only one single parameter in the cupola, e.g. because the coke and raw materials are not entirely homogeneous and they are often stored outdoor, so the weather conditions influences the amount of water in the raw materials and coke. The model development is described in article III[3].

The developed model of the stone wool cupola furnace is a static 1-D mathematical model. All variations in temperature, concentration, etc. are thus restricted to the vertical direction in the model. The model consists of mass and energy balances for six gas species, four different types of rock and coke.

In the model seven chemical reactions are included. The reactions are combustion of the coke, CO and H_2, gasification of the coke with CO_2 and H_2O, calcination of lime and reduction of iron oxides.

The model accounts for mass and heat balances of the gas phase, coke and four different raw material phases. Mass transfer between the gas and the coke is modelled as convection with a mass transfer coefficient correlation developed for a fixed bed. Heat transfer is modelled as both convection and radiation.

The model is discretised with orthogonal collocation[5] and the system of equations are solved with Levenberg-Marquardt[6] and Newton-Raphson[7] methods.

Since the model is one-dimensional it has limited ability to predict consequences of furnace design modifications. The potential of the model is that it predicts the output of the cupola for a given input, thus the coke percentage, coke type, raw material types, charge composition and blast air temperature, amount and composition is specified and then the model predicts melt capacity, flue gas

composition and temperature, melt temperature etc.

The model uses the properties of the coke determined from the measurements described in article I[2] and the properties of the raw materials determined in article II[1]. Furthermore a model for predicting raw material properties is implemented in the cupola model. The heat capacity can then be predicted from the chemical composition when experimental data is unavailable. The raw material model is described in article II[1].

The model has been calibrated against the input/output data and the calibrated model was subsequently validated against the probe measurements and the quenching results. The validation showed that the model has captured the essential phenomena in the cupola operation and describes these sufficiently accurate (all described in article III[3]). The model performance is illustrated in figure 3.8 and 3.9.

3.3 Application Results

Article IV[4] describes some application examples of the cupola model, and the model is compared with some rules of thumb that have been used for cupola operation in the stone wool industry.

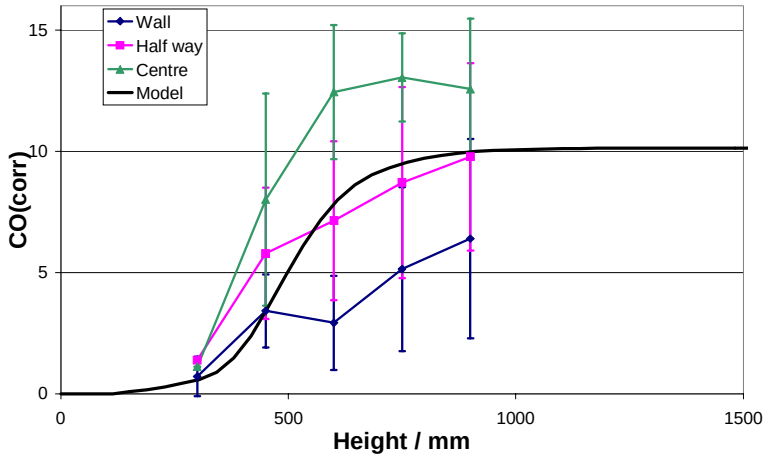

Figure 3.8. CO profile predicted and measured with the probes. (Vertical bars indicates the standard deviation of the measurement.)

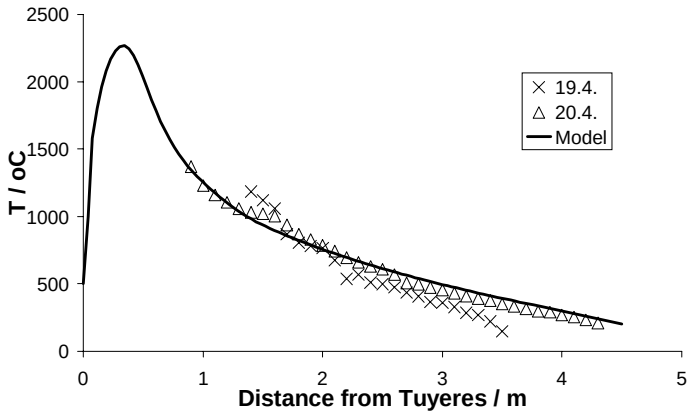

Figure 3.9. Model predicted gas temperature profile in the cupola and two gas temperature profiles measured with the top probes.

The model was used to test the impact of oxygen enrichment of the blast air. The background is that at some cupolas oxygen enrichment was beneficial while not on others. The model demonstrates how changes in other operation parameters (in this case the blast air temperature) affect the impact of the oxygen enrichment. The model shows that the issue has no definite answer, because oxygen enrichment can be beneficial on some lines while not on others depending on the operation conditions.

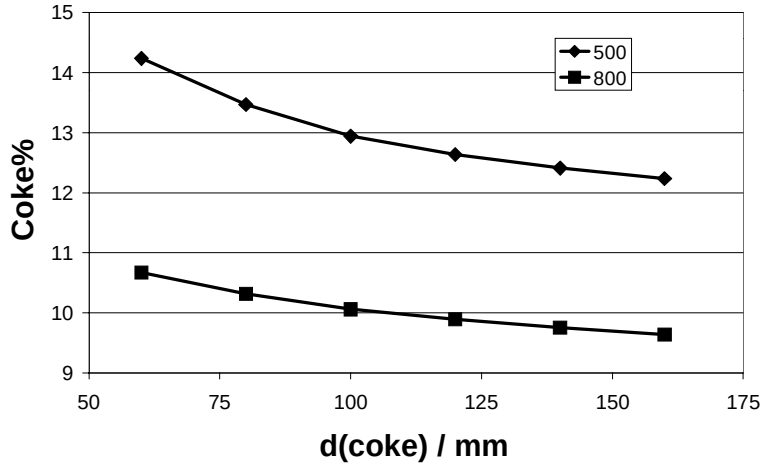

Figure 3.10. Coke consumption as function of coke size predicted by the model. The coke consumption is adjusted to sustain a given melt temperature.

The size of coke used in the cupola became an issue when the EU added an anti-dumping tax on Chinese foundry coke (large coke[8]). The model was then used to test cupola operation sensitivity towards coke size changes. The cupola model showed that the sensitivity is dependent on other operation parameters (illustrated with blast air temperature). Figure 3.10 shows that it cost two percent extra coke to change from largest coke to the smallest coke if the blast temperature is 500^oC while it only costs 1 percent if the blast air temperature is 800^oC.

Different coke reactivities were tested to investigate the impact on the cupola operation. The simulations showed that for maintaining the same melt temperature the coke percentage had to be increased from 13.5% to 17% if the coke is changed to one half as reactive towards CO_2 and O_2. On the other hand, the coke percentage could be decreased if the coke was changed to one with half the reactivity towards CO_2 while keeping the reactivity towards O_2. This result is not obvious since the CO_2 in the combustion zone acts as a carbon carrier since the CO_2 reacts with the coke forming CO that combusts in the gas phase, which speeds up the rate of coke combustion.

A rule of thumb for cupola operation is that an increase of coke in the charge by 1% will increase the melt temperature by 20 ± 20^oC. The model was compared to this and other rules of thumb and demonstrates generally good agreement. Deviations were observed, but as the simulations with the oxygen enrichment, the different coke sizes and the coke reactivity showed, the impact of input changes depends on the actual operation conditions.

The application examples show how the model can give insight into how different phenomena in the process constrain the cupola performance under different operation conditions.

4

Discussion

Through the experimental work and the development of the mathematical model improved understanding of the mineral melting cupola was obtained, however, much is still unknown.

The developed mathematical model explains several parts of the complex interaction, but the model is 1-D and can thus not predict radial influences in the cupola. The full scale measurements reveal some of the radial variances, however this knowledge can not be used quantitatively in a predictive manor but only qualitatively.

The developed model was also limited by crude reaction rate expressions since lumped expressions were used while other multiple step mechanisms could have been used accounting for e.g. radicals. The limitations of the model due to this were not explored. Especially the iron oxide reduction mechanism was simplified.

The mathematical model is a static model and can therefore not predict time variances. The cupola is in general operated at steady state, but some fluctuations are always present but neither the model nor the experiments gave information about this.

The full scale measurements are always difficult to reproduce. This may be because the cupola is never perfectly stable or because the coke and raw materials charged into the cupola is not homogeneous and changes slightly over time. This dissertation provides no answer to this since the model developed is static.

5

Conclusion

During the Ph.D project properties of cokes and raw materials have been measured and full scale experiments on mineral melting cupolas have been conducted. A mathematical model of a mineral melting cupola furnace has been developed. The experimental data has been used as input to the model for simulations, as calibration data and as validation data.

The reactivity towards CO_2 was measured for seven different coke types in lab scale measurements. The porosity, density and surface area were measured for three of the cokes. The cokes were ranked, and the measurements showed that the reactivity decreases as the baking time used in the production of the coke increases. A longer baking time results in a structure of the coke closer to that of graphite. The most reactive coke was approximate 10 times more reactive than the least reactive. In the cupola the most reactive coke is the most efficient since the combustion is more rapid, which more than compensates for the faster gasification.

The enthalpy required for heating, melting and superheating raw materials from 25^oC to 1500^oC was measured for nine raw materials used in stone wool production. Differences between raw materials were discovered, and the most energy consuming raw material requires 25% more energy than the least energy consuming among the materials tested. All the materials tested showed almost zero heat of fusion.

A model for predicting the raw material energy consumption has been developed based on a number of submodels. The model predicts the fraction solid and the enthalpy as a function of temperature and the chemical composition of the raw material. The best fit of the model was obtained by setting the heat of fusion to zero. The model type was selected to be differentiable for easy implementation in the cupola model.

Five different types of full scale measurements on operating cupolas have been

made. The data obtained was used for calibration and validation of the model.

Wall probes were used to measure the temperature, gas composition and collect melt samples in the region from the tuyeres and 1m up. The measurements showed that the combustion zone is located from the tuyeres and 0.3m upward. The reduction zone, where CO is formed is located from 0.3m above the tuyeres to approximately 1m above the tuyeres. Melt samples could be collected 0.9m above the tuyeres indicating that the upper limit of the melting zone is at least 0.9m above the tuyeres. The temperatures measured showed odd behaviour and no conclusions were made on this basis.

Probes were used to measure the gas temperature from the top of the cupola to approximately 1m above the tuyeres. The temperature increase from 150^o at the top til 1200^o 1m above the tuyeres.

Melt samples were collected with the wall probes and through the tuyeres. Analysis of the chemical composition showed that the iron reduction mainly occurs in the zone from the tuyeres and 0.5m upward.

An operating cupola was quenched during normal operation. The void of the cupola was filled with cement and the cupola was subsequently cut in two. The vertical cross section gave information about the bulk porosity and position of the melting zone. The bulk porosity was about $0.4 - 0.5$. The melting zone was identified in the region from $400 - 750$mm above the tuyeres which was low compared to the general perception in ROCKWOOL®.

A 1-D static mathematical model of the mineral melting cupola has been developed. The model describes chemical reactions, gas phase composition, temperatures of gas, coke and four raw material phases (solid or liquid), mass flow of each phase and heat and mass transfer between the different phases and the cupola wall as function of vertical position.

The cupola model was calibrated using experimental data, i.e. model parameters were estimated based on experimentally obtained input/output data. The model showed agreement with the experimental data within the experimental uncertainty.

The cupola model was validated against the data obtained in the wall and top probe measurements and in the quenching experiment. The model performs well indicating that the model has captured the essential phenomena, which have been described sufficiently accurate for the model to describe temperatures, gas composition and melting zone location.

During the project the knowledge about the cupola within the company has been increased and a tool, the mathematical model, for simulating cupola operation has been developed to improve cupola operation.

6

Future Work

The mathematical model could be further developed in several ways. The most beneficial improvements are listed below with the most beneficial first.

- Extend to 2-D or 3-D to obtain a model that can be used for furnace design issues.
- Better description of the chemical reactions.
  - Introduce a mechanism for FeO reduction, so that it can be used for analysing how the iron reduction can be reduced.
  - Add SO_x formation and reactions involving binder from recycled wool to be able to predict trace element content in the flue gas.
  - Use more detailed expressions for the reactions in stead of the lumped expressions that are currently used.
- Redo the calibration based on larger amount of data.
- Calculate the pressure as function of position.
- Introduce a submodel for bulk porosity as function of particle size distribution.
- Introduce a particle size distribution for the cokes and raw materials.
- Make the model dynamic e.g. to be able to explore the consequences of dynamic changes in production.

The experiments should also be extended as the model is further developed to support the development. The type of experiment is determined from the type of model improvement, e.g. the extension to more than one dimension of the model would require measurements inside the cupola at several vertical and horizontal positions such as the wall probe experiments.

References

[1] R. Leth-Miller, A. D. Jensen, P. Glarborg, S. B. Jørgensen, L.M. Jensen, and P.B. Hansen. Experimental investigation and modelling of heat capacity, heat of fusion and melting interval of rocks. *Thermochemica Acta (submitted)*, 2002.

[2] R. Leth-Miller, J. Jensen, A. D. Jensen, P. Glarborg, S. B. Jørgensen, L.M. Jensen, and P.B. Hansen. Compartive study of coke reactivity towards co_2. *Ironmaking and Steelmaking (submitted)*, 2002.

[3] R. Leth-Miller, A. D. Jensen, P. Glarborg, S. B. Jørgensen, L.M. Jensen, and P.B. Hansen. Experimental investigation and mathematical modelling of a mineral melting cupola furnace. *Industrial and Engineering Chemistry Research (submitted)*, 2002.

[4] R. Leth-Miller, A. D. Jensen, P. Glarborg, S. B. Jørgensen, L. M. Jensen, and P. B. Hansen. Application of a mathematical model of a mineral melting cupola. *Industrial and Engineering Chemistry Research (submitted)*, 2002.

[5] J. Villadsen and M.L. Michelsen. *Solution of Differential Equation Models by Polynomial Approximation.* Prentice Hall, 1978.

[6] J. E. Dennis and R. B. Schnabel. *Numerical Methods for Unconstrained Optimisation on Nonlinear Equations.* Prentice-Hall Inc., 1983.

[7] R.G. Rice and D.D. Do. *Applied Mathematical Modelling for Chemical Engineers.* John Wiley and sons Inc., 1995.

[8] R.H. Hafner. *Cupola Handbook.* American Foundrymen's Society, 5th ed. edition, 1984.

Article I

Experimental Investigation and Modelling of Heat Capacity, Heat of Fusion and Melting Interval of Rocks

R. Leth-Miller[†,‡*], A.D. Jensen[‡], P. Glarborg[‡],
L.M. Jensen[†], P.B. Hansen[†] and S.B. Jørgensen[‡]

[†]ROCKWOOL® International A/S, Denmark
[‡]Department of Chemical Engineering,
Technical University of Denmark
May 14, 2002

Abstract

The heat capacity and heat of fusion was measured for a number of minerals using Differential Scanning Calorimetry (DSC). The DSC measurements showed that the heat of fusion for the minerals is very low compared to the heat of fusion for pure crystalline phases reported elsewhere.

A model for the melting behaviour of mineral materials in terms of melting interval, heat capacities and heat of fusion has been developed. The only model input is the chemical composition of the mineral material. The model was developed to be implemented in a detailed model of a cupola furnace, thus the focus for the development was not only precision but also to obtain a model that was continuous and differentiable.

The model is based on several different submodels that each covers a part of the heating and melting of rocks. Each submodel is based on large amounts of empirical data. Comparison of the model and the DSC measurements showed good agreement.

Table 1. List of symbols.

a	Parameter in f_s model
$c_{p,l}$	Heat capacity of liquid rock material
$c_{p,s}$	Heat capacity of solid rock material
f_s	Fraction solid of a rock materials
ΔH_{fus}	Heat of fusion
T	Temperature
T_g	Glass transition temperature
T_m	Temperature at the middle of the melting interval or melting point temperature

$[X]$ denotes cation mole fraction of element X.

1 Introduction

In the production of ROCKWOOL® products rock materials are melted and heated to about 1500^{o}C. The energy requirements for heating and melting the rocks and superheating of the melt from the individual rock materials are considerable and together with the melting interval are of importance for determining the thermal efficiency of the cupola.

Models and experimental work for description of heat capacity, heat of fusion and melting temperature interval for rock materials have been developed earlier. Nathan and van Kirk [1] describe the melting curve (fraction solid as function of temperature) using an empirical model that predicts the composition of a mineral material in terms of crystalline phases. The model contains equations for estimating the liquidus temperature for nine phases as function of chemical composition, and uses these to construct a fraction solid function by solidifying a melt of a given chemical composition.

Methods for calculating the heat capacity of solid (crystalline and amorphic) and liquid rock materials based on their composition in terms of crystalline phases are described by Steppins et al. [2], and methods for calculating the heat of fusion of minerals based on their composition in terms of crystalline phases is described by Konnerup-Madsen [3]. These methods are simple weighted sums over the properties of each of the phases present in a mineral material.

The composition of mineral materials in terms of crystalline phases can be predicted by the CIPW method described by Best [4]. The CIPW method is an algorithm that estimates the crystalline phase composition based on the chemical composition taking 31 phases into account, but does not predict melting

*Corresponding author, e-mail: rasmus.leth.miller@rockwool.com

interval as the method of Nathan and van Kirk [1].

Experimental data of pure mineral crystals have been collected and published e.g. by Howie et al. [5] and by Bach and Krause [6]. Crystalline rocks consist of a number of phases that mixes during melting, but the heat of mixing is not well described in literature.

The purpose of this work is to obtain knowledge of the enthalpi requirements for heating, melting and superheating of different raw materials used in ROCKWOOL® production to be better able to improve the production process. Furthermore, the purpose is to obtain a predictive model that can be used in a detailed model of a stone wool producing cupola furnace [7] when experimental data is not available.

A model based on several submodels that each describes a part of the heating, melting and superheating is presented. The model aims at describing the heat requirements as function of temperature for heating a rock taking heat capacity, heat of melting and melting temperature interval into account. The model input is the chemical composition while the composition in terms of crystalline phases is estimated using an empirical correlation. The apparent heat capacities of nine mineral materials have been measured using DSC. The apparent heat capacity has other heat consuming or producing phenomena embedded such as melting, calcination of $CaCO_3$ and mixing of melt from different crystals. The DSC method is briefly introduced and the results of the measurements are presented. Finally the empirical model is compared to the experimental data.

2 Model

The energy used for heating, melting and superheating the raw materials/melt is an important factor for the cupola operation. For use in a mathematical model of the cupola it is an advantage that the enthalpy function is continuous and differentiable over the entire temperature interval. Thus the function proposed here is given by

$$H_r = \int_{298\mathrm{K}}^{T} c_{p,s} f_s dT + \Delta H_{fus}(1 - f_s) + \int_{298\mathrm{K}}^{T} c_{p,l}(1 - f_s) dT \qquad (1)$$

where f_s is the solid fraction of the mineral at a given temperature and $c_{p,s}$ and $c_{p,l}$ are heat capacity of solid and liquid and heat of fusion of the rock material as function of temperature. f_s is approximated with

$$f_s = \frac{1}{2}\left(1 - \tanh\left(a(T - T_m)\right)\right) \qquad (2)$$

The parameters a and T_m are model parameters that has to be estimated The parameter a has no physical interpretation, while T_m can be interpreted as the middle of the melting temperature interval, i.e. the temperature where 50% is molten.

The tanh function was chosen in order to obtain a continuous and differentiable function that is easy to use in detailed mathematical models of complex systems such as a cupola furnace (see [7]) where the melting is only one of the necessary submodels.

Determination of the values of $c_{p,s}$, $c_{p,l}$, ΔH_{fus}, a and T_m are described in the following sections.

Melting Temperature

Crystalline Raw Materials

The melting temperature is estimated with a model of magmatic crystallisation by Nathan and van Kirk [1], who consider the nine solid phases listed in table 2 in their model. The basic concept of the model is to calculate the liquidus temperature, T_{liq}, of all the nine phases corresponding to the composition of a melt. A small amount of the phase with the highest T_{liq} is then removed from the melt and a new composition of the melt is calculated. Then a new set of T_{liq} is calculated, more is removed from the melt and so forth until all the melt has been removed. The melting temperature interval is then the interval where the fraction solid is $0 < f_s < 1$.

The liquidus temperatures are calculated as

$$\begin{aligned} T_{liq,i} = a_{0,i} &+ a_{1,i}[Al] + a_{2,i}[Ti] + a_{3,i}[Fe(III)] + a_{4,i}[Fe(II)] \\ &+ a_{5,i}[Mg] + a_{6,i}[Ca] + a_{7,i}[Na] + a_{8,i}[K] \\ &+ a_{9,i}\ln(GM_i) + a_{10,i}\sqrt{[Al]([Na]+[K])} \end{aligned} \quad (3)$$

where $[X]$ represent the cation fraction of cation X in the melt, and GM_i is the geometric mean of the essential cations of phase i (see table 3). The coefficients, $a_{j,i}$, are given by Nathan and van Kirk [1].

For each of the solid solutions (e.g. (Fe,Ti) in magnetite in table 2) the composition is calculated from equilibrium constants for the cations. E.g. for magnetite the composition of the Fe(III)-Ti solid solution is calculated as

$$\frac{([Fe(III)]/[Ti])_{mag}}{([Fe(III)]^2/([Fe(II)]\cdot[Ti]))_{liq}} = k = 1.84 \quad (4)$$

Table 2. The solid phases considered in the crystallisation model. (X,Y) denotes solid mixture of X and Y.

Mineral	Abbreviation	Composition
Magnetite	Mag	$(Fe,Ti)_3O_4$
Olivine	Olv	$(Mg,Fe)_2SiO_4$
Hypersthene	Hyp	$(Mg,Fe)SiO_3$
Augite	Aug	$(Ca,Na)(Mg,Fe)Si_2O_6$
Plagioclase	Pla	$(Ca,Na)(Si,Al)_4O_8$
Orthoclase	Ksp	$(K,Na)AlSi_3O_8$
Quartz	Qtz	SiO_2
Leucite	Leu	$KAlSi_2O_6$
Nepheline	Nep	$(Na,K)AlSiO_4$

Table 3. The expressions for the geometric mean of the essential cations in the solid phases.

Mineral	Geometric Mean
Magnetite	$\sqrt[3]{[Fe(II)][Fe(III)]^2}$
Olivine	$\sqrt[3]{([Mg]+[Fe(II)])^2[Si]}$
Hypersthene	$\sqrt{([Mg]+[Fe(II)])[Si]}$
Augite	$\sqrt[4]{[Ca]([Mg]+[Fe(II)])[Si]^2}$
Plagioclase	$\sqrt[5]{([Na]+[K])[Al][Si]^3}$
Orthoclase	$\sqrt[5]{[K][Al][Si]^3}$
Quartz	1
Leucite	$\sqrt[4]{[K][Al][Si]^2}$
Nepheline	$\sqrt[3]{[K][Al][Si]}$

The remaining solution expressions are given by Nathan and van Kirk [1]. It must be noted that plagioclase ($(Ca,Na)(Si,Al)_4O_8$) consists of a mix of albite ($NaAlSi_3O_8$) and anorthite ($CaAl_2Si_2O_8$). It is therefore only necessary to calculate the ratio between Ca and Na to determine the composition of plagioclase (see e.g. Deer et al. [8]).

An example of a modelled fraction solid curve for the volcanic rock gabbro (chemical composition given in table tab:ChemComp) using the method of Nathan and van Kirk [1] is shown in figure 1. The figure shows that the first solid is formed at approximately 1220^oC when a liquid sample is cooled and all the material has solidified at approximately 1000^oC. The model of Nathan and van Kirk [1] considers only nine crystalline phases and thus fails to give a complete description of raw materials that contain crystals not represented among the nine. A consequence of this is that when most of the material has

solidified in the model the remaining elements can (in some cases) not form any of the nine phases. The model of Nathan and van Kirk [1] can thus often not reach a fraction solid equal unity as seen in figure 1.

Amorphic Phase

Amorphic materials do not melt as such, but the viscosity properties are chanced abruptly at a certain temperature, the glass transition temperature, T_g [9]. The amorphic materials thus changes from solid to liquid form at the glass transition temperature. No reliable models for estimating the glass transition temperature has been published. A rough estimate is that [10]

$$T_g = \frac{2}{3} T_{melt} \text{ [K]} \tag{5}$$

where T_{melt} is the melting point of the crystalline material with the same composition. The melting point (or interval) can often not be calculated using the model of Nathan and van Kirk [1] described above, since the amorphic materials frequently have a low silicon content and therefore form other crystalline phases than those used in the above model (equation 3). The glass transition temperature must then be found in phase diagrams for each new material encountered.

Estimation of a and T_m

The two parameters in equation 2, a and T_m, can be estimated by comparing the function in equation 2 to the solid fraction function calculated with the model of Nathan and van Kirk [1] in the case of crystalline materials. Illustration of the solid fraction curve and fitting of the f_s function is shown in figure 1.

In the case of amorphic materials the T_m-parameter in equation 2 is set equal to T_g and a must be adjusted to a value to obtain a reasonable value that depends on the what use the model is aiming at.

Specific Heat Capacity

Crystalline Phase

Crystalline mineral materials consist of a number of mineral phases. The equilibrium composition can be calculated from the total chemical composition with

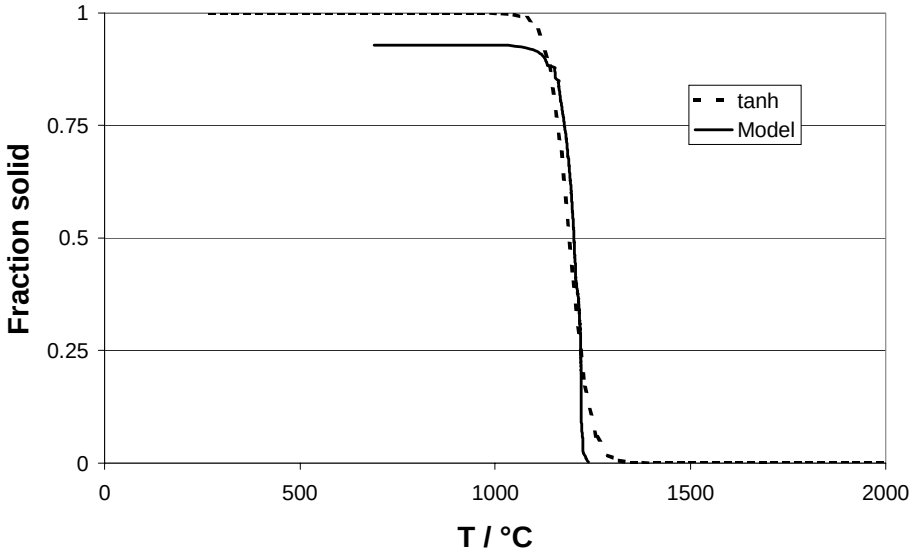

Figure 1. Solid fraction of the volcanic rock, Gabbro. Model by Nathan and van Kirk [1] and the fitted tanh in the f_s model plotted against temperature.

the CIPW method described by Best [4]. The CIPW method includes 31 different crystalline phases and is thus more detailed than the method of Nathan and van Kirk [1]. However, the CIPW method predicts only the composition of the solid mineral, and gives no information about the melting interval. The CIPW method is an algorithm that, based on the chemical composition, determines the amount of the each of the 31 crystals listed in table 8 in the appendix that are present in the mineral.

The heat capacity of the raw material can be assumed to be calculated as the weighted sum of the heat capacity of the phases [2].

$$c_{p,s} = \sum x_{phase,i} c_{p,s,i} \quad \left[\frac{\mathrm{J}}{\mathrm{mole} \cdot \mathrm{K}}\right] \tag{6}$$

Correlations for the specific heat capacity for each phase are given in appendix A. The correlations for c_p (table 9 and 10) that are used in the model are only valid over a limited temperature range, but the correlations were used as a best guess beyond the range of validity. When the heat of fusion or heat capacity data for a crystal was not available (see table 9 and 10) the value for that crystal was set to the weighted average of the values for the other crystals present in the mineral.

Amorphic Phase

According to Steppins et al. [2] the heat capacity of amorphic minerals can be calculated as

$$c_{p,amorph,s} = \sum a_i x_i + \sum b_i x_i T + \sum c_i x_i T^{-2} \quad \left[\frac{\mathrm{J}}{\mathrm{mole} \cdot \mathrm{K}}\right] \tag{7}$$

where x_i are the mole fractions of the oxides. The coefficients are listed in table 4.

Liquid Phase

According to Steppins et al. [2] the heat capacity of liquid minerals can be calculated as

$$c_{p,l} = \sum x_i c_{p,i} \quad \left[\frac{\mathrm{J}}{\mathrm{mole} \cdot \mathrm{K}}\right] \tag{8}$$

where x_i are the mole fractions. The heat capacities are listed in table 5.

Heat of Fusion

The heat of fusion of the amorphic mineral materials is zero, since it is a supercooled liquid. The heat of fusion of the crystalline mineral materials is calculated as the weighted sum of the heat of fusion of the phases [3].

$$\Delta H_{fus} = \sum x_{phase,i} \Delta H_{fus,i} \quad \left[\frac{\mathrm{J}}{\mathrm{mole}}\right] \tag{9}$$

The composition can be calculated from the total chemical composition as described in appendix A. The heat of fusion for each phase is listed in table 9 and 10 in appendix A.

3 Measurement Procedures

The experimental data in this work was obtained using Differential Scanning Calorimetry (DSC). DSC has previously been used for measuring heat capacity, heat of fusion, melting interval and other transition quantities [12, 13]. The materials that have been analysed by DSC include heavy metal fluoride glass

Table 4. Coefficients for calculating the specific heat capacity of silicate glasses (400K - 1000K). $c_{p,amorph}$ and $c_{p,cryst}$ are the heat capacities at 700K of amorphic and crystalline magma respectively. (Data retrieved from [2])

	a_i	$b_i \cdot 10^2$	$c_i \cdot 10^{-5}$	$\frac{c_{p,amorph}}{3R}$	$\frac{c_{p,cryst}}{3R}$
SiO_2	66.354	0.7797	-28.003	0.88	0.88
TiO_2	33.851	6.4572	4.470	1.07	0.92
Al_2O_3	91.404	4.4940	-21.465	0.96	0.94
Fe_2O_3	58.714	11.3841	19.915	1.14	1.18
FeO	40.949	2.9349	-7.6986	1.20	1.13
MgO	32.244	2.7288	1.7549	1.04	0.98
CaO	46.677	0.3565	-1.9322	0.98	1.03
Na_2O	69.067	-3.2194	2.9101	1.11	1.18

Table 5. Specific heat capacity of liquid mineral materials (1200K - 1850K). The heat capacities are independent of temperature. [2]

	$c_{p,liq}\ \left[\frac{\text{J}}{\text{mole}\cdot\text{K}}\right]$
SiO_2	80.0 ± 0.9
TiO_2	111.8 ± 5.1
Al_2O_3	157.6 ± 3.4
Fe_2O_3	229.0 ± 18.4
FeO	78.9 ± 4.9
MgO	99.7 ± 7.3
CaO	99.9 ± 7.2
Na_2O	102.3 ± 3.6

[14], pure metals [15], ashes and deposits from high-temperature coal-straw co-firing [16], ashes from solid fuel combustion [17] and polymers [12].

Differential Scanning Calorimetry is based on measureing the heating rate of a sample and of a known reference material in a specified atmosphere. The underlying assumption is that the heat transfer rate is proportional to the temperature difference between the surroundings and the sample/reference material, i.e. Fourier's law applies, and that the heat transfer coefficients are independent of material. Höhne et al. [18] discuss the theoretical background of DSC and provide an extensive introduction to practical DSC.

The equipment used in this work is a Netzsch STA 409 C. The measuring part of the STA 409 C is shown in a side view in figure 2. During experiments, the sample material is placed in the sample crucible and the reference material in the reference crucible on top of the sample carrier (figure 2, No 3 and figure

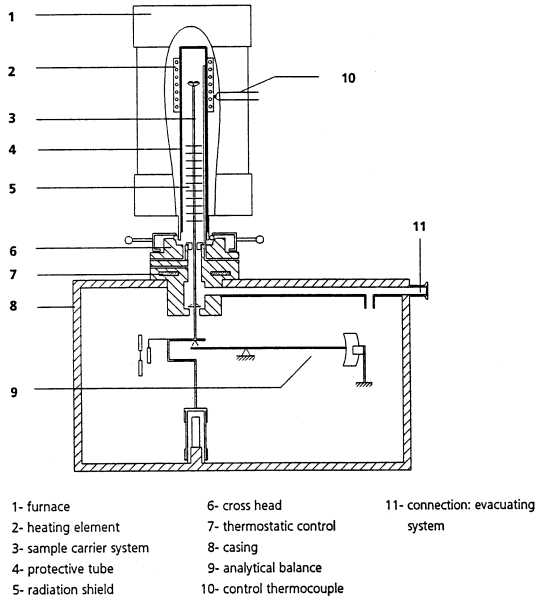

Figure 2. Cross section of the measuring part of the STA 409 C (from [11]).

3). To the bottom of each crucible is mounted a thermocouple, allowing continuous measurement of the temperature difference between the sample and the reference material. The sample carrier is located on top of a highly sensitive analytical balance (No 9), located in a vacuum tight casing (No 8), containing connections for gas inlet/outlet or evacuation (No 11). The balance operates according to the principle of a substitution beam balance with electromagnetic weight compensation. The bottom part of the sample carrier is equipped with a radiation shield (No 5) to prevent errors introduced due to heat radiation to the balance system. In addition, the vacuum tight connection (No 6) between the reaction and the balance chamber is equipped with a thermostatic control (No 7). The high temperature furnace (No 1) is heated by tubular SiC heating elements and operates at temperatures from 25 to 1550^{o}C with possible heating rates between 0.1 and 50^{o}C/min.

The measurement procedure was as follows. First the reference line is established by measuring approximately 20mg sapphire in one crucible and approximately 20mg α-alumina in the other. These materials are heated from room temperature to 1475^{o}C at 10K/min and the temperature difference is recorded in terms of a mV signal. The crucibles are made of platinum and equipped with a lid that is not hermetically sealed. For this measurement the following equation is valid

$$c_{p,Al} m_{Al} \beta - c_{p,sap} m_{sap} \beta = K_\Phi(T) \cdot (\Phi_{Al} - \Phi_{sap}) \tag{10}$$

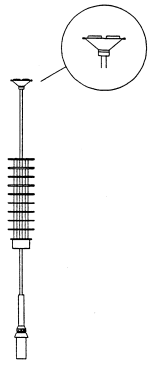

Figure 3. The sample carrier system (from [11]).

where $K_\Phi(T)$ is the temperature dependent calibration factor and $(\Phi_{Al} - \Phi_{sap})$ is the DSC signal. Subscript Al and sap denotes α-alumina and sapphire respectively and β is the heating rate. Now the sample is measured the same way as the sapphire, i.e. approximately 20mg sample in one crucible and approximately 20mg α-alumina in the other. In analogy with the above the following equation is valid

$$c_{p,Al} m_{Al} \beta - c_{p,sam} m_{sam} \beta = K_\Phi(T) \cdot (\Phi_{Al} - \Phi_{sam}) \tag{11}$$

Combining the two equations to eliminate $K_\Phi(T)$ and β, the heat capacity of the sample can be found as

$$c_{p,sam} = \frac{1}{m_{sam}} \left[c_{p,Al} m_{Al} - (c_{p,Al} m_{Al} - c_{p,sap} m_{sap}) \frac{\Phi_{Al} - \Phi_{sam}}{\Phi_{Al} - \Phi_{sap}} \right] \tag{12}$$

This is the equation that is used to determine the specific heat capacity of the sample as function of temperature. If the crucibles do not have identical mass (which they rarely have) this must be accounted for by introducing the term $\Delta m_{crucible} c_{p,crucible} \beta$ on the left hand side of equation 10 and 11. In case of phase transition the heat required for the transition will be embedded in the heat capacity.

From the heat capacity an enthalpy function can be obtained by integration as

$$H(T) - H(298.15\text{K}) = \int_{298.15\text{K}}^{T} c_p dT \tag{13}$$

4 Results and Discussion

The direct result of the measurements is the heat capacity as function of temperature, but with the heat of fusion embedded. Figure 4 shows an example of

the resulting c_p curve (for gabbro). The value of the heat capacity t 500^{o}C is 1.3J/g/K. A peak is observed at around 800K and again at 1200K and 1500K. The DSC measurements do not identify which transition a peak represents, but for the minerals investigated here it is known that the melting point is above 1100^{o}C. The peaks at 800K and at 1200K are caused by transitions other than melting, e.g. recrystallisation, calcination of $CaCO_3$ or evaporation of crystal bound water (the mass signal indicate whether it is recrystallisation or calcination/evaporation). The peak at 1500K correspond to the melting. The width of the peak indicates the melting temperature interval. The heat of fusion can be determined as the area under the peak of the resulting c_p curve (see an example in figure 4). Figure 5 shows the measured apparent heat capacity of all the mineral materials included in this work. The chemical composition of the materials are shown in table 11 in appendix A.

Since the melting temperature interval is indicated by the resulting c_p curve the two parameters in equation 2 can be estimated. Figure 6 shows the predicted melting curve and the c_p curve for a basalt. The model (equation 2) is then manually tuned to the c_p curve and also plotted. The manual tuning is done so that the f_s function is (almost) unity below the melting interval and (almost) zero above. The melting interval is illustrated with the grey area in figure 4.

The measurements show some variance as illustrated with three measurements of Gabbro (a mineral material) in figure 7. The curves are shifted vertically, however, the positions of the peaks are at the same temperature for all three measurements and the peaks are of the same size. The reason for the discrepancy is not clear.

When the solid fraction curve has been determined the modelled enthalpy function can be estimated using equation 1, 6, 8 and 9. Figure 8 shows the modelled enthalpy curve along with the measured (for gabbro). The plot shows good agreement between the modelled and the measured ΔH (evaluated through equation 13) since the two curves are parallel both below and above the melting interval. However the predicted heat of fusion is overestimated. On the experimental curve there is very little evidence of a heat of fusion. Figure 8 shows the modelled enthalpy curve along with the measured, in the case where the heat of fusion has been set to zero in the model.

The very low heat of fusion was found for all the materials tested (table 6). The best agreement between the model and the measurements was in all cases found when the heat of fusion was set to zero. Table 6 shows the energy requirements for each material for heating, melting and superheating from 25^{o}C to 1500^{o}C, both measured and predicted values (heat of fusion set to zero in the predicted values). Table 7 contains an overview of which phases the minerals contain according to the CIPW model. Anorthosite and Zuzel slag are the only two minerals containing quartz (Q) and they are the minerals for which the enthalpy

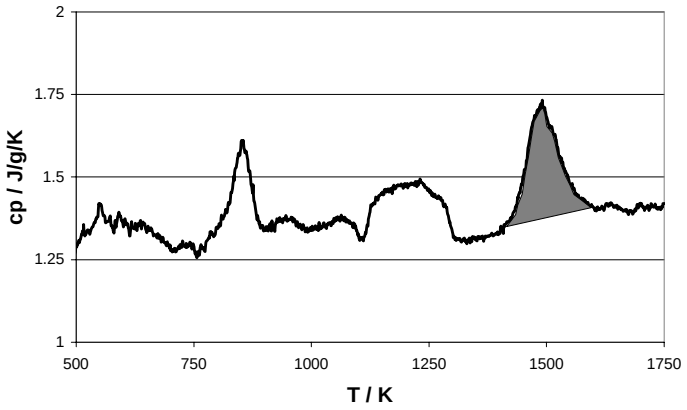

Figure 4. The heat of melting (or other transition heats) can be extracted from the resulting heat capacity function as the grey area, assuming that the heat capacity follows the base line of the grey area.

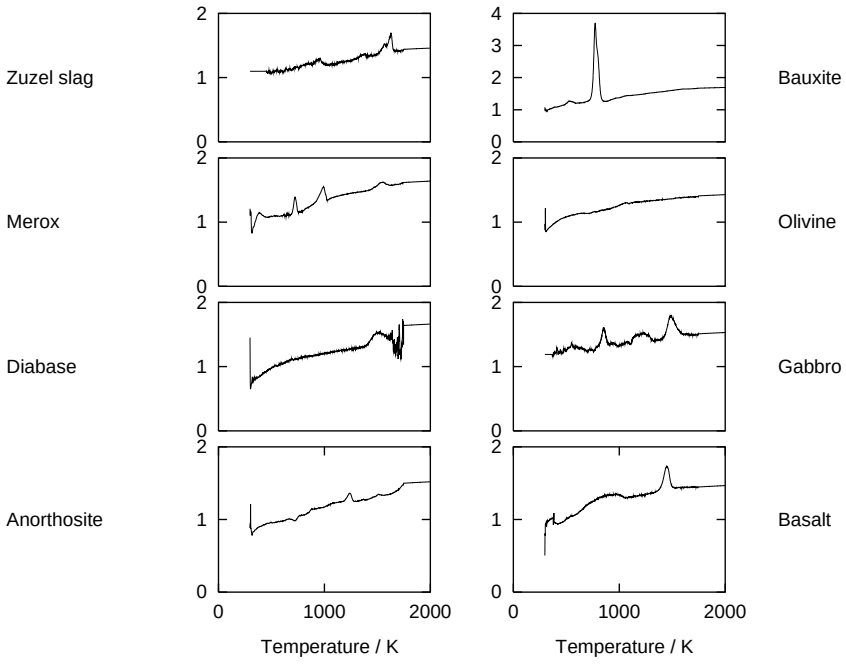

Figure 5. Measured apparent heat capacity as function of temperature. The heat capacity is given in J/g/K.

Table 6. Modelled and measured energy requirements (heating from 25^oC to 1500^oC including melting) for a number of raw materials.

	Model J/g	Exp J/g	Error %
Anorthosite	2463	1715	43.62
Basalt	1750	1896	-7.70
Bauxit	2212	2162	2.31
Gabbro	1685	2064	-18.36
Diabase	1812	1777	1.97
Merox	1825	1984	-8.01
Olivine	1869	1822	2.58
Zuzel slag	2110	1845	14.36

Table 7. Crystalline phases present in the minerals according to the CIPW model.

	Q	C	Z	Or	Ab	An	Lc	Ne	Kp	Hl	Th	Nc	Ac	Ns	Ks	Di	Wo	Hy	Ol	Cs	Mt	Cm	Il	Hm	Tn	Pf	Ru	Ap	Fl	Pr	Cc
Anorthosite	x	x		x	x	x												x				x		x				x			
Basalt				x		x	x	x								x			x				x					x			
Bauxit		x				x	x	x	x										x									x			
Gabbro				x	x	x		x								x			x				x					x			
Diabase		x		x	x	x												x	x				x					x			
Merox						x	x	x	x										x	x			x					x			
Olivin		x			x	x												x	x			x	x								
Zuzel slag	x	x		x	x													x					x								

Available data

H	x	x	x	x	x	x	x	x	x	x	x	x		x	x	x	x	x	x	x	x	x	x	x	x	x		x	x		
cp	x	x	x			x	x	x	x	x	x		x	x	x	x	x	x	x	x	x	x	x	x	x	x	x		x	x	x

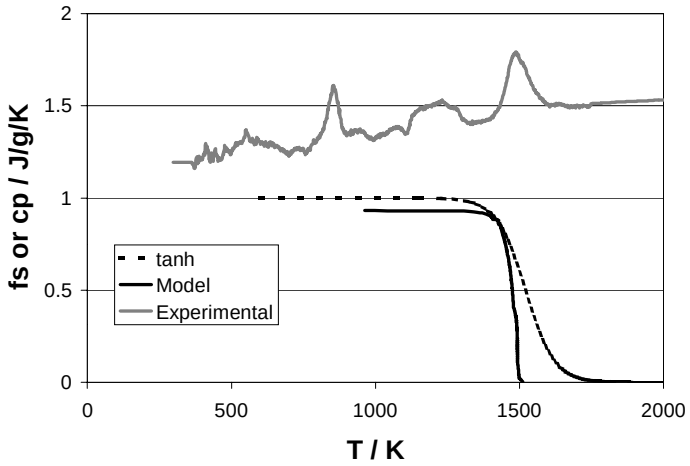

Figure 6. Fraction solid of a Gabbro (a mineral material) as function of temperature predicted by the melting model and the f_s model with fitted constants. Also the heat capacity from the DSC measurements is plotted on the fraction solid axis (J/g/K). The c_p curve was used to determine the parameters in the f_s model.

model gives the largest positive error. Gabbro contains 49% anorthite (An) according to the CIPW model[4], but data was not found for the heat capacity of anorthite, and thus the accuracy of the prediction must be expected to be limited.

During the melting the chemical composition of the solid and liquid phase is assumed constant (equal to the total composition) in the model when the heat capacities are evaluated. This assumption will, however, only introduce a small error compared to the total energy needed for heating the minerals from 25^{o}C to 1500^{o}C.

The measurements showed that the minerals exhibited almost no heat of fusion. Other works (see e.g. table 9 and 10 in appendix A) demonstrate considerable heat of fusion of the crystalline phases that the minerals consist of. The different behaviour in the minerals may be caused by heat of mixing.

5 Conclusion

A model for predicting the melting behaviour of mineral materials in terms of melting interval and heat consumption based only on the chemical composition was developed. The model was compiled from a number of existing models that each describes part of the phenomenon.

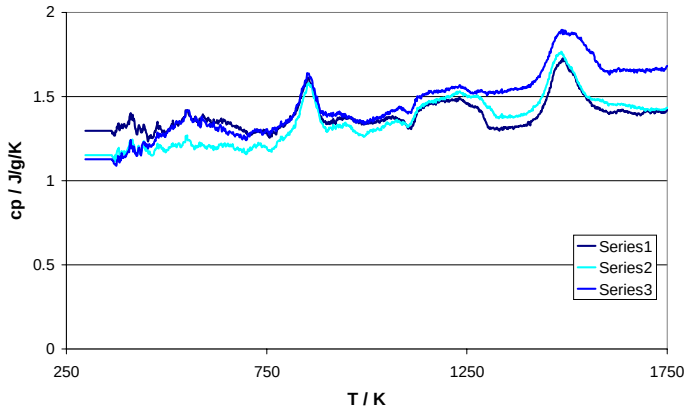

Figure 7. Measured heat capacity of Gabbro as function of temperature. The figure contains results of three independent measurements.

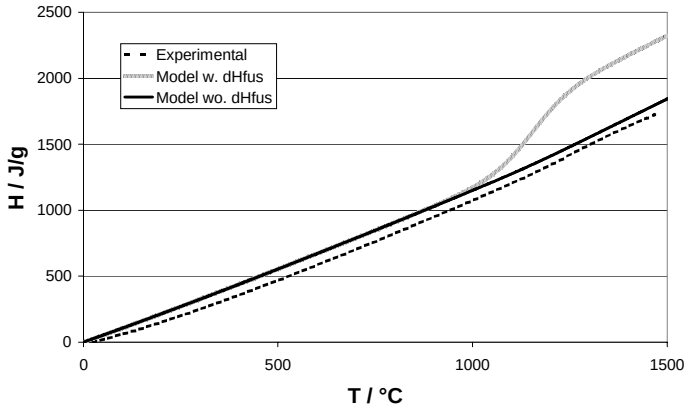

Figure 8. The enthalpy, modelled and measured, plotted against temperature. The modelled curves are with and without the heat of fusion term, i.e. either the heat of fusion was estimated using equation 9 or it was set to zero.

A number of minerals relevant to production of ROCKWOOL® products have been investigated with DSC technique to obtain information about their melting interval, heat capacity and heat of fusion. The measurements showed that the minerals exhibited only very low heat of fusion.

The model has been compared with the experimental data and showed good agreement when the heat of fusion was set to zero in the model.

The model was developed for use in a model of a mineral melting cupola furnace, where minerals are heated, melted and superheated from 25^oC to about 1500^oC. If the model is to be used for describing the phase transition precisely, the challenge of describing the heat of mixing should be addressed and the model should be refined with respect to both the f_s function and the evaluation of the heat capacities should be made dependent of the actual compositions of the solid and liquid phase during the melting.

Acknowledgement

This work is part of the research programme of ROCKWOOL® International A/S in cooperation with CAPEC (Computer Aided Process Engineering Centre) and CHEC (Combustion and Harmful Emission Control) at the Department of Chemical Engineering at the Technical University of Denmark. The project is funded by ROCKWOOL® and The Danish Ministry of Business and Industry.

References

[1] H.D. Nathan and C.K. van Kirk. A model of magmatic crystallisation. *Journal of Petrology*, 19:66 – 94, 1978.

[2] J.F. Steppins, I.S.E. Carmichael, and L.K. Moret. Heat capacities and entropies of silicate liquids and glasses. *Contributions to Mineralogy and Petrology*, pages 131 – 148, 1984.

[3] J. Konnerup-Madsen. *Energi-behovet ved opsmeltning af mineraler og bjergarter (Energy Requirements for Melting of Minerals and Rocks, in Danish).* Institut for Petrologi, Københavns Universitet, 1982.

[4] M.G. Best. *Igneous and Metamorphic Petrology.* W.H. Freeman and Company, 1982.

[5] R.A. Howie, B.S. Hemmingway, and J.R. Fisher. *Thermodynamic Properties of Minerals and Related Substances at* $298.15K$ *and 1bar (*10^5 *Pascals)*

Pressure and at Higher Temperatures. United States Government Printing Office, Washington, 1978.

[6] H. Bach and D. Krause. *Analysis of the Composition and Structure of Glass and Glass Ceramics*. Springer-Verlag, 1999.

[7] R. Leth-Miller, A.D. Jensen, P. Glarborg, S. B. Jørgensen, L.M. Jensen, and P.B. Hansen. Experimental investigation and mathematical modelling of a mineral melting cupola furnace. *Industrial and Engineering Chemistry Research (submitted)*, 2002.

[8] Deer, Howie, and Zussmann. *An Introduction to the Rockforming Minerals*. Longman group limited, Essex, Eng., 14th ed. edition, 1983.

[9] L. H. van Vlack. *Elements of Material Science and Engineering*. Addison-Wesley, 6th ed. edition, 1989.

[10] H. Scholze. *Glas; Natur, Structur und Eigenschaften (in German)*. Springer-Verlag, 1988.

[11] Simultaneous thermal analysis - STA 409 c - instruction manual. Netzsch, Thermal Analysis, 1993.

[12] E. Verdonck, K. Schaarp, and L.C. Thomas. A discussion of the principles and applications of modulated temperature DSC. *International Journal of Pharmaceutics*, 192:3 – 20, 1999.

[13] B. Wunderlich, A. Boller, I. Okazaki, and K. Ishikiriyama. Heat-capacity determination by temperature-modulated DSC and its seperation from transition effects. *Thermochimica Acta*, 304/305:125 – 136, 1997.

[14] R. Mossadegh, C.T. Moynihan, A.J. Bruce, and M.G. Drexhage. DSC studies of melting behaviour of heavy metal fluoride glass compositions. *Material Research Bulletin*, 22:593 – 600, 1987.

[15] N. Clavaguera, M.T. Clavaguera-Mora, J. Fontán, and J.L. Touron. Melting vs. solidification of a pure metal analysed by DSC. *Material Research Society Symposium Proceedings*, 481:33 – 38, 1998.

[16] L. A. Hansen, F. J. Frandsen, K. Dam-Johansen, H. S. Sørensen, and B.-J. Skrifvars. Characterisation of ashes and deposits from high-temperature coal-straw co-firing. *Energy and Fuels*, 13 (4):803 – 816, 1998.

[17] L. A. Hansen, F. J. Frandsen, K. Dam-Johansen, and H. Sørensen. Quantification of fusion in ashes from solid fuel combustion. *Thermochimica Acta*, 326:105 – 117, 1999.

[18] G.W.H. Höhne, W. Hemminger, and H.-J. Flammersheim. *Differential Scanning Calorimetry, An Introduction to Practioneres*. Springer Verlag, 1996.

[19] L.B. Pankratz, J.M. Stuve, and N.A. Gocken. *Thermodynamic Data for Mineral Technology, Bulletin 677.* United States Department for the Interior, Bureau of Mines, 1984.

A Raw Material Data

Table 8. Names, abbreviations, chemical formulas and formula weights for the minerals. [4]

Name and abbreviation	Chemical formula	Formula weight
Quartz (Q)	SiO_2	60.1
Corundum (C)	Al_2O_3	102
Zircon (Z)	ZrO_2, SiO_2	183
Orthoclase (Or)	K_2O, Al_2O_3, $6SiO_2$	556
Albite (Ab)	Na_2O, Al_2O_3, $6SiO_2$	524
Anorthite (An)	CaO, Al_2O_3, $2SiO_2$	278
Leucite (Lc)	K_2O, Al_2O_3, $4SiO_2$	436
Nepheline (Ne)	Na_2O, Al_2O_3, $2SiO_2$	284
Kaliophilite (Kp)	K_2O, Al_20_3, $2SiO_2$	316
Halite (Hl)	NaCl	58.4
Thenardite (Th)	Na_2O, SO_3	142
Sodium carbonate (Nc)	Na_2O, CO_2	106
Acmite (Ac)	Na_2O, Fe_2O_3, $4SiO_2$	462
Sodium metasilicate (Ns)	Na_2O, SiO_2	122
Potassium metasilicate (Ks)	K_2O, SiO_2	154
Diopside (Di)	CaO, (Mg,Fe)O, $2SiO_2$	217-248(a)
Wollastonite (Wo)	CaO, SiO_2	116
Hypersthene (Hy)	(Mg,Fe)O, SiO_2	100-132(a)
Olivine (Ol)	2(Mg,Fe)O, SiO_2	141-204(a)
Dicalcium silicate (Cs)	2CaO - SiO_2	172
Magnetite (Mt)	FeO, Fe_2O_3	232
Chromite (Cm)	FeO, Cr_2O_3	224
Ilmenite (Il)	FeO, TiO_2	152
Hematite (Hm)	Fe_2O_3	160
Sphene (Tn)	CaO, TiO_2, SiO_2	196
Perovskite (Pf)	CaO, TiO_2	136
Rutile (Ru)	TiO_2	79.9
Apatite (Ap)	3.3CaO - P_2O_5	310
Fluorite (Fl)	CaF_2	78.1
Pyrite (Pr)	FeS_2	120
Calcite (Cc)	CaO, CO_2	100

(a) These two numbers represent the weights of the pure Mg- and Fe-end members, respectively.

The correlations referred to in the tables in this appendix are equation a, b and

c given by

$$c_p = a + bT + cT^{-0.5} + dT^{-2} \qquad \text{(a)}$$

$$c_p = a + bT^{0.5} + cT + dT^2 + eT^{-1} \qquad \text{(b)}$$

$$c_p = a + bT + cT^2 + dT^{-0.5} + eT^{-2} \qquad \text{(c)}$$

Table 9. Heat of fusion, melting temperature and specific heat capacitites for the minerals.

Phase	ΔH_{fus} kJ/mole	ref.	T_m K	ref.	a	b	c	d	e	eq	Range	ref.
Q	9.6	II			$4.46030 \cdot 10^{1}$	$3.77540 \cdot 10^{-2}$	0	$1.00180 \cdot 10^{6}$		a	$298 - 844$K	I
					$5.89280 \cdot 10^{1}$	$1.00310 \cdot 10^{-2}$	0	0		a	$844 - 1800$K	I
C	107	II	2345	I	$1.57360 \cdot 10^{2}$	$7.18990 \cdot 10^{-4}$	$9.88040 \cdot 10^{2}$	$1.89690 \cdot 10^{6}$		a	$298 - 1800$K	I
Z	144	II			$2.36950 \cdot 10^{2}$	$-1.78790 \cdot 10^{-2}$	$-2.26780 \cdot 10^{3}$	$-1.49600 \cdot 10^{5}$		a	$298 - 1600$K	I
Or	158.9	II										
Ab	118.6	II										
An	146	II										
Lc	150.4	II			$2.96840 \cdot 10^{2}$	$2.68500 \cdot 10^{-1}$	0	$4.32900 \cdot 10^{6}$		a	$298 - 955$K	I
					$3.92940 \cdot 10^{2}$	$5.53320 \cdot 10^{-2}$	0	$2.45220 \cdot 10^{7}$		a	$955 - 1800$K	I
Ne	150.8	II			$5.54800 \cdot 10^{1}$	$5.90800 \cdot 10^{-1}$	0	0		a	$298 - 467$K	I
					$2.24180 \cdot 10^{2}$	$1.34220 \cdot 10^{-1}$	0	0		a	$467 - 1180$K	I
					$3.44000 \cdot 10^{2}$	$1.10400 \cdot 10^{-2}$	0	0		a	$1180 - 1525$K	I
Kp	133.8	II			$3.77760 \cdot 10^{2}$	$1.10374 \cdot 10^{-1}$	$-2.95740 \cdot 10^{3}$	0		a	$298 - 810$K	I
Hl	28.158	I	1073.8	I	$4.51510 \cdot 10^{1}$	$1.79740 \cdot 10^{-2}$	0	0		a	$298 - 1073.8$K	I
Th	23.723	I	1155	I	$1.21930 \cdot 10^{2}$	$8.14130 \cdot 10^{-2}$	0	0		a	$514 - 1155$K	I
Nc	27.67874	III	1123	III	$6.50000 \cdot 10^{1}$	$2.10000 \cdot 10^{-1}$	0	0		a	$298 - 723$K	III
					$5.70000 \cdot 10^{1}$	$1.50000 \cdot 10^{-1}$	0	0		a	$723 - 1123$K	III
Ac												
Ns	51.82268	III	1362	III	$1.53000 \cdot 10^{2}$	$4.50000 \cdot 10^{-2}$	0	$-3.50000 \cdot 10^{6}$		a	$298 - 1362$K	III
	52.3	II										
Ks	50.2	II			$1.41000 \cdot 10^{2}$	$5.30000 \cdot 10^{-2}$	0	$-2.00000 \cdot 10^{6}$		a	$298 - 1200$K	III
Di	*	*	*	*	*	*	*	*	*	*	*	
Wo	82.2				$1.11250 \cdot 10^{2}$	$1.43730 \cdot 10^{-2}$	$1.69360 \cdot 10^{1}$	$-2.77790 \cdot 10^{6}$		a	$298 - 1400$K	I
	27.405	I	1817	I	$1.07100 \cdot 10^{2}$	$1.74810 \cdot 10^{-2}$	0	$-2.29650 \cdot 10^{6}$		a	$298 - 1700$K	I
Hy	*	*	*	*	*	*	*	*	*	*	*	
Ol	*	*	*	*	*	*	*	*	*	*	*	
Cs	168.1	II	2403	I	$2.48710 \cdot 10^{2}$	$-8.31450 \cdot 10^{-4}$	$-2.05210 \cdot 10^{3}$	$-9.07700 \cdot 10^{4}$		a	$298 - 970$K	I
					$1.34557 \cdot 10^{2}$	$4.61080 \cdot 10^{-2}$	0	0		a	$970 - 1710$K	I
Mt	138.072	I	1870	I	$-3.55800 \cdot 10^{3}$	$3.34730 \cdot 10^{2}$	-9.30900	$2.53880 \cdot 10^{-3}$	$1.42730 \cdot 10^{5}$	b	$298 - 848$K	I
	138.1	II			$9.68230 \cdot 10^{1}$	$5.27330 \cdot 10^{-2}$	0	$5.64130 \cdot 10^{7}$		a	$848 - 1800$K	I
Cm					$3.01840 \cdot 10^{2}$	$4.15710 \cdot 10^{-2}$	$1.14700 \cdot 10^{-5}$	$-2.80270 \cdot 10^{3}$	$4.87690 \cdot 10^{5}$	c	$298 - 1800$K	I
Il	90.667	I	1640	I	-2.98950	$6.50490 \cdot 10^{-2}$	$2.42660 \cdot 10^{3}$	5.10570		a	$298 - 1640$K	I
Hm	74.9	II	1895	I	-838.61	$8.65250 \cdot 10^{1}$	-2.34340	$6.05190 \cdot 10^{-4}$	$2.78210 \cdot 10^{4}$	b	$298 - 950$K	I
					$-1.09570 \cdot 10^{3}$	$2.72670 \cdot 10^{-1}$	$3.39600 \cdot 10^{4}$	-1.02390		a	$950 - 1800$K	I
Tn	123.805	I	1670	I	$1.76730 \cdot 10^{2}$	$2.38520 \cdot 10^{-2}$	0	$3.99050 \cdot 10^{6}$		a	$298 - 1670$K	I
Pf	112.1		2188	I	$1.24960 \cdot 10^{1}$	$4.51560 \cdot 10^{-2}$	$2.46200 \cdot 10^{3}$	6.30180		a	$298 - 1530$K	I
Ru			2103	I	$6.30790 \cdot 10^{1}$	$1.13070 \cdot 10^{-2}$	5.61600	$9.86260 \cdot 10^{5}$		a	$298 - 1800$K	I
Ap	224.8	II										
Fl	29.706	I	1691	I	$-2.46920 \cdot 10^{1}$	$5.80950 \cdot 10^{-2}$	$1.87060 \cdot 10^{3}$	$2.87740 \cdot 10^{6}$		a	$298 - 1424$K	I
Pr					$-2.03190 \cdot 10^{1}$	$5.02990 \cdot 10^{-2}$	$1.78700 \cdot 10^{3}$	$-3.20020 \cdot 10^{6}$		a	$298 - 1000$K	I
Cc					$9.97150 \cdot 10^{1}$	$2.69200 \cdot 10^{-2}$		$2.15760 \cdot 10^{6}$		a	$298 - 1200$K	I

References: I: Howie et al. [5]; II: Bach and Krause [6]; III: Pankratz et al. [19]. The crystals Di, Hy and Ol (marked with * in stead of data) contains solid solution with varying compositions. The data for the components in the crystals are listed in table 10.

Table 10. Heat of fusion, melting temperature and specific heat capacitites for the minerals.

Phase	ΔH_{fus} kJ/mole	ref.	T_m K	ref.	a	b	c	d	e	eq	Range	ref.
Olivine												
Forsterite(Mg)	71.1	II	2163	I	$2.27980 \cdot 10^2$	$3.41390 \cdot 10^{-3}$	$-1.74460 \cdot 10^3$	$-8.93970 \cdot 10^5$		a	$298 - 1800$K	I
Fayalite(Fe)	92.173	I	1490	I	$1.72760 \cdot 10^2$	$-3.40550 \cdot 10^{-3}$	$2.24110 \cdot 10^{-5}$	0	$-3.62990 \cdot 10^6$	c	$298 - 1490$K	I
	92	II										
Diopside												
CaMg(SiO3)2	77.404	I	1664.5	I	$1.91820 \cdot 10^2$	$8.30790 \cdot 10^{-2}$	$-2.17180 \cdot 10^{-5}$	0	$4.27950 \cdot 10^6$	c	$298 - 1600$K	I
	128.4	II										
CaFe(SiO3)2												
Hyperstene												
Clinoenstatite(Mg)	61.505	I	1830	I	$2.05560 \cdot 10^2$	$-1.27960 \cdot 10^{-2}$	$-2.29770 \cdot 10^3$	$1.19260 \cdot 10^6$		a	$298 - 1600$K	I
	75.3	II										
Fe-enstatite	61.1	II										

References: I: Howie et al. [5]; II: Bach and Krause [6]; III: Pankratz et al. [19].

Table 11. Chemical composition of the minerals.

	SiO_2	Al_2O_3	K_2O	Na_2O	CaO	NaCl	Fe_2O_3	FeO	MgO	Cr_2O_3	TiO_2	P_2O_5	MnO
Diabase	0.4950	0.1410	0.0110	0.0290	0.0690	0.0000	0.0000	0.1170	0.0960	0.0000	0.0210	0.0060	0.0000
Merox	0.1220	0.0200	0.0010	0.0010	0.4120	0.0000	0.0000	0.2310	0.1000	0.0000	0.0120	0.0050	0.0290
Basalt	0.4095	0.1135	0.0105	0.0385	0.1275	0.0000	0.0000	0.1150	0.1155	0.0000	0.0280	0.0080	0.0010
Gabbro	0.4935	0.1450	0.0010	0.0280	0.1365	0.0000	0.0000	0.0650	0.0870	0.0000	0.0075	0.0010	0.0010
Zuzel	0.3880	0.0800	0.0040	0.0060	0.0000	0.3440	0.0000	0.0030	0.0830	0.0000	0.0030	0.0000	0.0050
Briquette	0.4060	0.1420	0.0090	0.0180	0.1470	0.0000	0.0000	0.0900	0.1130	0.0000	0.0140	0.0040	0.0010
Bauxite	0.1010	0.5050	0.0040	0.0010	0.0170	0.0000	0.0000	0.1930	0.0020	0.0000	0.0000	0.0010	0.0010
Olivin	0.4130	0.0030	0.0000	0.0010	0.0010	0.0000	0.0000	0.0670	0.4970	0.0020	0.0010	0.0000	0.0000
Anorthosite	0.4860	0.2940	0.0030	0.0300	0.1370	0.0000	0.0150	0.0000	0.0070	0.0002	0.0020	0.0010	0.0002

Article II

Comparative Study of Coke reactivity towards CO_2

R. Leth-Miller[†,‡*], A.D. Jensen[‡], J. Jensen[‡],
P. Glarborg[‡], L.M. Jensen[†], P.B. Hansen[†] and S.B. Jørgensen[‡]

[†]Rockwool® International A/S, Denmark
[‡]Department of Chemical Engineering,
Technical University of Denmark
June 10, 2002

Abstract

The reactivity towards CO_2 of seven types of commercial coke used in stone wool production have been measured in a Thermo Gravemetric Analyser (TGA). The cokes originated from Western and Eastern Europe and from China. For three of the cokes the porosity, density and surface area were determined. The directly measured porosities of the cokes was slightly low indicating that there are pores that are not connected with the outer surface. This is supported by the measured densities and micro photos.

The measurements showed that the Chinese cokes were the least reactive while the European cokes made on American coal were the most reactive. The reactivity of the one Eastern European coke in the measurements had an intermediate reactivity.

Simulations with a cupola model show that 25% more coke is needed for stone wool production if the coke type is changed to a type with half the reactivity towards O_2 and CO_2.

The TGA method proved to be a good method for ranking the coke with respect to reactivity with CO_2.

*Corresponding author, e-mail: rasmus.leth.miller@rockwool.com

Introduction

Coke is the main energy source for melting rocks in cupolas used for stone wool production and for melting iron in the foundry cupolas. The coke quality has influence on the cupola operation, e.g. on how much coke is needed, CO emissions etc. The CO emissions affect the reduction of iron oxides to metallic iron, which is a purpose in foundry blast furnaces, but undesired in the cupolas for stone wool production, since metallic iron is a waste product.

Coke is produced heating coal for a period of time without presence of oxygen to remove the volatiles. Two different types of ovens have been used for manufacturing the cokes that are investigated in this work, the coke battery and the beehive coke oven. The two production types differ by oven design as well as baking time. The cokes produced in batteries are baked for 20-50 hours while the cokes produced in beehives are baked for up till 5 days, both processes at 900-1100^{o}C.[1]

Several parameters influence the quality of coke e.g. hardness, porosity, reactivity, etc. The heterogeneous reaction between coke and CO_2 (C + CO_2 $\rightarrow$ 2CO) is important for the stone wool production process since the endothermic reaction is an important source of energy loss. In foundry blast furnaces the reaction is also important for production of CO for reduction of iron oxides to metallic iron. The product in stone wool production is the glass (or slag) and the useless byproduct is iron, i.e. opposite of iron production. The reactivity of the coke with CO_2 is therefore an important parameter but for different reasons. Reactivity towards CO_2 may also provide an indication of the reactivity with other species, e.g. combustion with O_2. The combustion of particles has been described with the so called double layer theory, where CO_2 reacts with the coke to give CO. The CO formed then diffuses through a gas film to react with O_2. The CO_2 formed then diffuses partly away from the particle through an outer gas layer and partly back to the particle[2]. According to the double film theory, CO_2 is the actual coke oxidising agent even in the combustion, and the CO_2 gasification is thus in itself important to the combustion.

Coke reactivity towards CO_2 has been investigated by several researchers[3–10]. These reactivity studies have been made in an atmosphere containing N_2 and CO_2 and in some cases CO and the particle sizes were in the interval of 1mm to 30mm. The amount of specimen in the measurements varies from 7g to 20kg. The temperature range is 750^{o}C - 1200^{o}C. The rate expression for the gasifications has been reported to be a Langmuir-Hinshelwood expression[2–4,11]

$$r = \frac{K_1 P_{CO_2}}{1 + K_2 P_{CO} + K_3 P_{CO_2}}. \quad (1)$$

Hobbs et al.[12] reports reaction rates of char gasification with CO_2 following the

expression

$$r = kC_{CO_2} \tag{2}$$

In this work the coke reactivity with CO_2 of a range of commercial cokes is investigated in a TGA. Density and porosity measurements have further been made to provide explanations to the results. The cokes selected for the investigations are of the type that are typically categorised as foundry coke (cokes of size up to 220mm) in contrast to the metallurgical coke (sized approx. 50mm) [1].

This paper is organised as follows. First the seven cokes studied in this work are presented in terms of production method, chemical composition and physical properties. Then the experimental setup and the measurement procedures are described. The results are presented and compared to results reported. Finally simulation based investigation is performed to illustrate the significance of the coke reactivity upon cupola operation.

Coke Selection and Characterisation

Seven commercial cokes were selected for the reactivity investigations. The cokes will not appear under their trade name but as e.g. *Euro 1* or *Chinese 1*. Five types of European cokes were selected and two types of Chinese. Table 1 shows the coal origin and production method of the cokes.

The chemical composition and calorific value of the seven cokes are shown in table 2. All the cokes contain very little S, N and H. The four European cokes made on American coal (*Euro 1,2,4* and *5*) contain approximately 7% ash, while *Euro 3* and *Chinese 1* and *2* contain more than 10% ash. The cokes containing

Table 1. Coke production parameters

Coke	Production process	Coal origin
Euro 1	Battery	USA
Euro 2	Battery	USA
Euro 3	Battery	Poland
Euro 4	Battery	USA
Euro 5	Battery	USA
Chinese 1	Beehive	China
Chinese 2	Beehive	China

Table 2. Coke compositions and calorific values

	Calorific value* [MJ/kg]	Ash [%]	Water [%]	S [%]	H [%]	C [%]	N [%]
Euro 1	31.0	7.2	0.9	0.73	0.17	89.8	1.1
Euro 2	31.2	6.5	0.9	0.79	<0.1	90.8	1.1
Euro 3	29.7	10.5	1.1	0.72	0.15	86.5	0.95
Euro 4	31.1	6.2	0.8	0.64	0.11	91.1	1.1
Euro 5	28.6	6.8	8.4	0.58	0.3	82.3	1.1
Chinese 1	29.6	10.4	1.4	0.64	0.33	85.2	1.3
Chinese 2	29.7	10.2	1.1	0.60	0.22	86.3	1.2

* Lower heating value, i.e. the water product has not condensed to liquid (see Turns[13]).

much ash have the lowest heating values. *Euro 5* also have a low heating value, but that is due to the high content of water.

Physical Properties

The porosity, density and surface area was determined for three of the cokes, *Euro 2*, *Euro 3* and *Chinese 2*. These three cokes were selected because they cover the different combinations of coal and production oven that are included in this work.

The porosity was determined by weighing a batch of particles before and after absorption of water into the pore system under vacuum[14]. The particle density was obtained by measuring the volume of a batch of fine sand particles before and after a known mass of coke particles was added to the container[14]. No information about the pore size distribution and surface area was obtained. The coke particles used in the measurements were approximately 0.7mm. The measurements by both methods were repeated several times and the 'water' method was tested by systematically varying the applied particle size. In the case of *Chinese 2*, more than 10 experiments were carried out by the water method. In general the two simple methods were found to give repeatable results.

The results of the porosity and density measurements from the simple method, *sand and water*, are shown in table 3. The Chinese coke is more dense and less porous than the European cokes. The coke made from polish coal, *Euro 3*, is the most dense and least porous of the two European cokes. The solid density of graphite is about 2.25 g/cm^3 and a solid density of about 2 g/cm^3 is expected for amorphous carbons[15]. The measured values are thus of a realistic

Table 3. Coke physical data by 'sand' and 'water' method.

Coke	Particle density [g/cm^3]	Porosity (%)	Solid density [g/cm^3]
Euro 2	0.93	42	1.60
Euro 3	1.09	35	1.68
Chinese 2	1.34	34	2.03

size, however slightly low in two of the cases.

The surface area obtained through BET measurements (using He) are shown in table 4. The measurements show that the *Chinese 2* coke has approximately ten times higher surface area than the two European cokes.

Figure 1 shows a photograph of the pore structure of the *Chinese 2* coke. It appears that most of the large pores are connected by regions of micro porosity only.

Experimental Methods

The reactivities of the cokes with CO_2 are measured in a thermo gravimetric analyser (TGA). A sketch of the used TGA Netzsch STA 409C is shown in figure 2. The TGA measures the sample mass as function of time and temperature while the gas composition is controlled. The temperature can be controlled as desired, in several isothermal or dynamic (heating or cooling) sequences. The data from TGA may be represented by the direct measurement result, i.e. the sample mass, as a function of time or temperature, or by the derivative of the signal (DTG), i.e. the rate of mass change, against time or temperature.

The measurement procedures are initially conducted with an empty crucible

Table 4. BET surface area measurements of the three selected cokes.

Coke	BET area [m^2/g]
Euro 2	0.414
Euro 3	0.497
Chinese 2	4.951

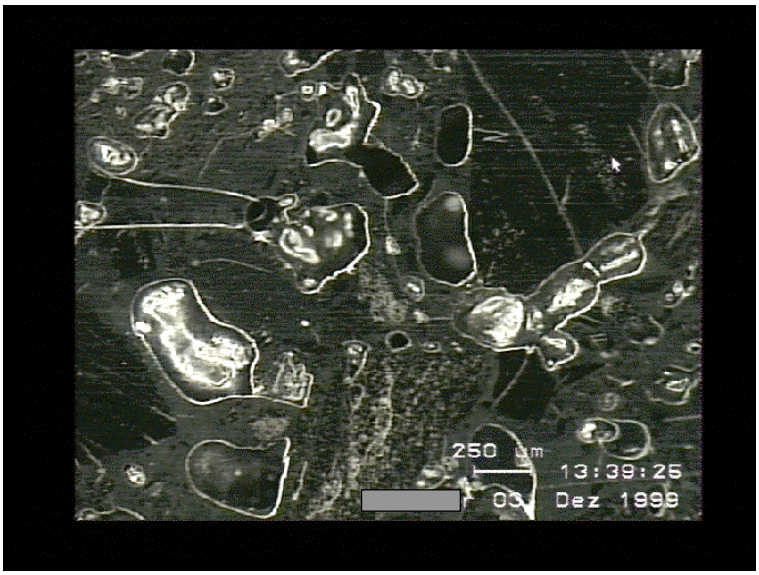

Figure 1. Photograph of the pore structure in the *Chinese 2* coke.

placed in the sample carrier to obtain a reference curve. The reference curve is subsequently subtracted from the sample curve to account for buoyancy and other systematic disturbances.

The reactivities were measured in a N_2-CO_2 atmosphere (in some cases also CO). Approximately $1-5$mg sample was used for each measurement and the particle size was $90-105\mu$m, which is smaller and less than what was used in the works of[3–10]. Preliminary experiments showed that larger sample masses and/or larger particle size reduced the reactivity (indicating that transport phenomena may play a significant role). Volatile matter released below 1073K in the cokes is present in so small amounts that mass loss could hardly be detected. The measurements reported here therefore start at 1073K because the rate of chemical reactions in the system is virtually zero below this temperature. The CO_2 concentration was fixed in each measurement but varied between 5vol% and 20vol%. The heating rate was also constant in each measurement, but varied between 5K/min and 20K/min. When the temperature reaches 1573K it is kept constant until full conversion of the coke is obtained. The temperature is not increased beyond 1573K to avoid ash sintering to the platinum crucibles.

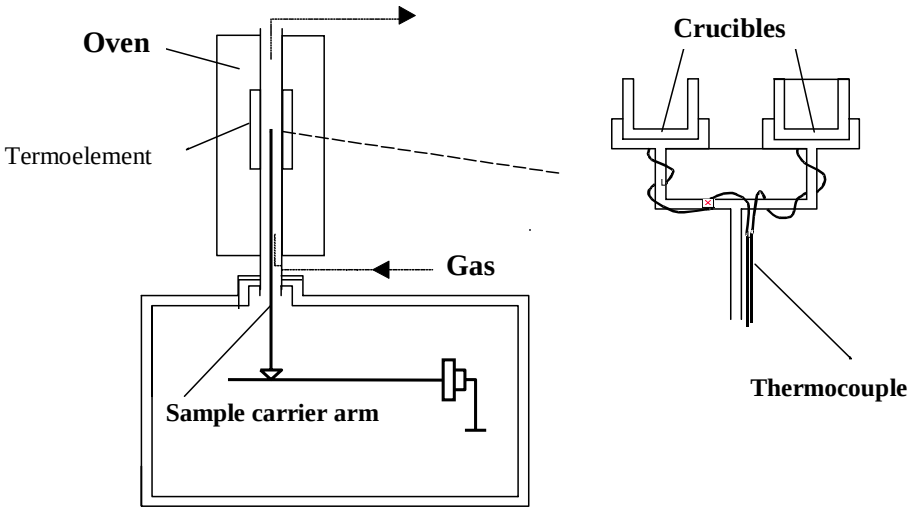

Figure 2. Sketch of TGA equipment, type Netzsch STA 409 C[16]. To the right a crucible carrier is sketched. In this case for two crucibles for DSC measurements, one for the sample and one for the reference. This setup enables measurement of heat of reaction.

Results

This section describes the results of the TGA measurements in terms of reaction kinetics. The coke conversion for the seven cokes are shown in figure 3. The European group of cokes starts to convert (reach 10% conversion) after approximately 40min, i.e. at $T = 1273$K. The rate of conversion gets faster until the conversion has reached $\approx 80\%$. The cokes are fully converted in a little less than 100min, i.e. at $T = 1573$K. The *Euro 3* coke reacts a little slower than the other European cokes and reaches full conversion after a little more than 100min. The initial conversion of the Chinese cokes are comparably slow with 10% conversion after 45min, i.e. at $T = 1300$K. They and reach full conversion after 115min, i.e. at $T = 1573$K in the isotherm segment of the heating procedure. Figure 3 shows that the two Chinese cokes are the least reactive and have very similar reactivity. The *Euro 3* coke is intermediate between the Chinese and the remaining four European cokes, the latter group being the most reactive.

The repeatability of the method was good as illustrated in figure 4.

Quantitative kinetics for the three cokes are determined using a volumetric reaction model[17], assuming that the reaction is first order with respect to the

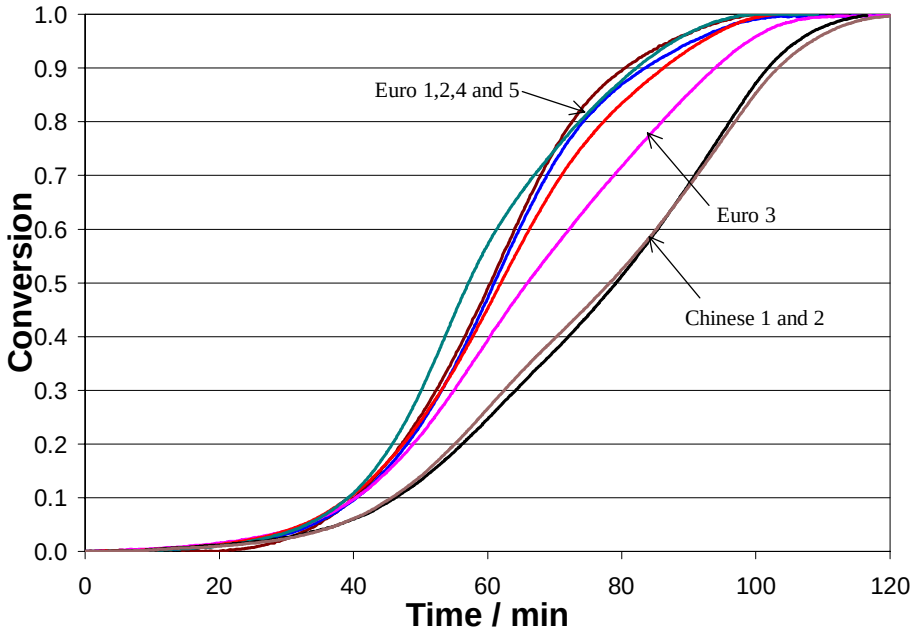

Figure 3. Conversion as function of time. The temperature is $T = 1073$K at time $t = 0$. The heating rate is 5K/min.

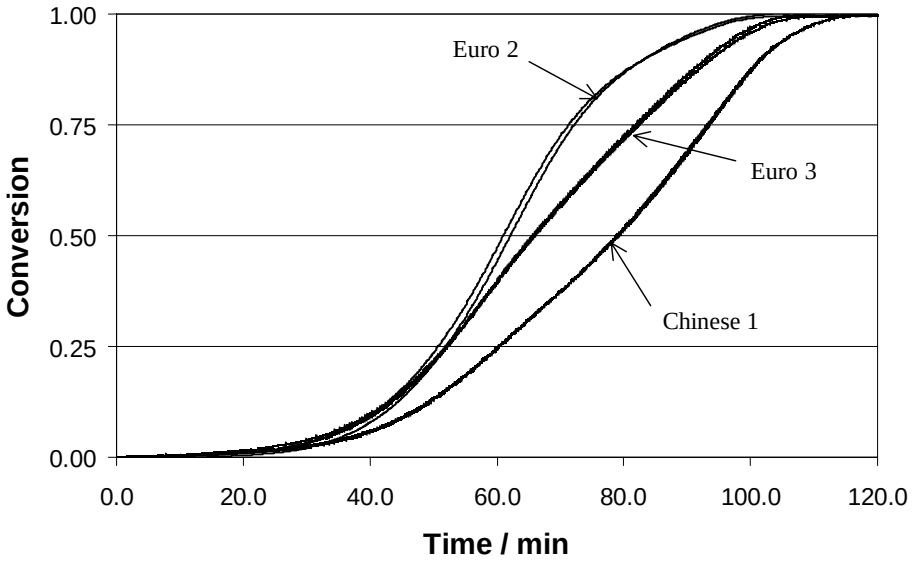

Figure 4. Repeatability. Two measurement series for each of the three cokes, *Euro 2*, *Euro 3* and *Chinese 1*, in terms of conversion plotted against time. At time 0min the temperature is 1073K, and at time 100min the temperature is 1573K whereafter it is kept constant.

coke and n'th order with respect to CO_2. The rate of reaction is thus given by

$$\frac{\mathrm{d}X}{\mathrm{d}t} = p_{CO_2}^n k_0 \exp\left(\frac{-E_a}{RT}\right)(1-X) \tag{3}$$

where X is the fraction of coke conversion. The factor $(p_{CO_2}^n k_0)$ and the activation energy, E_a, have been estimated numerically using an in house computer code based on the VA07AD algorithm[18]. The code enables parameter estimation using as basis up to three sets of data with fixed CO_2 partial pressure. The pre-exponential factor, k_0, and the reaction order, n, is hereafter estimated exploiting that

$$\ln(p_{CO_2}^n k_0) = n\ln(p_{CO_2}) + \ln(k_0) \tag{4}$$

and using data from measurements with different p_{CO_2}.

During the estimation procedure it was discovered that it was inappropriate to give all data the same weight, i.e. the parameter values had high standard deviation. The data for coke conversions higher than 80% was weighted by zero to obtain unambiguous results. This indicates that the volumetric reaction model is less appropriate at high conversion or that the coke deactivates due to thermal annealing[19,20].

Figure 5 compares experimental data and model prediction of the coke conversion plotted against temperature for the *Chinese 2* coke. The figure shows that the model in general describes the data well but has some difficulties describing the reaction at small coke conversions whereas the model describes the reaction well at intermediate coke conversions. The data at higher conversion have been given more weight in the parameter estimation, and this (partly, at least) causes the slightly better agreement at intermediate conversion.

The model can be fitted to single experiments with good result. However, the fits for *Euro 2* and *Euro 3* gave ambiguous results with respect to the activation energy, E_a. This problem may arise because the assumption that the mass transport is negligible may not be valid for the more reactive cokes and the given sample mass. Also the well known compensation effect[21] is to account for that, i.e. k_0 and E_a are correlated.

The resulting parameters in the reaction model for the three cokes are listed in table 5. The parameters have been obtained based on measurements with heating rates of both 5 and 20 K/min.

The results are compared to the results of Aderibigbe and Szekely[3] and Wu (Wu's results are extracted from Aderibigbe and Szekely[3]) in figure 6. The results from this work are extrapolated beyond the temperature range were it was measured (1073K - 1573K). The figure shows that the present results lies in the same order of magnitude as the most reactive metallurgical cokes referred

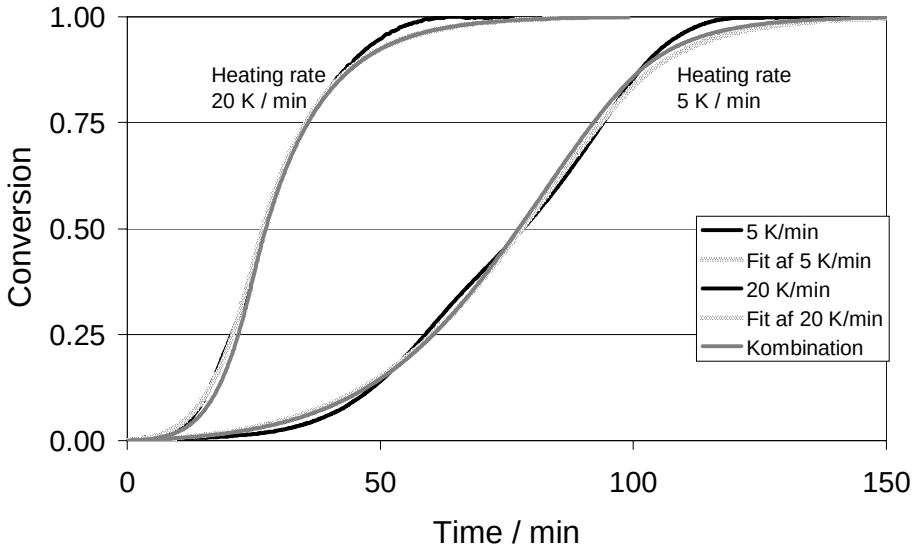

Figure 5. Experimental data and fitted model for *Chinese 2* coke at 20% CO_2.

Table 5. Parameters in the reaction model for the three cokes

Coke	n	E_a / $\frac{\text{kJ}}{\text{mole}}$	k_0 / $(\text{atm}^n\text{s})^{-1}$
Euro 2	1.11 ± 0.33	200 ± 0.3	$(1.59 \pm 0.1) \cdot 10^7$
Euro 3	0.79 ± 0.35	161 ± 0.2	$(3.32 \pm 0.5) \cdot 10^4$
Chinese 2	0.97 ± 0.32	146 ± 0.1	$(1.54 \pm 0.4) \cdot 10^5$

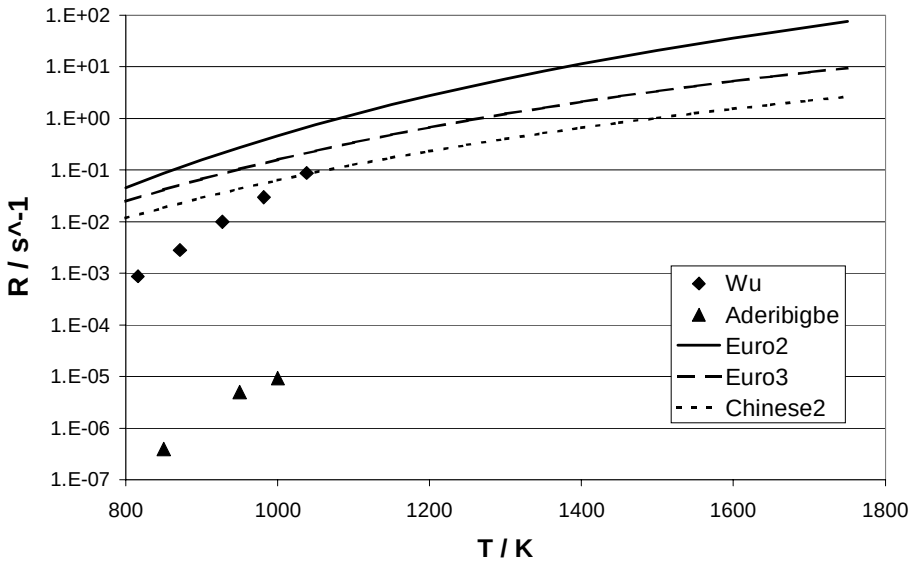

Figure 6. Comparison of reactivity at $p_{CO_2} = 0.20$atm found in this work (extrapolated beyond the temperature range were it was measured, 1073K - 1573K) and results from the literature. (Wu's results are extracted from Aderibigbe and Szekely [3])

to by Aderibigbe and Szekely[3]. However the apparent slope of the measured points of Aderibigbe and Szekely[3] is steeper than the apparent slope of the reactivities of this work. The reactivities found in this work are higher than what is found in literature. However, the activation energies found in this work is lower than those reported, Aderibigbe and Szekely[3] and Wu.

The difference between the results of this work and the work Aderibigbe and Szekely[3] and of Wu may be explained by particle size or temperature range. The results of this work were extrapolated beyond the temperature interval of the measurement to compare it to literature data and it may not valid to do so, and thus conclusion based on the comparison should be drawn with caution.

The influence of CO in the gas phase on the reactivity towards CO_2 was also investigated for the three cokes *Euro 2* and *3* and *Chinese 2*. The investigations showed that the CO concentration had little effect on the reaction rate. Figure 7 shows the conversion curves for *Euro 2* that was most sensitive to the CO concentration. The delay for full conversion compared to the 0% CO case is approximately the same for both 5% and 15% CO in the gas. The delay is approximately 4min of the total reaction time of more than 50min. The influence of CO in the gas phase on the two other cokes *Euro 3* and *Chinese 2* is even less obvious.

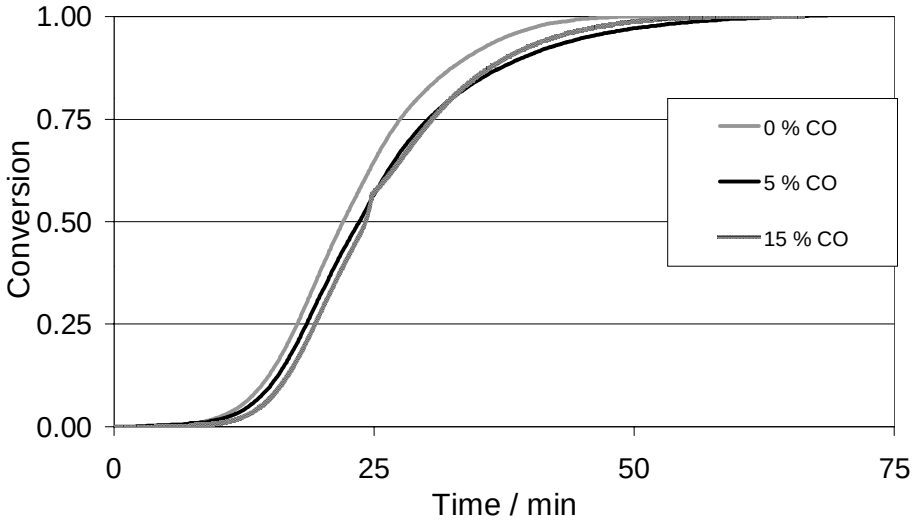

Figure 7. Conversion curves for *Euro 2* at a heating rate of 20K/min and with 20% CO_2 and varying amounts of CO in the atmosphere.

Coke Reactivity Impact on Cupola Operation

In this section the impact of different coke reactivities on cupola operation is investigated using a mathematical model of a cupola used for stone wool manufacturing. The model is developed by Leth-Miller et al.[22]. The cupola furnace is a vertical shaft furnace with water cooled walls that is fed with raw materials (rocks, briquettes, etc.) and coke at the top, and air for combustion of the coke is blasted through tuyeres at the bottom of the cupola. Simulations have been made with two different types of coke, where the most reactive has double the reactivity of reactions with CO_2 and O_2 as the least reactive. To sustain the same temperature of the melt it was necessary to increase the coke content from 13.5% of the charge to 17% when the most reactive coke was replaced with the least reactive. Thus the simulations shows that approximately 25% more coke is needed if the reactivity of a coke towards CO_2 and O_2 is halved. This indicates the importance of the coke reactivity.

Figure 8 shows that the gas temperature for the highly reactive coke has a more narrow peak than the profile for the less reactive coke, and that the temperature of the gas close to the bottom is higher in the case of the highly reactive coke. The higher temperature at the bottom assures that the melt leaves the cupola at a higher temperature.

These results contradicts the old perception in ROCKWOOL® that a less reactive

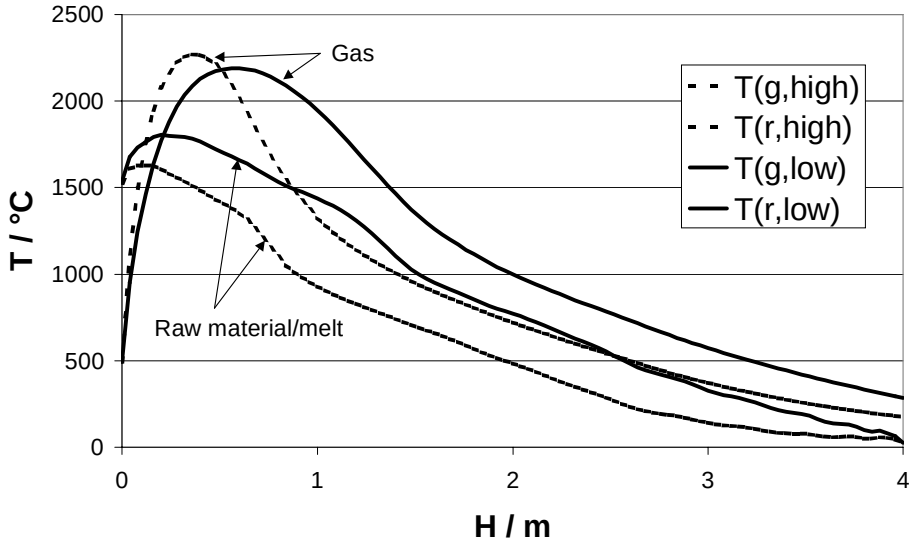

Figure 8. Temperature profiles in the cupola with a high and a low reactive coke. $H = 0$ is at the bottom of the cupola, and $H = 4$m is at the top.

coke would produce less CO and thus the loss would be smaller and less coke was needed. However, the present simulation indicate that with a more narrow gas temperature peak obtained with reactive coke less heat is lost to the cooling water, and thus coke can be saved.

Thus these simulations result indicate the potential significance of obtaining proper information about coke reactivity for a specific application.

Discussion

It is characteristic that the cokes which have been baked for longer time are more dense and have a lower reactivity. The results found are also in good agreement with results found in literature. The measured surface areas surprisingly show that the least reactive coke has the highest surface area, however, the difference is not extreme, and the results thus show that the surface area is not the key factor determining the reactivity. The directly measured porosities of the cokes was slightly low indicating that there are pores that are not connected with the outer surface.

For the cupola operation the coke reactivity plays an important role for both the combustion and especially the CO formation. The simple interpretation is

that the more reactive the coke is the more CO will be formed. However, since the combustion is also affected the temperature profile in the cupola is changed and thereby the conditions for CO formation are also changed. In stone wool production the more efficient combustion with the most reactive cokes makes it possible to reduce the coke consumption and the CO emissions. The foundrys may benefit in a similar way from this knowledge.

A fast and cheap screening of coke reactivity can be done with the TGA. The results needed for decisions regarding cupola operation need not necessarily be quantitative. The results shown in figure 3 are for most purposes sufficient, since it ranks the cokes after reactivity. The ranking also strongly indicates which cokes are the most porous and which are the most dense.

Conclusion

Seven commercial cokes have been investigated for reactivity towards CO_2 in the temperature range 1073K - 1573K.

There are clear differences between Western European cokes (*Euro 1, 2, 4* and *5*), Eastern European coke (*Euro 3*) and Chinese cokes. The most reactive cokes are the Western European cokes (*Euro 1, 2, 4* and *5*) and the least reactive are the Chinese cokes. The Eastern European coke (*Euro 3*) has intermediate reactivity. The differences were explained with difference in baking time, with longer baking time leading to more dense graphite-like coke with lower reactivity.

Experiments with up till 15vol% CO showed that CO has negligible influence on the gasification rate.

Simulations with a cupola model shows that 25% more coke is needed for stone wool production if the coke type is changed to a type with half the reactivity towards O_2 and CO_2. The more reactive coke gives a higher temperature at the bottom of the cupola which assures that the melt leaves the cupola with a higher temperature and lower heat loss to the cooling water.

The results of this work show that there can be large differences in reactivity of different cokes, and the simulations indicate that there is significant impact of the coke reactivity on the cupola operation in stone wool production.

Acknowledgement

This work is part of the research programme of ROCKWOOL® International A/S in cooperation with CAPEC (Computer Aided Process Engineering Centre) and CHEC (Combustion and Harmful Emission Control) at the Department of Chemical Engineering, Technical University of Denmark. The project is funded by ROCKWOOL® and Erhvervsfremmestyrelsen (Danish Ministry of Business and Industry).

References

[1] R.H. Hafner. *Cupola Handbook*. American Foundrymen's Society, 5th ed. edition, 1984.

[2] N.M. Laurendeau. Heterogeneous kinetics of coal char gasification and combustion. *Progress in Energy and Combustion Science*, 4:221–270, 1978.

[3] D.A. Aderibigbe and J. Szekely. Studies in coke reactivity: Part 1 reaction of conventionally produced coke with CO-CO2 mixtures over temperature range 850°C - 1000°C. *Ironmaking and Steelmaking*, 1:11, 1981.

[4] J.A. Menéndez, R. Álvarez, and J.J. Pis. Determination of metallurgical coke reactivity at INCAR: NSC and ECE-INCAR reactivity tests. *Ironmaking and Steelmaking*, 26:117 – 121, 1999.

[5] J.J. Pis and A. Cagigas. *Rev. Metal, Madrid*, 22, (3):169 – 177, 1986.

[6] S.I. Pinchuk and A.V. Ostapchenko. *Coke Chem. USSR*, 2:59 – 62, 1978.

[7] J.J. Pis, A. Cagigas, P. Simon, and J.J. Lorenzana. *Fuel Proc. Technol.*, 20:307 – 316, 1988.

[8] J.A. Menéndez, R. Alverez, and J.J. Pis. Relationship between different methods of determination of coke reactivity (spanish). *Rev. Metal, Madrid*, 29, (4):214 – 222, 1993.

[9] A. Bernard, J.M. Duchéne, and D. Isler. *Rev. Métall., Cah. Inf. Tech., Dec*, pages 849 – 860, 1985.

[10] S. Okstad and A. Hoy. Proceding 2nd Conf. on 'Industrial Carbon and Graphite', Society of Chemical Industry, London, 1965.

[11] R.G. Squires P.C. Koenig and N.M. Laurendeau. Evidence of a two side model of char gasification by carbon monoxide. *Carbon*, 23(5):531–536, 1985.

[12] M. L. Hobbs, P. T. Radulovic, and L. D. Smoot. Combustion and gasification of coals in fixed-beds. *Prog. Energy Combustion Science*, 19:505 – 586, 1994.

[13] S.R. Turns. *An Introduction to Combustion*. McGraw & Hill, 1996.

[14] Y. Wanibe and T. Itoh. *New Quantitative Approach to Powder Technology*. John Wiley & Sons, 1998.

[15] W.E. White, C.H. Bartholomew, W.C. Hecker, and D.M. Smith. Changes in surface area, pore structure and density during fomation of high-temperature chars from representative U.S. coals. *Adsorption Science Technology*, 7:180–209, 1991.

[16] M. Stenseng and L.A. Hansen. Practical experience obtained using Netzsch STA 409 C, CHEC report no.9812, 1998.

[17] M. Ishida and C. Y. Wen. Comparison of zone-reaction model and unreacted-core shrinking model in solid-gas reactions - part I isothermal analysis. *Chemical Engineering Science*, 26:1031 – 1041, 1971.

[18] R. Fletcher. A modified marquardt subroutine for non-linear squares. *Harwell Report AERE R 6799*, 1971.

[19] R. Hurt, J.-K. Sun, and M. Lunden. A kinetic model of carbon burnout in pulverized coal combustion. *Combustion and Flame*, 113:181 – 197, 1998.

[20] A. Zolin, A. Jensen, and K. Dam-Johansen. Coupling thermal deactivation with oxidation for predicting the combustion of solid fuel. *Combustion and Flame*, 125:1341 – 1360, 2001.

[21] E. Chornet and C. Roy. Compensation effect in the thermal decomposition of cellulosic materials. *Thermochimica Acta*, 35:389–393, 1980.

[22] R. Leth-Miller, A. D. Jensen, P. Glarborg, S. B. Jørgensen, L.M. Jensen, and P.B. Hansen. Experimental investigation and mathematical modelling of a mineral melting cupola furnace. *Industrial and Engineering Chemistry Research (submitted)*, 2002.

Article III

Experimental Investigation and Mathematical Modelling of a Mineral Melting Cupola Furnace

R. Leth-Miller[1,2], A.D. Jensen[2], P. Glarborg[2], L.M. Jensen[1], P.B. Hansen[1], S.B. Jørgensen[2]

[1]Rockwool® International A/S, Denmark
[2]Department of Chemical Engineering, Technical University of Denmark
May 14, 2002

Abstract

Full scale measurements on a mineral melting cupola furnace for stone wool production have been made. The measurements include probe measurements of gas concentration, solid/liquid phase and gas temperature and melt composition at several vertical and radial positions in the cupola. A cupola has been quenched and the content fixed in concrete before it was cut open such that the position of the melting zone and other characteristics could be determined.

A mathematical model of a mineral melting cupola furnace for stone wool production has been developed for improving cupola operation. The 1-D, first engineering principle model includes mass and heat balances for the gas phase, five solid phases and four liquid phases. The gas and solid/liquid phases flow countercurrently. Seven chemical reactions account for conversion of coke, iron oxide, limestone and gaseous species. The heterogeneous reactions of coke conversion are limited by both kinetics and mass transport. Heat transfer between phases is modelled including both convection and radiation.

The model predicts gas concentration, mass flow rates and temperature profiles of solid, melt and gas in the cupola and the heat loss to the water cooled walls. Input to the model is the coke, rock and blast air properties and blast air amount and coke percentage in the charge. The unknown model parameters have been estimated based on input/output measurements. Comparison of model predicted and measured concentration and temperature profiles inside the cupola shows good agreement.

List of symbols

a	:	Specific surface area	m^2/m^3
A	:	Area	m^2
C	:	Concentration	$mole/m^3$
d	:	Diameter	m
D	:	Diffusion coefficient	m^2/s
f_c	:	Weight percentage of coke in the feed	
H	:	Height	m
j_D	:	Chilton-Colburn factor	
J	:	Jacobian	
k	:	Reaction rate constant	$mole^n/(m^3)^n/s$
k_m	:	Mass transfer coefficient	$mole/m^2/s$
l	:	Length	m
L	:	A characteristic length	m
m	:	Mass flow rate	kg/s
M	:	Molecular weight	$kg/mole$
N	:	Molar flow rate	$mole/s$
P	:	Pressure	Pa
q	:	Heat transfer	$\mathrm{J/m^3}$
r	:	radius	m
r	:	Rate of reaction	$mole/m^3/s$
R	:	Universal gas constant	$J/mole/K$
T	:	Temperature	K
v	:	Velocity	m/s
V	:	Volume	m^3
w	:	Dimensionless rate of reaction	
X	:	Mole fraction	
x	:	Dimension less molar flow rate	
z	:	Axial position	m
ε	:	Porosity	
ϵ	:	Emissivity	
ζ	:	Dimensionless axial position	
μ	:	Viscosity	$kg/m/s$
ρ	:	Density	kg/m^3
υ	:	Reaction coefficient	
Φ	:	Dimensionless pressure	
Θ	:	Dimensionless temperature	

Bold face characters denotes either vectors or matrices.

Subscripts

A	:	Species A
b	:	Bulk
c	:	Coke
f	:	Furnace
g	:	Gas
M	:	Mass based
p	:	Particle
r	:	Rocks
ref	:	Reference
s	:	Property at surface

Dimensionless Numbers

$Da = \frac{r(C_0)L}{V_g C_0}$	:	Damköhler number. Chemical reaction.
$Nu = \frac{hL}{k}$	:	Nusselt's number. Heat transfer.
$Pr = \frac{c\mu}{k}$	:	Prandtl's number. Heat capacity.
$Re = \frac{\rho v L}{\mu}$	:	Reynold's number. Velocity.
$Sc = \frac{\mu}{\rho D}$	:	Schmidt's number. Diffusivity.
$Sh = \frac{k_m L}{D}$	:	Sherwood's number. Mass transport

where L is a characteristic length. For particles the characteristic length is the diameter, d_p. For furnace it is the diameter, d_f.

Introduction

Production of stone wool products involves melting rock materials and subsequent spinning of the melt to fibers (wool). The melting of the rocks is usually carried out in a cupola furnace. Cupolas are widely used in the foundry industry and cupola models have previously been developed. However, the focus of previous cupola model developments have aimed at foundry related problems which are different from those of stone wool production. Stanek *et al.* (1–10) developed a steady state 1-D model that includes heat and mass balances. A primary aim of this model is to predict the composition of the melt leaving the cupola. The composition of the melt from a foundry cupola is much more complex than the composition of melt in a stone wool cupola, since few chemical reactions take place in the melt of a stone wool cupola. On the other hand stone wool production requires an accurate prediction of the melt temperature, and this is not possible with the model of Stanek *et al.* (1) where radiation is neglected.

A 3-D model of a foundry cupola has also been developed (11). Predictions with this model compares favourably with reported experimental data of gas

composition and gas temperature. However, 3-D CFD calculations are computationally expensive, and systematic calibration of the model may be virtually impossible. Also it may be necessary to make several simplifications and assumptions not necessary in a 1-D model. Selection of the number of spatial dimensions is of course closely linked to the aim of the model. Based on the 3-D model Viswanathan *et al.* (11) conclude that the gas is in plug flow from 300mm above the tuyeres and upwards. This conclusion is the basis for the 1-D assumption made for the model developed in this work.

Models of blast furnaces, which are similar to cupolas, have also been developed (12–15). The models are focused on on-line control of different aspects of the blast furnace. Among the models are a simple distributed model (12), a state-space model (13), a model for prediction of slag viscosity using neural networks (14) and an expert system for on-line diagnoses of blast furnace conditions (15). The models were developed based on extensive experimental data that qualitatively can be used to assess the experiments that have been performed on stone wool cupolas. The experimental data include probe measurements of the temperature and gas composition inside a blast furnace.

Not many experimental investigations of the conditions inside cupolas have previously been reported, probably due to the harsh environment of high temperature and particles. Measurements in foundry cupolas have been reported (11; 16; 17). The results of these measurements are not directly comparable to stone wool cupola operation because the CO concentration is higher in the foundry cupolas, the properties of the iron charged in foundry cupolas are different from the rocks used in stone wool cupolas. The information provided by these investigations does, however, provide indications of the conditions in a stone wool cupola. Experimental data for fixed bed coal gasifiers, referred by (18), can also be used for qualitative comparison with stone wool cupola measurements.

In stone wool cupolas the reduction of iron oxides to metallic iron is unwanted opposite in the foundry cupolas. The location and mechanism of reduction of iron oxides in the raw materials are not well known in a cupolas. Mass transport of FeO in foundry slag is reported to be rate controlling (19–22) while others found that the reduction of iron oxide with CO at the slag-gas interface was rate controlling (23). Yet other authors report that the CO formation rate in the Boudouard reaction ($C(s) + CO_2(g) \rightarrow 2CO(g)$) is rate controlling (24). In any of the proposed mechanisms the iron reduction can not take place until it has melted, i.e. in the lower first meter of the cupola and in the melt bath.

The aim of this work is through experimental work and mathematical modelling to obtain new insights about the conditions inside the cupolas used for stone wool production, and thereby to develop a tool that can be used for optimisation of the operation, for trouble shooting and for predicting the impact of opera-

tional changes, such as the introduction of new raw materials in the process. The thermal efficiency of stone wool cupolas is only approximately 50%, i.e. approximately 50% of the heat released from combustion of the coke is used for heating and melting the rocks while the rest is lost to the surroundings, mainly to the cooling water and as CO in the flue gas. Thus there is a large potential for improvement of the energy efficiency of the cupola.

To achieve the goals of this work an elaborate set of experimental investigations were carried out both of the coke and raw materials properties and on full scale operating cupolas. The latter experiments are reported after the mineral melting cupola has been described. Subsequently development of a mathematical model of a mineral melting cupola is presented together with the procedure applied for its solution. Finally the model is calibrated to experimental input/output data and the model predictions of internal conditions are validated against the obtained experimental data.

Process Description

A cupola furnace for melting rocks is a vertical shaft furnace, $4-6$m tall, with a circular cross section with a diameter of $1-2.5$m (cupolas in the foundry industry are often larger), see figure 1. Preheated air is blasted through a number of tuyeres (4 to 20) at the bottom of the furnace and coke and raw materials (rocks, briquettes, limestone) are fed from the top. The coke burns at the bottom of the furnace and the combustion proceeds until oxygen is consumed approximately 0.5m above the tuyeres. The hot combustion products flow upwards through the cupola heating the raw materials and coke which move down during operation. Melting of the rocks takes place in a zone about $0.5-1$m above the tuyeres (the melting zone), and the melt is collected in a melt bath. The level in the melt bath is maintained by a simple siphon. The furnace is made of steel and is cooled with water in a cooling jacket to prevent that the steel melts. Evaporation of the cooling water in the jacket circulates the cooling water from the jacket to a tank above the cupola. Steam leaves at the top of the jacket and water from the tank comes into the jacket at the bottom. The cupola operates at a pressure of approximately 10kPa overpressure at tuyere level and a slight underpressure at the top.

Coke is a fuel made through pyrolysis of coal at high temperatures ($\approx 1000^o$C) for several days. The remaining char contains only very little volatiles (25). The coke used in stone wool cupolas is foundry coke, i.e. with an average diameter of ≈ 200mm. The coke contains typically between 3 and 15% ash.

The raw materials fed to a mineral melting cupola can be rocks, briquettes and limestone. The rocks are typically formed in volcanos and could be diabase,

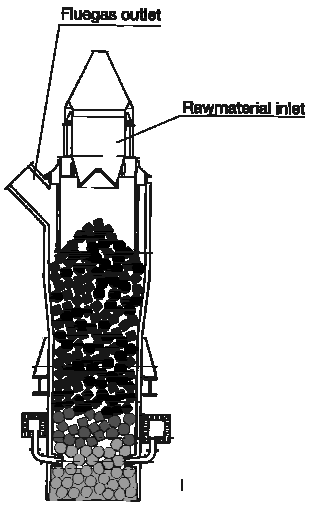

Figure 1. Cupola furnace.

gabbro or basalt. The briquettes are made of various minerals as e.g. olivine or basalt, diabase and gabbro. Waste stone wool can also be recycled in the briquettes. The limestone is mostly added to adjust the viscosity of the melt to the requirements of the spinning process. The raw material particles typically have an average diameter of $50 - 150$mm.

Approximately 30% of the iron oxides in the minerals are reduced to metallic iron in the cupola. The metallic iron sinks to the bottom of the melt bath, where it accumulates and must be tapped off before the iron level reaches the siphon. The iron reduction is an undesired reaction since metallic iron is a waste of material and the production must be stopped two or three times a day for iron tapping.

In order to develop and calibrate reliable first engineering principle based mathematical models for mineral melting cupolas it is necessary to obtain information about the behaviour of the cupola and their internal condition. To obtain such information a detailed experimental plan was developed. The results from these experiments are reported next.

Experimental

In this section four experiments are described that aim at measuring the internal cupola state. Also measurements of the inputs and outputs of the cupola are

also described. The results of the measurements provide new useful information about the cupolas and they will be used for model calibration and model validation.

Gas concentration, melt composition, gas and solid/liquid temperatures are explored using several different probes. Two types of probes have been used; a set of probes inserted horizontally through the wall (wall probes) and probes inserted vertically from the top of the cupola. The location of the melting zone in the inside of cupola is explored through quenching of an operating cupola using nitrogen. Melt sample collection through the tuyeres and at the siphon outlet is conducted to determine the location of the iron reduction. The full scale experiments have been made on ROCKWOOL® cupolas.

Wall Probes

The gas concentration, melt composition and solid/liquid temperature in the hot part of an operating cupola was measured using wall probes located from 300 to 900mm above the tuyeres.

Procedure

To perform a measurement, the probe is placed on a stand and driven horizontally into the cupola with an electrical motor. The probe is then left in the cupola for 1-2min while the samples are collected. A picture of the three types of probes is shown in figure 2. The gas probe is a steel tube with a tip welded to the end of the pipe, and with a hole on the bottom side close to the tip. The temperature probe is a steel tube connected to a IR- pyrometer. At the end of the probe a loose tip is attached with adhesive tape before a trial. The melt sample probe is a solid rod with three pockets on the top side distributed along the length of the probe. Stone wool cupolas operates at a slight overpressure so when the gates in the wall are opened sparks, hot gas and molten rocks are blown out of the cupola. A ceramic insulation material is wrapped around the tip of the probe. The insulation is fixed in a clamp shell where it remains when the probe is pushed into the cupola. In this way sparks and hot gases are avoided in the working area outside the cupola.

Five gates were installed on the cupola. Each gate consists of a pipe open directly at the cupola inner wall and closed at the outside by a ball valve. Gate 1 was positioned 300mm above the tuyeres, and gate 2,3,4 and 5 were positioned with 150mm interval. Gate 1 was blocked with melt after two probings, so only gas concentrations were measured at this position. The gate was attempted

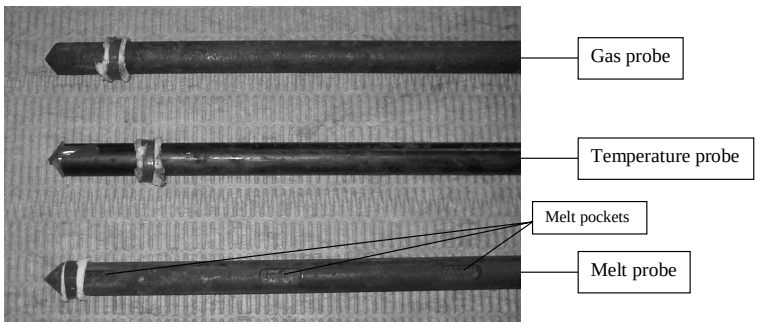

Figure 2. Probes used to measure gas concentration, temperature and melt composition in the cupola.

cleared, but when a small hole was opened with an air hammer, the hot gas from the inside of the cupola heated the pipe in the gate enabling the melt to flow further out in the pipe and eventually damage the ball valve so that the gate had to be blocked with clay.

The gas measurements are made at three radial positions: at the wall, half radial position and at the centre of the cupola. The gas sample is sucked out through the hole in the tip of the probe by a pump. The gas was lead from the probe to the pump in an ordinary plastic tube, and collected in a plastic bag. The composition was subsequently measured offline. Before collecting the gas at each position the system was ventilated to avoid interference with the gas that was already in the tube and probe before the probe was positioned.

The melt sample probe is driven to the centre immediately and left there for approximately 60sec. Then it is pulled out. Melt is collected in three pockets. Melt will of course also be collected in the pockets as the probe is moving in or out, but the time that the probe is moving is in total less than 5sec, so the disturbance of that is expected to be negligible. At some trials empty pockets were observed. This was probably because of the presence of a coke particle just above the pocket in the cupola.

Initially the temperature probe is driven past the centre of the cupola, then pulled back to the centre. On the way back the loose tip (the adhesive tape melts or burns once it comes into the cupola) falls off and the temperature can be measured with the IR-pyrometer that receives photons through the 1.8m tube. The tip is lost at each measurement and must be replaced. After the measurement at the centre the probe is moved to the two other radial positions for additional measurements. When the tip falls off nitrogen is blown through the probe to maintain a clear view. The IR-pyrometer is designed to measure surface temperatures, i.e. the temperatures measured are the temperatures of coke, rocks and melt. There is, however, no way of telling from which phase or

phases that the IR-pyrometer receives photons. The reading on the display was oscillating a lot ($\pm 50^o$C) during the measurements and an average was manually determined.

Results

Gas Concentrations
Figure 3 shows the results of the CO concentration measurements made at the centre of the cupola plotted against vertical position. The measurements were made on several days. The concentration is less than 1% at 300mm above the tuyeres and then increases to between 5% and 15%. The measurements are very scattered even though the cupola operation is not changed very much between the measurements on the individual days. The concentrations of O_2 and CO_2 are not shown because the conclusions are made primarily based on the CO concentration.

For clarity the average of the CO concentration measurements at each position was calculated. Figure 4 shows these results as function of vertical position at the wall, half way at the centre and at the centre. The reaction between CO and oxygen is very fast at high temperatures, hence CO and oxygen can not co-exist in the hot part of the cupola if perfect mixing is assumed. The CO concentration is therefore most likely zero until the oxygen has been consumed. Reactions in the probe may disturb the measurements, i.e. CO and oxygen that may be present due to non-ideal mixing may react in the probe. Above the position where all oxygen is consumed the CO concentration increases due to gasification. At gate 1, 300mm above the tuyeres, the CO concentration is close to 0% indicating that the oxygen level has just dropped to 0%. At gates 4 and 5 the results indicate that the gasification rate is significantly reduced, probably caused by the drop in temperature. Figure 4 shows that the concentration of CO rises faster at the centre than towards the wall indicating that the gasification of coke is fastest at the centre. The difference in gasification rate between the wall and the centre is probably caused by the lower temperature at the water cooled wall.

Temperature Profiles
Figure 5 shows the average temperature profiles. The temperature is between 1400^oC and 1650^oC 450mm above the tuyeres and then decreases upwards through the cupola. 900mm above the tuyeres it is between 1250^oC and 1400^oC. There are two points in the plot that deviate from the expected behaviour. At gates 4 and 5 (750 and 900mm above the tuyeres) the temperature is rising at the wall. Also it is surprising that the temperature is lower at the centre than half way to the centre. There is no obvious explanation for this behaviour. However, two factors can be suggested to cause these observations

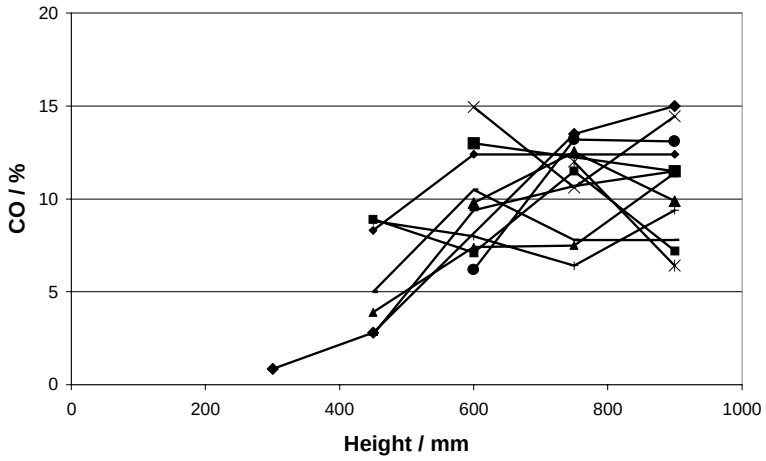

Figure 3. CO profile at the centre of the cupola measured with the probes.

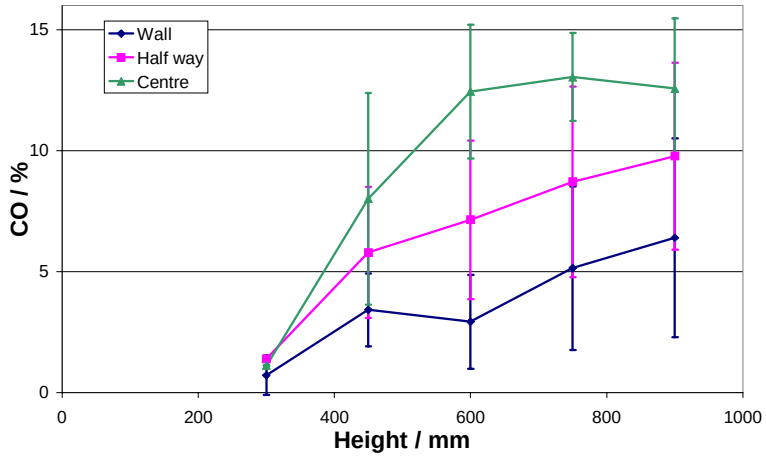

Figure 4. Average CO profile measured with the probes. (Vertical bars indicate the standard deviation of the measurement.)

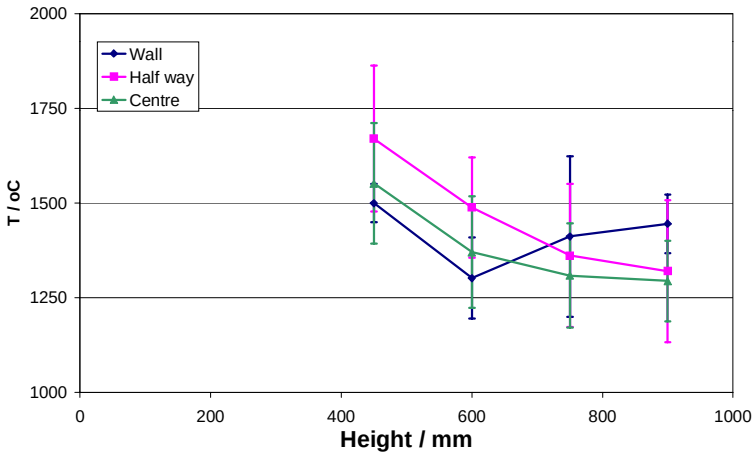

Figure 5. Temperature profile measured with the probes. (Vertical bars indicate the standard deviation of the measurement.)

1. High rate of gasification of coke due to less oxygen at the centre take up energy and thereby lowering the temperature

2. High melting rate at the centre gives a faster movement of new colder raw materials down through the cupola

For all the measurements there were large variances or disturbances. The difficulty of obtaining reliable temperature measurements using the wall probes can be associated with the fluctuations in the temperature reading which indicates presence of high frequency noise. To account for this a reliable filtering procedure should have been adopted rather than attempting to average visually. The plots show only an average of the measurements, which is a crude way to treat the data, since the precise conditions of the operation were not identical during all the measurements. The operation changed mostly in terms of melting rate, i.e. the charge composition was relatively unchanged, but blast air flow rate changes. Changes were only made to account for higher or lower rates of production and for moisture variations in the coke, i.e. more (or less) coke is needed. Nevertheless, the average values presented here still provide valuable information.

The melt samples showed that the melting zone extends as far up as above 900mm above the tuyeres, but the probes can not determine at which height all the raw materials have melted. The melt composition results are described in the following section.

Iron Reduction

Part of the minerals charged to the cupola is iron oxides, which are present in the different raw materials. The iron oxide content is important for the properties of the stone wool product because it provides fire resistance to the wool. In the cupola approximately 30% of the iron oxides are reduced to metallic iron. The metallic iron is immiscible with the glass melt and the metallic iron sinks to the bottom of the melt bath at the bottom of the cupola. As a result the level of the iron in the melt bath increases during the operation and must be tapped out of the bottom of the cupola before the iron level reaches the outlet.

As a first step towards understanding the iron reduction, which is a premise of avoiding or reducing it, melt samples were taken out through the tuyeres and from the siphon. The chemical compositions of the samples were analysed using a magnet for determining the content of metallic iron and X-ray analysis for the remaining composition. Melt samples from the probe measurements described above were also analysed. The values are averages over two samples for the siphon and the tuyere samples. The results for the probes are averages of analyses of six samples, two at each of three radial positions that the melt samples are collected in each probe. The results of the analyses are shown in table 1.

The analyses show that the composition of the samples from the tuyeres and from the siphon are similar when the metallic iron is removed from the tuyere sample. A slightly higher content of SiO_2 and FeO was found in the tuyere sample while the Al_2O_3 was a little lower. The reason for the observed differences may be that the melt has not been well mixed above the melt bath but also that iron reduction take place in the melt bath. However, it appears that most of the iron reduction occurs above melt bath.

The compositions of the melt samples taken with the probes show that some metallic iron has been formed at all the positions. The amount is, however, only slightly above that in the siphon, except for probe 5. The high content of free iron in the sample from probe 5 was actually only found in one of the five samples (not six since one of the pockets was empty after one of the probings), while the remaining values were below 1. It is most likely that the one measurement with the extremely high content is an unsuccessful measurement since it was only seen once. This means that the major part of the iron reduction probably occurs below 0.45m above the tuyeres, which is the lowest position that the wall probes were used at for collecting melt samples.

The conclusion from these measurements is that the iron reduction happens from the melt bath and approximately 0.5m up. Reduction above 0.5m above the tuyeres can be neglected and the iron reduction in the melt bath is limited

Table 1. Chemical composition (in w/w%) of the melt samples collected to investigate the iron reduction. The probe samples are from another cupola than the tuyere and siphon sample. The Gate position above the tuyeres are: 2: 450mm, 3: 600mm, 4: 750mm and 5: 900mm above the tuyeres.

		Composition excluding the free iron									
Sample	Fe	SiO_2	Al_2O_3	TiO_2	FeO	CaO	MgO	Na_2O	K_2O	P_2O_5	MnO
Siphon	0.21	42.6	19.2	1.6	5.9	19.7	7.8	1.8	1.0	0.3	0.1
Tuyere	3.6	43.5	18.3	1.7	7.5	17.5	7.7	2.0	1.0	0.5	0.1
Gate 2	0.4	40.2	18.2	1.6	10.4	18.4	7.4	1.9	1.3	0.4	0.1
Gate 3	0.7	40.5	18.0	1.6	9.4	19.3	7.4	1.9	1.4	0.5	0.1
Gate 4	0.6	37.5	17.1	1.5	15.1	18.0	6.7	2.0	1.5	0.5	0.1
Gate 5	7.2	42.0	20.6	1.8	3.9	20.1	7.3	2.1	1.6	0.5	0.1

and can probably be neglected. The results are surprising since the reduction was expected to depend on the oxygen and CO concentration in the gas phase. The iron reduction was expected to be largest in a zone with high CO concentration and low O_2 concentration, but the measurements show the opposite. This indicates that the mechanism of the iron reduction in stone wool cupolas involves reaction of the molten iron oxide with the coke surface, which is the only reducing reactant in the zone from the tuyeres and 0.5m up.

Top Probes

Procedure

In addition to the wall probes the temperature has also been measured using a six meter long steel probe that is inserted from the top of the cupola a little into the rocks and coke packing. Then the burden of the charge pulls the probe with a thermocouple inside down. The probe cannot be pulled out again, and simply melts in the cupola. The thermocouple is pulled out as the temperature comes near to the upper limit of the thermocouple ($\approx 1500^o$C) and the measurements stop.

As the probe moves down the temperature is logged as function of the position of the probe. The measured temperature is that of the gas since the thermocouple is not in physical contact with the solid materials and it is well shielded from radiation by the pipe.

The top probe is inserted near the wall, i.e. less than 300mm from the wall (cupola diameter was 1.8m). The results are thereby to some extent affected by the water cooled wall. The precise location of the probe tip can not be determinated since it is the charge that pulls the probe down through the cupola, and the flow pattern of the charge is not known.

Measurements above the melting point temperature of the steel probe ($\approx 1000^o$C) should be interpreted with caution, because some of the pipe may have melted and the determination of the position of the thermocouple is not very precise.

Results

The temperature profiles are shown in figure 6 for two experiments on the same cupola. The temperature profiles show that 1m above the tuyeres the temperature is approximately 1300^oC. The temperature then decreases almost linearly to approximately 150^oC at the top of the cupola. There is a little difference between the two measured profiles, since the operation conditions were not changed, and the difference is probably due to the different paths that the probes have taken down through the cupola. The temperature profiles obtained with the wall probes are also plotted in figure 6. The temperature profiles of the different probes are in qualitative agreement, but the wall and top probes were used on different cupolas and the temperatures obtained with the wall probes are for solid/liquid phase, so the temperature measurements are not immediately comparable.

Quenching a Cupola

Given the high temperatures and the tight packing of the coke and rocks it is difficult to get an overview of the properties inside the cupola in terms of e.g. bulk density and location of melting zone. Therefore an operating cupola was quenched to obtain such an overview.

Procedure

The quenching of the cupola was carried out by interrupting the blast air and injecting nitrogen to stop the combustion and other chemical reactions and to cool the furnace. The nitrogen was injected from the top of the cupola to avoid that the nitrogen picks up heat from the melt bath and then keeps melting the rocks even after the combustion is stopped. Just before the quenching

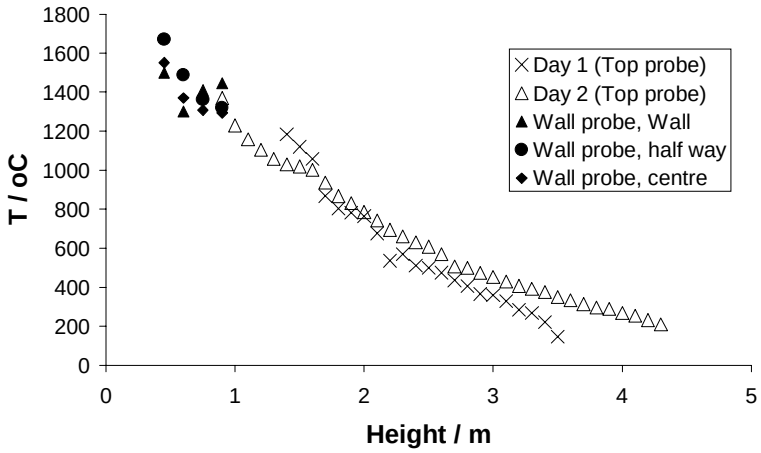

Figure 6. Gas temperature profiles measured two different days with the top probe and the temperature profiles obtained with the wall probes.

the cupola was tapped for all iron and melt in the melt bath and the hole in the bottom was used as outlet for the nitrogen. The injection of nitrogen was continued until the temperature in all regions in the cupola was below the self ignition temperature of the coke (600°C). Then the cupola was left for a couple of weeks until it reached ambient temperature. The void in the cupola was then filled with cement and when the cement had cured and dried the big lump was cut open to give a picture of the state inside the operating cupola. The quenched cupola was charged with basalt, briquettes and coke the period before the quenching.

Results

The results (displayed in figure 7) show that the melting zone is located slightly higher near the tuyeres than closer to the centre. The extent of the melting zone is not distinctively related to the position, i.e. near the wall or the centre. The briquettes melt over an interval of 350mm; from 400mm to 750mm above the tuyeres and the basalt over an interval of 250mm; from 450mm to 700mm above the tuyeres. Figure 8 shows an example of a basalt rock in the melting process. A droplet has been frozen just before it drips off and is captured in the concrete. Another indication of melting is when the surface edges are not sharp and bubbles are present.

There is evidence of an iron build-up in the bottom (i.e. in the melt bath) of the furnace caused by iron that has solidified during the week of production and never melted again, and thus it makes the melt bath volume smaller, which

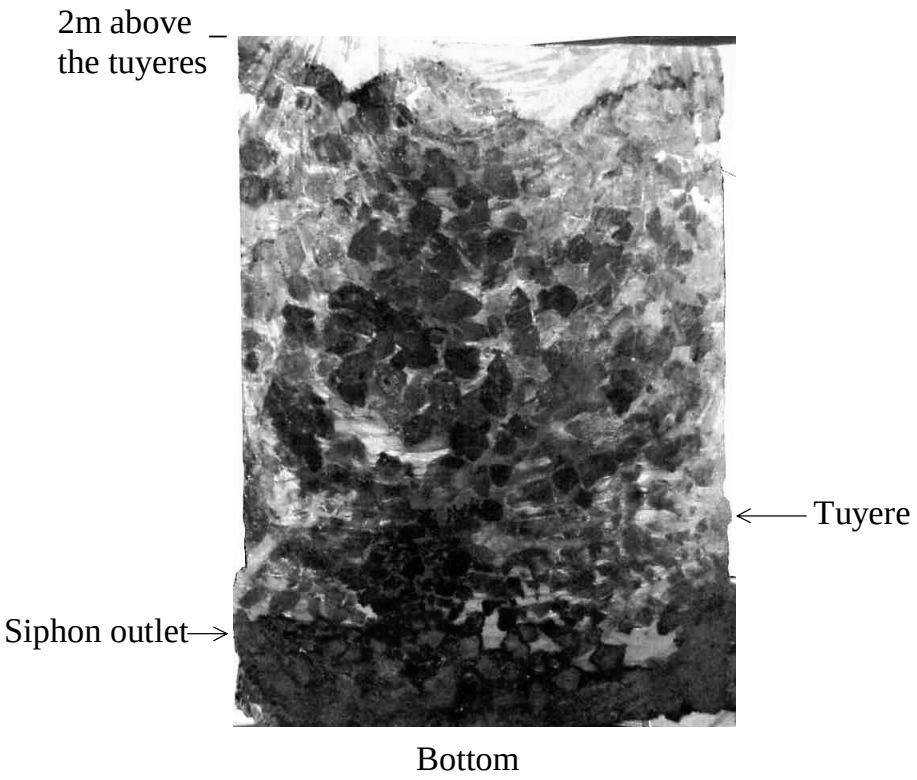

Figure 7. Cross section of the open quenched cupola. (Picture height and width are 2.5m and 1.8m.)

necessitates more frequent tappings. The build-up is lowest near the tapping holes and highest furthest away.

The melt zone is located a little higher near the wall than closer to the centre. This is surprising since it was expected that the furnace was hottest at the centre furthest away from the water cooled wall. The extent of the melt zone is thus apparently not dependent of the radial position (i.e. whether at the wall or at the centre).

An impression of the bulk porosity of an operating cupola can be retrieved from the cross section of the quenched cupola. The bulk porosity was before the quenching was estimated to be $0.4 - 0.5$, which the picture in figure 7 supports. The picture has not been systematically analysed, e.g. by image analysis, so here it can only be concluded there is no apparent contradiction between the perception of the bulk porosity before and after the quenching.

The interpretation of the quenching experiment should be taken with some

Figure 8. Basalt droplet captured in the quenched cupola. (The total width of the picture is 70mm.)

caution, since the quenching did not happen instantaneously. It took at least 15min before the nitrogen injection was working properly, and after this all melt was of course not frozen instantaneously. In this period part of the melt may have escaped to the melt bath and the visible cross section is then not the true image concerning the melted fraction in the operating cupola.

Measured Input/Output data

Some of the input to and standard output from the cupola have been measured at several occasions in connection with development projects in ROCKWOOL®. The input parameters include the amount and type of coke and raw materials charged and the amount and properties of the blast air. The output data are the temperature of melt, the temperature of flue gas, CO content in flue gas and cooling water loss. To determine the CO concentration in the flue gas the O_2 concentration must also be measured to determine the amount of false air that dilutes the flue gas. The gas concentrations are measured with an IR analyzer for CO_2 and CO and the O_2 was measured in a chemical cell. The flue gas

temperature is measured with an ordinary thermocouple. The temperature of the melt is regularly measured manually with a thermocouple that is put into the melt jet as it leaves the siphon. The cooling water loss (i.e. the amount of water evaporated from the cooling water tank) is not measured continuously, but can be measured manually in terms of how much water is filled into the cooling water tank.

The above input/output data from full scale cupola operation have been collected, and are used in this work for calibrating the cupola model.

The uncertainty of the measurements are estimated as follows , based on many years of experience

- Melt temperature: $\pm 20^o$C of $\approx 1500^o$C
- Flue gas temperature: $\pm 2^o$C of $\approx 150^o$C
- CO in the flue gas: $\pm 0.5\%$ of $\approx 5\%$
- Cooling water loss: $\pm 0.1 \mathrm{m}^3/\mathrm{h}$ of $\approx 4 \mathrm{m}^3/\mathrm{h}$

The melt temperature is difficult to measure, because the surface cools when the melt leaves the siphon. The melt is very black and thus there is almost only heat radiation loss from the surface and not from deeper in the melt. This results in large temperature gradients, hence the value read from the instrument is very dependent of where in the melt the thermocouple is placed.

The flue gas temperature is between 100^oC and 200^oC, which is a temperature range where the temperature can be measured very precisely. However, the temperature is measured in a relatively large duct, so flow profile and heat loss can affect the precision of the measurement. Also false air will disturb the temperature measurement. Measurement of the CO concentration in the flue gas is also disturbed by false air.

The precision of the cooling water loss measurement is affected by the heat loss from the pipes and tanks etc. in the cooling water system. The heat loss from the surfaces has been estimated using heat transfer correlations from (26), and it was found that approximately 1% was lost this way. The cooling water tank is filled to a high level when the water level is low. For this reason the level in the tank should be noted at the beginning and end of a measurement, which was not done. Only the total amount of new water filled into the tank was registered. The measurements usually goes on for more than six hours and the meter indicating how much water has been filled to the cooling water tank is controlled regularly (e.g. once per hour), and the average is then found.

It is seldom possible to make the energy balance fit from the measurements. Typically the energy measured in the output streams is less than the energy supply in the coke and the hot blast air. The reason for the discrepancy is not clear, but may partly be attributed to by the uncertainty in the blast air flow rate. This value affects the calculated energy in the flue gas, both thermal and in CO. Other errors sources include the leaks in the system that are known to exist (the O_2 measurements can only discover leaks in positions with under pressure).

Discussion of Experimental Results

The experiments performed to map the conditions inside a mineral melting cupola furnace described in this section have provided much new information. The concentration and temperature profiles inside the cupola have been measured, the location of the melt zone has been determined and the location of the iron reduction has been indicated. These results provide a better understanding of cupola operation, and later in this paper the obtained experimental results are used to validate the model presented in the next section.

The wall and top probe measurements show behaviour similar to those of foundry cupolas, blast furnaces and fixed bed coal gasifiers. The measurements of (11; 16–18) show that oxygen is rapidly consumed followed by an increase in the CO concentration to a steady level when the temperature has decreased so much that the gasification reactions have virtually stopped. Also the temperature profiles found in gasifiers, blast furnaces and foundry cupolas qualitatively compares with the profiles found in this work.

The location of the melting zone has been indicated by both the wall probes and the quenching experiment. There is qualitative agreement, but quantitative difference between the two experiments, since the quenching indicates that the melting zone lies below 750mm above the tuyeres, while melt was collected in the wall probes 900mm above the tuyeres. The two experiments were made on different cupolas, so different operation conditions could explain the difference. It is also likely that the position of the melting zone in the quenched cupola has moved somewhat down either during the tapping or during the time when the nitrogen injection did not work properly or both.

Overall, valuable information has been obtained through this experimental programme. This information provides a quantitative basis for the development of a mathematical model and subsequent calibration and validation of the model. The model development is described next.

Model

The mathematical model of the cupola furnace developed is a static 1-D model, i.e. the properties in any cross section are assumed constant, and the variations are limited to the vertical direction. The model is based on process knowledge, i.e. it is a first engineering principles model. The model is based on a number of assumptions whereof the most important are listed in table 2. Assumptions are necessary because of the complex, heterogeneous chemical and physical nature of coal prohibits the development of a truly molecular scale model of fixed bed gasification (18). Both coke and mineral materials are also complex and heterogeneous hence the cupola can also not be modelled truly on a molecular scale.

The development of the model has focused on more detailed descriptions of the chemistry and mass and heat exchange mechanisms rather than on spatial dimensions. Three dimensions and detailed chemistry are not yet an option, but the development in CFD tools and computer hardware seems to make such combination possible within relative near future.

In the following sections the different parts of the model are presented. First the balance equations are presented, then the constitutive equations and correlations. In the subsequent solution of the equations the constitutive equations are substituted into the balance equations.

The model can handle one coke type and four different types of raw materials (rocks) in each simulation, i.e. the model calculates mass and energy balance for four rocks with independent physical properties. The fractions in the charge are defined as

$$f_c = \frac{\dot{m}_c}{\dot{m}_c + \sum_i \dot{m}_{r_i}} \tag{1}$$

$$f_{r_j,s} = \frac{\dot{m}_{r_j,s}}{\sum_i \dot{m}_{r_i,s}} \tag{2}$$

Both the coke fraction and the raw material fractions are functions of position since the coke burns and the raw materials melts in the cupola. At the top of the cupola ($z = H_f$) the fractions are given as the charge composition.

In the model the pressure is assumed constant 1atm (assumption A.2). In the real cupola the pressure is approximately 1.1atm at the tuyeres and slightly under 1atm at the top. The pressure affects the concentrations that are used for computing the reaction rates. The rates should have been 10% higher at the bottom, but this is neglected and compensated by a higher mass transfer coefficient (this will be estimated in the *Calibration* section).

Table 2. Assumptions made during the mathematical model development.

A.1 Steady state

A.2 The pressure is assumed constant.

A.3 Ideal gas law applies.

Geometric assumptions

A.3 Radially homogeneous properties, i.e. 1-D assumption

A.4 The bulk porosity is constant

A.5 Heterogeneous reactions occur only on the outer surface of the coke

A.6 Coke particles are spherical

A.7 The coke particles do not disintegrate in any way

A.8 Raw material particles of each type are spherical

A.9 The raw material particles do not disintegrate in any way

A.10 All droplets are spherical

A.11 All droplets are the same size

Mass related assumptions

A.14 The vertical heat conduction and mass diffusion is negligible

A.15 Negligible axial mass dispersion

A.16 Net mass flow away from the reacting coke does not influence mass and heat transfer

A.17 The ash is assumed not to interact with anything in the cupola and leave as fly ash in the flue gas at the same temperature as it enters.

A.18 Chemical reactions apart from those in table 4 do not affect the overall mass and energy balances

A.19 Coke particles are initially the same size and shrink uniformly during conversion

A.20 There is no ash layer on the reacting coke surface

A.21 Raw materials melts on the outer surface only

A.22 Raw material particles of each type are initially the same size

Thermal Assumptions

A.23 Heat of gas phase reactions is released in the gas phase

A.24 Heat of the heterogeneous reactions is released in the coke

A.25 The vertical heat conduction in the solid phase and heat dispersion is negligible

A.26 Thermally homogeneous coke and raw material particles

A.27 The radiation between non-gaseous phases are not damped by the gas

A.28 The heat transfer between non-gaseous phases through physical contact, i.e. conduction is neglected

Mass Balances

Using matrix and vector notation the mole balance equation is written as

$$0 = -\frac{\partial \mathbf{N}}{\partial z} + A_f \cdot \boldsymbol{\upsilon} \cdot \mathbf{r} \tag{3}$$

where the molar flow vector, $\dot{\mathbf{N}}$, is given by

$$\mathbf{N} = [N_{CO_2}\ N_{CO}\ N_{O_2}\ N_{H_2O}\ N_{H_2}\ N_C]^T \tag{4}$$

The matrix of stoichiometric coefficients, $\boldsymbol{\upsilon}$, and the vector of chemical reactions, $\mathbf{r}$, are defined in the chemical reaction section. The mass balance of the rocks can be calculated from the coke balance using algebraic equations only. The inlet boundary conditions for the gas species are given as input to the model in terms of blast air flow rate and composition. The blast air is typically ordinary atmospheric air but it may be enriched with oxygen. For the coke the boundary condition is that $N_C = 0$ at $z = 0$.

In the formulation of the mass balance plug flow of gas and particles is assumed, i.e. dispersion is neglected (assumption 15).

The mass balances of the rocks are trivial since the mass flow rate is constant through the cupola and the fraction of coke and each of the rock types in the charge are inputs to the model.

Energy Balances

In the enthalpy balances the enthalpies are calculated with reference to the temperature $T_{ref} = 298.15\text{K}$. The heats of reactions in the model are for $T = T_{ref}$.

Gas Phase

The energy balance for the gas phase is formulated as

$$0 = -\frac{\partial}{\partial z}\left(N_g M_{w,g} \int_{T_{ref}}^{T_g} c_{p,g} dT_g\right) + \varepsilon_b \sum_i -\Delta H_{r_g,i} r_{g,i} + \sum_i q_i \tag{5}$$

where

$-\frac{\partial}{\partial z}\left(N_g M_{w,g} \int_{T_{ref}}^{T_g} c_{p,g} dT_g\right)$	:	Energy transport by convection.
$\varepsilon_b \sum_i -\Delta H_{r_g,i} r_{g,i}$	:	Energy released in homogeneous gas phase reactions.
$\sum_i q_i$	:	Heat transferred from coke, rocks, briquettes, melt and furnace wall by convection and radiation.

The temperature of the blast air that is given as input to the model serves as boundary condition, i.e. at $z = 0$. The blast air temperature is typically 500^oC to 800^oC. It is assumed that the heat released in the gas phase reactions are released in the gas phase (assumption A.23).

Coke Particles

The energy balance for the coke particles is formulated as

$$0 = -\frac{\partial}{\partial z}\left(N_c M_{w,c} \int_{T_{ref}}^{T_c} c_{p,c} dT_c\right) + \sum_i -\Delta H_{r_c,i} r_{c,i} a_c + \sum_i q_i \qquad (6)$$

where

$-\frac{\partial}{\partial z}\left(N_c M_{w,c} \int_{T_{ref}}^{T_c} c_{p,c} dT_c\right)$	:	Energy transport by convection.
$\sum_i -\Delta H_{r_c,i} r_{c,i} a_c$	:	Energy released by the heterogeneous chemical reactions involving coke (assumption 24).
$\sum_i q_i$	:	Heat transferred from gas, rocks, briquettes, melt and furnace wall by convection and radiation.

The temperature of the coke as it enters the cupola at the top (i.e. at $z = H_f$) is given as input to the model and provides the required boundary condition. The coke is not preheated, so the temperature is the ambient temperature, i.e. -10^oC to 30^oC depending on which factory and the time of year. The storage facilities of the coke also result in varying amounts of moisture content, typically 5w/w% but values of up to 17w/w% have been encountered. In the cupola and in the model the coke is dried which takes up some energy.

Rocks

The energy balances for rock particles cover both solid and liquid rock. It is assumed that the melt from different rocks does not mix until they reach the melt bath, i.e. outside the control volume of the model. Katz (27) has found evidence of this in foundry cupola probe measurements. The energy balance is formulated as

$$0 = -\frac{\partial}{\partial z}\left(H(T_r)\cdot \dot{N}_r\right) + \sum_i -\Delta H_{r_r,i} r_{r,i} + \sum_i q_i \tag{7}$$

where

$-\frac{\partial}{\partial z}\left(H(T_r)\cdot \dot{N}_r\right)$	:	Energy transport by convection.
$\sum_i -\Delta H_{r_r,i} r_{r,i}$	:	Energy released by the chemical reactions.
$\sum_i q_i$	:	Heat transferred from coke, gas and furnace wall by convection and radiation.

The heat of fusion is taken care of in the enthalpy function, $H(T_r)$. The enthalpy function, $H(T_r)$, is further described in the Raw Material Properties section.

The boundary condition is the temperature of the rocks at the inlet of the cupola. The inlet temperature of the rocks is the same as for the coke, since they are stored in the same building.

Mass Transfer

The mass transfer between the gas phase and the coke, $\dot{n}_{A,g\to c}$, is modelled using the film model, i.e. Fick's law in a gas film surrounding the particles (see e.g. (28)). The equations needed for the mass transfer model are listed in table 3. The mass transfer coefficient for species A, $k_{m,A}$, is modelled as a function of the diffusion coefficient and the Sherwood number. In the evaluation of Reynold's number it is assumed that the ideal gas law applies since the cupola runs at $1 - 1.1$bar. In the first equation in table 3 a_c is the surface area of the coke per volume cupola. The calculation of a_c is described in the Coke Properties section.

The formation of CO in the gasification reactions between CO_2 or H_2O and coke forms two gas molecules from only one gas molecule. Thus there will be a

Table 3. Model equations describing the mass transfer between the gas phase and the particle surface.

Equation	Ref.
$n_{A,g\to c} = k_{m,A}\left(C_{A,g} - C_{A,c}\right) a_c$	(28)
$k_{m,A} = \frac{Sh_A \cdot D_A}{2r_c}$	(26)
$D_{O_2} = 2.2 \cdot 10^{-4} \left(\frac{T}{1000K}\right)^{1.75} \frac{1atm}{P} \frac{m^2}{s}$	(29)
$D_{CO_2} = 1.6 \cdot 10^{-5} \left(\frac{T}{393K}\right)^{1.75} \frac{1atm}{P} \frac{m^2}{s}$	(29)
$D_{H_2O} = 2.2 \cdot 10^{-5} \left(\frac{T}{273K}\right)^{1.75} \frac{1atm}{P} \frac{m^2}{s}$	(29)
$Sh_A = j_D Sc_A^{1/3} Re_p$	(26)
$\rho_g = \frac{m_g}{V_g} = \frac{P}{RT} \sum_i x_i M_i$	(30)
$j_D = \frac{1}{\varepsilon_b} \frac{0.357}{Re_p^{0.359}}$	(26)

net flow away from the particle, known as Stephan flow (18; 31), however this is neglected (assumption 16).

The surface area of the coke is calculated from the mass, assuming that the coke particles are spherical (assumption 6) and that all the cokes have the same size (assumption 19). To simplify the model it is assumed that there is no size distribution of the coke.

The correlation for the mass transfer to the particles in fixed beds is a general correlation. However, the coke and raw material particles are unusually large compared to typical fixed beds, and for this reason a correction factor will be estimated based on experimental data on full scale cupolas. The mass transfer coefficient is thus $k_{m,A,eff} = k_{m,A} * corr_{k_m}$, and in the ideal case $corr_{k_m} = 1$.

Heat Transfer by Convection

The cupola model contains five solid phases (coke and four types of raw material) and four liquid phases (melt from the four types of raw material) which interact with the gas. The gas also exchanges heat with the water cooled wall.

The convective transfer between gas and particles in a fixed bed is modelled as transfer through a thin gas film. The heat transfer coefficient is calculated from the correlation

$$h_{gx} = 0.61 \cdot Re^{-0.41} \gamma \cdot c_g \cdot \frac{\dot{m}_g}{A_f} \cdot Pr^{2/3} \tag{8}$$

where subscript x is either c for coke, r for raw material or l for melted raw material. The equation is valid for $Re > 50$ based on d_f (28). The factor γ is a

shape factor (for spheres $\gamma = 1.00$).

The convective heat transfers from the gas phase to the liquid melt droplet and to the solid raw material are modelled as

$$q_{gl,i} = h_{gl,i}(T_g - T_{l,i}) \cdot a_{l,i} \tag{9}$$

$$q_{gr,i} = h_{gr,i}(T_g - T_{r,i}) \cdot a_{r,i} \tag{10}$$

where $a_{l,i}$ and $a_{r,i}$ are the surface area of liquid and solid rock, type i, per volume cupola. The calculation of the surface areas are described in a following section.

The convective heat transfer from gas to coke is modelled using the expression

$$q_{gc} = h_{gc}(T_g - T_c) \cdot a_c \tag{11}$$

where a_c is the surface area of the coke per volume cupola. The calculation of a_c is described in a later section.

The convective heat transfer to or from a reacting coke surface has been reported to be more difficult to model than that due to Stephan flow (18; 32). Correction models accounting for Stephan flow exist (33), but are not used here since the mass flow away from the particles is low.

The heat transfer from the gas phase to the water cooled wall is modelled as convection using an expression similar to that used for the particles,

$$q_{gw} = h_{gw}(T_g - T_w) \cdot a_w \tag{12}$$

where the surface area of the wall per volume cupola is simply $a_w = 2/r_f$ since the cupola is a cylinder. The heat transfer coefficient, h_{gw}, is calculated from a correlation valid for fixed beds (16)

$$\mathrm{Nu}_{gw} = \frac{h_{gw} d_f}{k_g} = 0.069 \cdot \frac{(6 \cdot (1 - \varepsilon_b))^{0.185}}{\varepsilon_b} \cdot Re^{0.815} \cdot \left(\frac{T_w}{T_g}\right)^{-0.73} \cdot Pr^{0.5} \tag{13}$$

Heat transfer by Radiation

In the cupola model a simple model for radiation is used. The wave length spectrum is not considered and the emission is calculated as

$$\frac{q_{rad}}{A} = \epsilon \sigma T^4 \tag{14}$$

where σ is Stephan Bolzmann's constant ($\sigma = 5.672 \cdot 10^{-8} \mathrm{W/m^2/K^4}$) and ϵ is the emissivity.

The values for the gas emissivity and absorption ratio depends on content of CO, CO_2 and H_2O (*diathermal* molecules). Values of the emissivity and adsorption ratio as function of gas composition and temperature have been published (34). For simplicity the emissivity was set equal to the absorption ratio and was given a constant value. The value were set to $\epsilon_g = 0.01$ found for $p_{CO_2} = 0.1$atm, $p_{H_2O} = 0.01$atm, $l = 0.01$m and $T > 1200$K, where l is an average distance between two non-gaseous phases. Determination of l is based on an assessment of the quenched cupola. The emissivity may vary but the value was chosen for a high temperature since the radiation is modest at low temperatures.

The net radiation from the gas phase to a liquid or solid phase (raw materials, coke or cupola wall) is modelled as (28)

$$\dot{q}_{rad,gx} = \sigma\epsilon_g(T_g^4 - T_x^4) \cdot a_x \text{ where } x = l_i, r_i, c, w \tag{15}$$

where a_x is the surface area of the liquid or solid phase per volume cupola.

In the following expressions for radiation between solid and liquid bodies are presented. For all the expressions the absorption of radiation in the gas phase is neglected, i.e. the radiation emitted from a solid/liquid body is also assumed to reach another solid liquid body. For simplicity the dampening of the radiation is not subtracted from the radiation emitted from one solid/liquid phase to another.

The solid/liquid particles/droplets are assumed to have so little physical contact that the only mechanism for heat exchange is radiation (assumption 28). The coke-melt radiation is modelled as

$$\dot{q}_{cl_i} = \sigma(\epsilon_c T_c^4 - \epsilon_{l_i} T_{l_i}^4) \cdot a_{l_i} \tag{16}$$

The surface area of liquid is used because it is assumed that the liquid hold-up is so small that the droplets are not visible to each other. The surface area of the coke is larger, but this only leads to coke-coke radiation, and since the coke particles all have the same temperature at a given axial position, this radiation need not be accounted for. It is also assumed that there are no solid raw materials present in positions in the cupola where melt is present. That is not the case in the melting zone where solid and liquid raw materials co-exist, but for simplicity this is not considered. The coke is an almost perfect black body, so the emissivity is set to $\epsilon_c = 1$. The liquid is known to have an emissivity around $\epsilon_l = 0.85$ (unpublished work at ROCKWOOL®).

For the radiation from the coke to the rocks, it is assumed that in the region where rocks are present in solid form coke particles are not visible to each other and melt droplets are not present. Thus the radiation is

$$\dot{q}_{rad,cr} = \sigma(\epsilon_c T_c^4 - \epsilon_r T_{r_i}^4) \cdot a_c \cdot f_{s,r_i} \cdot f_{r_i} \tag{17}$$

The coke surface area is moderated with the factors f_{s,r_i} and $f_{r,i}$ to account for the disappearance of the rock as it melts and to account for the fact that the radiation is divided onto the four different rocks. The rock emissivity is the same as for the liquid rock, i.e. $\epsilon_r = 0.85$.

The coke is assumed not to be in contact with the wall, so the heat is only exchanged by radiation. The radiation is calculated as

$$\dot{q}_{rad,cw} = \sigma(\epsilon_c(r_{T_{c,w}} T_c)^4 - \epsilon_r T_w^4) \cdot a_c \tag{18}$$

where T_w is the temperature of the inside of the wall. The factor $r_{T_{c,w}}$ is a correction factor accounting for the fact that the coke surface temperature is lower at the wall than the average value of T_c that the cupola model determines. The parameter $r_{T_{c,w}}$ eventually has to be estimated based on experimental data.

The rock-rock radiation is neglected, since the temperature difference is small.

Heat Transport in the Water Cooled Wall

The wall temperature is calculated from ordinary heat conduction equations and taking heat transfer from the steel to the cooling water into account. The temperature of the wall can thus be determined from equation (26)

$$q_{rad,gw} + q_{rad,cw} + q_{gw} = \left(\frac{1}{h_{wo}} + \frac{\lambda_w}{d_w}\right)^{-1} \cdot (T_w - T_{water}) \tag{19}$$

where T_{water} is the temperature of the boiling water in the cooling jacket and h_{wo} is the heat transfer coefficient between the cooling water and the outside of the inner cupola wall. Heat transfer coefficient, h_{wo}, is estimated based on experimental data.

Chemical Reactions

The chemical reactions in the cupola model are listed in table 4. Coke reacts with oxygen forming CO. CO_2 and H_2O also reacts with the coke forming CO and in the case of H_2O also H_2. The H_2 and CO reacts with oxygen in the gas phase forming H_2O and CO_2. The rate constants for the heterogeneous reactions may not be so important to know precisely because mass transport limitations also affects the rates of reactions. Hobbs *et al.* (18) conclude based on reviews of (35–42) that the most important parameter with respect to the dominant reaction mechanism of large particle combustion and gasification is the diameter. For large particles ($> 5 - 20$mm) gas film resistance is often

the dominant mechanism (18; 43), at least at temperatures over 1200K. Hence especially the coke combustion reaction rate constant need not be determined with high accuracy.

In the coke-O_2 reaction the ratio of CO to CO_2 formation ratio is very high at high temperatures. A reported correlation for the ratio is (39)

$$\frac{\mathrm{CO}}{\mathrm{CO_2}} = A \cdot \exp\left(\frac{E_a}{RT}\right) \tag{20}$$

were $A = 10^{2.5}$ and $E_a = 24 - 36$kJ/mole. Using this expression the ratio is more than 25 at 1500^oC, and the CO_2 production is neglected in the model.

In the mineral phase three reactions are included, calcination of lime stone and reduction of iron oxides (FeO and Fe_2O_3) to metallic iron and CO in reaction with the coke surface. These are important chemical reactions related to the minerals, because they consume a considerable amount of energy.

No fundamental model of iron reduction is available in literature. The iron reduction reaction expression used in the model is developed based on measurements of melt composition at tuyere level and higher up in the cupola referred to earlier in this paper. The reaction rate constant is adjusted so that 30% of the iron oxides are reduced in the cupola.

The calcination reaction (reaction VI in table 4) is modelled as illustrated in figure 9. The reaction rate function is zero below 750^oC then raises to maximum at 800^oC and thereafter decreasing to zero again at 850^oC (46). The reaction rate function is then scaled to satisfy the mass balance in the cupola model. The calcination is not modelled using an Arrhenius type expression because it would increase the number of equations to solve in the model. The chosen reaction rate function requires only one equation to find the scaling factor whereas an Arrhenius type expression would require the $CaCO_3$ concentration in the four types of rock as function of vertical position requiring $4 \cdot (N_{nodes} + 1)$ extra variables and equations to solve, where N_{nodes} is the number of internal nodes in the grid used for the numerical discretisation of the system of equations. Furthermore the calcination of the limestone only represents less than 3% of the energy consumption and so the exact location is less important. The scaling factor is determined from an overall carbon balance of the cupola.

The reaction rate vector used in the mass and enthalpy balances, $\mathbf{r}$, is given by

$$\mathbf{r} = [r_{CO_2}\ r_{H_2O}\ r_{O_2}\ r_{CO}\ r_{H_2}\ r_{CaCO_3}\ r_{FeO}\ r_{Fe_2O_3}]^T \tag{21}$$

Table 4. Chemical reactions accounted for in the model. (ΔH_r are given at 298.15K.)

	Reaction
I	$\mathrm{C(s) + CO_2(g) \rightarrow 2\ CO(g)}$ $k_{CO_2} = 4 \cdot 10^8 \cdot \exp\left(-\frac{30000\mathrm{K}}{T}\right)\ /\ (m/s)$ $r_{CO_2} = k_{CO_2} C_{CO_2,s} a_c\ /\ (mole/s/m^3)$ Reference: (42) $\Delta H_{r,CO_2} = 172,340 \frac{\mathrm{J}}{\mathrm{mole}}$ Reference: (44)
II	$\mathrm{C(s) + H_2O(g) \rightarrow H_2(g) + CO(g)}$ $k_{H_2O} = 1.2 \cdot 10^9 \cdot \exp\left(-\frac{30000\mathrm{K}}{T}\right)\ /\ (m/s)$ $r_{H_2O} = k_{H_2O} C_{H_2O,s} a_c\ /\ (mole/s/m^3)$ ($k_{H_2O} = 3 \cdot k_{CO_2}$ assumed based on (42) $\Delta H_{r,H_2O} = 131,328 \frac{\mathrm{J}}{\mathrm{mole}}$ Reference: (44)
III	$\mathrm{C(s) + \frac{1}{2}\ O_2(g) \rightarrow CO(g)}$ $k_{O_2} = 600T \cdot \exp\left(-\frac{18000\mathrm{K}}{T}\right)\ /\ (m/s)$ $r_{O_2} = k_{O_2} C_{O_2,s} a_c\ /\ (mole/s/m^3)$ Reference: (42) $\Delta H_{r,O_2} = -110,490 \frac{\mathrm{J}}{\mathrm{mole}}$ Reference: (44)
IV	$\mathrm{CO(g) + \frac{1}{2}\ O_2(g) \rightarrow CO_2(g)}$ $k_{CO} = 1.3 \cdot 10^{10} \cdot \exp\left(-\frac{20130\mathrm{K}}{T}\right)\ /\ (1/s/(mole/m^3)^{(3/4)})$ $r_{CO} = k_{CO} C_{CO} C_{H_2O}^{1/2} C_{O_2}^{1/4}\ /\ (mole/s/m^3)$ Reference: (42) $\Delta H_{r,CO} = -282,830 \frac{\mathrm{J}}{\mathrm{mole}}$ Reference: (29)
V	$\mathrm{H_2(g) + \frac{1}{2}\ O_2(g) \rightarrow H_2O(g)}$ $k_{H_2} = 1.631 \cdot 10^9 \cdot T^{-3/2} \cdot \exp\left(-\frac{3420\mathrm{K}}{T}\right)\ /\ (1/\mathrm{s}/(\mathrm{mole/m^3}))$ $r_{H_2} = k_{H_2} C_{H_2}^{3/2} C_{O_2}\ /\ (mole/s/m^3)$ Reference: (45) $\Delta H_{r,H_2} = -241,818 \frac{\mathrm{J}}{\mathrm{mole}}$ Reference: (29)
VI	$\mathrm{CaCO_3(s) \rightarrow CaO(s) + CO_2(g)}$ $\Delta H_{r,CaCO_3} = 177,500 \frac{\mathrm{J}}{\mathrm{mole}}$ Reference: (46)
VII	$\mathrm{FeO(s) + C(s) \rightarrow Fe(s) + CO(g)}$ $r = k_{FeO,red} \cdot (1 - z)$ for $0 < z < 1$ $r = 0$ for $1 < z$ $\Delta H_{r,FeO} = 75,340 \frac{\mathrm{J}}{\mathrm{mole}}$ Reference: (44)
VII	$\mathrm{Fe_2O_3(s) + 3C(s) \rightarrow 2\ Fe(s) + 3\ CO(g)}$ $r = k_{Fe_2O_3,red} \cdot (1 - z)$ for $0 < z < 1$ $r = 0$ for $1 < z$ $\Delta H_{r,Fe_2O_3} = 238,220 \frac{\mathrm{J}}{\mathrm{mole}}$ Reference: (44)

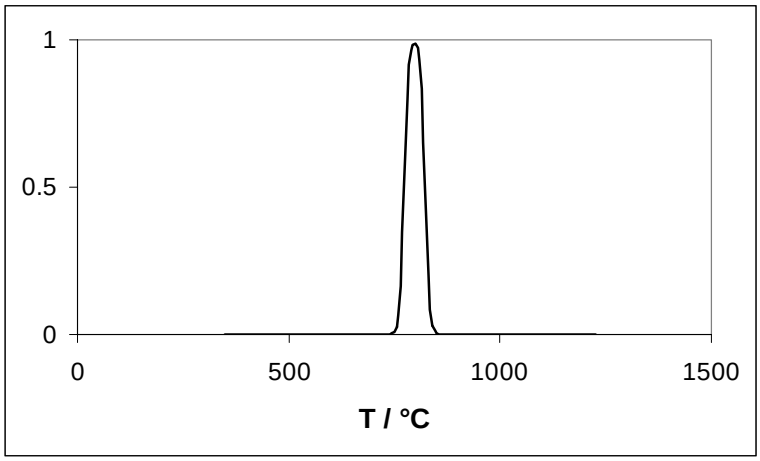

Figure 9. Normalised rate of calcination reaction

and the reaction coefficient matrix, $\boldsymbol{v}$, is given by

$$\boldsymbol{v} = \begin{bmatrix} \boldsymbol{v}_{CO_2} \\ \boldsymbol{v}_{CO} \\ \boldsymbol{v}_{O_2} \\ \boldsymbol{v}_{H_2O} \\ \boldsymbol{v}_{H_2} \\ \boldsymbol{v}_{C} \end{bmatrix} = \begin{bmatrix} -1 & 0 & 0 & 1 & 0 & 1 & 0 & 0 \\ 2 & 1 & 1 & -1 & 0 & 0 & 0 & 0 \\ 0 & 0 & -\frac{1}{2} & -\frac{1}{2} & -\frac{1}{2} & 0 & \frac{1}{2} & \frac{3}{2} \\ 0 & -1 & 0 & 0 & 1 & 0 & 0 & 0 \\ 0 & 1 & 0 & 0 & -1 & 0 & 0 & 0 \\ -1 & -1 & -1 & 0 & 0 & 0 & 1 & 3 \end{bmatrix} \tag{22}$$

The gas phase concentrations at the coke surface needed to evaluate the rates of the heterogeneous reactions are found using the ideal gas law and setting up a mass balance over the gas film, i.e.

$$C_A = \frac{N_A}{N_g} \cdot \frac{P}{RT} \tag{23}$$

and

$$C_{O_2,s} = \frac{2k_{m,O_2}}{k_{O_2} + 2k_{m,O_2}} C_{O_2,g} \tag{24}$$

$$C_{CO_2,s} = \frac{k_{m,CO_2}}{k_{m,CO_2} + k_{CO_2}} C_{CO_2,g} \tag{25}$$

$$C_{H_2O,s} = \frac{k_{m,H_2O}}{k_{H_2O} + k_{m,H_2O}} C_{H_2O,g} \tag{26}$$

The numerical solver used in the model had difficulties handling the very fast CO combustion reaction, so the expression for the rate of CO oxidation was modified to

$$r^*_{CO} = (1 - f) \cdot r_{CO} + f \cdot (r_{O_2} + 2r_{CO_2} + r_{H_2O}) \tag{27}$$

where f is given by

$$f = 0.5 \cdot (\tanh(100 \cdot *(z - 0.03)) + 1) \tag{28}$$

The modification is made so that all CO formed as long as the O_2 concentration is high will combust immediately, and when the O_2 concentration is low the kinetic expression is used.

Coke Properties

The density of the coke is approximately 1000kg/m^3 (more precise data for some types of coke are reported by (25)). The ash in the coke is assumed to leave the cupola as fly ash at T_{ref} and not to interact with any of the phases (assumption 17).

The heat capacity of coke is determined from the equations (47)

$$c_{p,c} = 3\frac{R}{a} \cdot g\,(z) \quad \left[\frac{\mathrm{J}}{\mathrm{kg} \cdot \mathrm{K}}\right] \tag{29}$$

$$a = \left(\sum_i \frac{w_i}{M_{w,i}}\right)^{-1} \tag{30}$$

$$g(z) = e^z \left(\frac{z}{e^z - 1}\right)^2 \text{ where } z = \frac{1200K}{T} \tag{31}$$

and w_i is the weight fraction of element i (e.g. C, H or O).

The coke surface area per volume cupola is needed for computing the rates of heterogeneous reactions. An expression for the surface area is derived as follows. A constant number of coke particles flow, $N_{c,p}$ at all vertical positions can be assumed since all the coke particles are initially identical (assumption 19), i.e.

$$\frac{\mathrm{d}N_{c,p}}{\mathrm{d}z} \equiv 0 \tag{32}$$

From this assumption and the formulas for the volume of a sphere and the connection between mass, volume and density, the expression for coke radius can easily be derived as

$$r_c = r_{c,in} \sqrt[3]{\frac{m_c}{m_{c,in}}} = r_{c,in} \sqrt[3]{\frac{N_c}{N_{c,in}}} \tag{33}$$

where r_c and N_c are the coke radius and the carbon molar flow rate at a given vertical position. The expression for the surface area of coke per volume of

cupola, a_c, can easily be derived from equation 33, the definitions of f_c, $f_{r,i}$ and ε_b and formulas for volume and surface area of a sphere. The expression for a_c is

$$a_c = \frac{3}{r_c} \frac{1-\varepsilon_b}{1+\sum_i \frac{\rho_c}{\rho_{r,i}} \frac{1-f_c}{f_c} f_{r,i}} \tag{34}$$

Equation 33 and 34 represents the unreacted shrinking particle model (assumption 5) that easily can be implemented as two algebraic equation. In the unreacted shrinking particle model it is assumed that the coke reacts at the outer surface only. This assumption is reasonable since the Thiele modulus for reaction with O_2 is large, of magnitude

$$\phi^2 = \frac{kC_s\rho_p S_p r_p}{D_e(C_s-0)/r_p} \approx \frac{10\frac{\mathrm{m}}{\mathrm{s}} \cdot 10\frac{\mathrm{mole}}{\mathrm{m}^3} \cdot 10^3\frac{\mathrm{kg}}{\mathrm{m}} \cdot 10^4\frac{\mathrm{m}^2}{\mathrm{kg}} \cdot 0.1\mathrm{m}}{10^{-5}\frac{\mathrm{m}^2}{\mathrm{s}} \cdot 10\frac{\mathrm{mole}}{\mathrm{m}^3}/0.1\mathrm{m}} = 10^{11} \tag{35}$$

The Thiele modulus is the ratio surface reaction rate to the diffusion rate into the particle, and a large number indicates that the reaction at the surface is dominating and transport into the particle is negligible (48). This conclusion is supported by literature (49; 50).

Only an insignificant ash layer is assumed to be formed due to the small amount of ash in the coke and the fast gas flow (assumption 20). It is additionally assumed that the coke does not break in the cupola (assumption 7). The only mechanism to break the coke particles in the cupola is mechanical stress, and the coke particles are assumed to be sufficiently strong to withstand the stress in the bed, which is supported by observations when the cupola is emptied for maintenance.

The reactivity with CO_2 has been measured for a number of cokes in a TGA (see (25)).

Raw Material Properties

The raw materials used in the stone wool cupolas are rocks, briquettes and lime. The rocks consist of different crystalline phases with different chemical composition, and they are typically of volcanic origin. Briquettes are composed of granulated wool waste from the production line, different powder mineral materials and cement to bind the powder. Briquettes are useful for tailoring the chemical composition of the charge and for recycling waste wool. Limestone is especially used on lines without briquettes for adjusting the viscosity of the melt.

The cupola model needs an enthalpy function for each of the four raw materials that are included in the model. The enthalpy function is the heat capacities

and the heat of fusion integrated as

$$H_{r_i}(T) = \int_{T_{ref}}^{T} c_{p,s,r_i} f_{s,r_i} dT + \Delta H_{fus,r_i}(1-f_{s,r_i}) + \int_{T_{ref}}^{T} c_{p,l,r_i}(1-f_{s,r_i})dT \quad (36)$$

where f_{s,r_i} is the fraction solid as function of temperature. Experimental studies of a number of raw materials (51) show that the heat of fusion for the raw materials is very small and can be neglected. Leth-Miller *et al.* (51) further presents a model that predicts the composition of a rock in terms of crystalline phases, heat capacity of the material in solid and liquid form, the heat of fusion and the fraction solid function, all only based on the chemical composition of the material. The model is an empirical model based on several submodels (52–60) that each are based on extensive experimental data.

The limestone melts at very high temperature, so the transformation from solid to liquid state in the cupola can not be melting, but is rather dissolution in the melt of the other raw materials. The cupola model assumes that there is no contact between the different raw materials, so in the model the solution is modelled as melting with no heat of fusion assuming a function for the fraction solid. The fraction solid curve used is a tanh-function that (almost) has the value 1 until e.g. 1200^{o}C and then decreases to (almost) 0 around e.g. 1300^{o}C.

The decrease in size of the raw material particles in the cupola can be described in the same way as the coke particles since the same assumptions are applied except that the raw materials shrink by melting (assumption 21). The shrinking particle assumption is reasonable since the raw materials are heated from the outside, even though the model assumes that there is no internal temperature gradient (assumption 26). The raw materials consist of several different crystalline phases which melts at different temperatures, but still it is assumed that the raw materials melts on the surface only. The size of the raw material particles can be evaluated from

$$r_{r_i} = r_{r_i,0}\sqrt[3]{\frac{m_{r_i}}{m_{r_i,0}}} = r_{r,0}\sqrt[3]{\frac{N_{r_i}}{N_{r_i,0}}} \quad (37)$$

where r, m and N are radius, mass flow rate and molar flow rate of the raw material.

The expression for the surface area of rock per volume of cupola, $a_{r,j}$, can easily be derived from the definitions of f_c, $f_{r,i}$ and ε_b and formulas for volume and surface area of a sphere. The expression is

$$a_{r,j} = \frac{3}{r_{r,j}} \frac{1-\varepsilon_b}{\frac{\rho_{r,j}}{\rho_c}\frac{f_c}{1-f_c}\frac{1}{f_{r,j}} + \sum_i \frac{\rho_{r,j}}{\rho_{r,i}}\frac{f_{r,i}}{f_{r,j}}} \quad (38)$$

The subscripts i and j indicates raw material type. The model handles four types of raw material that have independent physical properties such as melting

point and heat capacity. The rocks only change size due to melting on the surface and do not break or disintegrate in any way (assumption 9).

An empirical correlation is used for the liquid hold-up, H_l, (6)

$$H_l = 21.2 \left(\frac{d_c \frac{m_l}{A_f}}{\mu_l} \right)^{0.51} \left(\frac{d_c^3 g \rho_l}{\mu_l} \right)^{-0.44} \left(d_c \frac{S_c}{V_c} \right)^{-0.60} \tag{39}$$

where the hold-up is defined as

$$H_l \equiv \frac{V_l}{V_f} \tag{40}$$

The correlation is developed for melted steel and iron in a coke bed, but is assumed also to be valid for the raw materials used for stone wool production.

The liquid surface are per volume furnace, a_l, is evaluated as

$$a_l = \frac{N_{drops}}{V_f} A_{drop} = H_l \frac{3}{r_d} \tag{41}$$

where $A_{drop} = 4\pi r_d^2$ is the surface area of one droplet. The droplet radius is unknown, where the quenching experiment indicates the size range, but otherwise the size must be estimated based on experimental data.

Gas Phase Heat Capacity

The heat capacities of gas depend on temperature and gas composition. Despite this, most fixed bed models published assume that the gas heat capacity is independent of temperature and gas phase composition (18). In this cupola model the heat capacities are dependent of both temperature and gas phase composition.

The heat capacity of a gas mixture is calculated as (61)

$$c_{p,g,mix} = \sum_i X_i c_{p,i} \tag{42}$$

where X_i is the mole fraction of species i.

Expressions for heat capacities for the gas species N_2, O_2, CO_2, CO and H_2O were taken from (61) The heat capacity of H_2, c_{p,H_2}, was obtained from a chart in (26), but for simplicity and because H_2 is present in low concentrations and since c_{p,H_2} is almost independent of temperature, c_{p,H_2} was assumed constant, $c_{p,H_2} = 30 \frac{\mathrm{J}}{\mathrm{mole \cdot K}}$.

Numerical Solution

The model consists of equation 3, 5, 6 and 7 together with the boundary conditions at $z = 0$ and $z = H_f$ and the constitutive equations concerning mass and heat transfer and the rates of reactions substituted into the balance equations. The model is discretised using orthogonal collocation (62). The method of orthogonal collocation uses polynomial approximation of the differential equations resulting in a set of algebraic equations. The set of algebraic equations is solved using a Levenberg-Marquardt method (L-M) (63) which starts in the steepest descent direction and as convergence is obtained switches gradually to the Newton-Raphson direction (N-R) (64). The L-M method is slower than N-R but has a larger convergence radius so the solver starts using the L-M and then when the error has decreased sufficiently the N-R method is used. To further stabilise the solver, backtracking (65) is used. Backtracking means that the full L-M or N-R step is not used if the residual function value is not decreased. Then the step is decreased until the residual function decreases. To improve the numerical solution the model equations have been made dimensionless with the blast air flow rate.

for the simulations presented here 30 internal nodes and one node at each of the two boundaries were used. The solution has been tested with 50 internal nodes, and the result is virtually the same indicating that 30 internal nodes gives a sufficiently accurate solution. The model was solved on a Pentium III, 700 MHz, in approximately 2 minutes if the initial guess is sufficiently good. If no initial guess is available the model can be solved in a number of steps, where the energy balance is not solved initially. When the gas concentration equations have been solved based on a fixed temperature profile the energy balance is solved without changing the gas concentrations, rates of reactions and the fraction solid curves. Finally the entire model is solved by using first the coke temperature, then the gas phase temperature and as the last step the raw material temperatures. This safe way of solving takes approximately 15 minutes. The solution does not converge if too little coke is fed to the cupola. In practice it means that the cupola is extinguished.

Model Results

The developed cupola model can predict the capacity of the cupola (kg melt/hour), the temperature of the melt and flue gas and the composition of the flue gas. The model also predicts the gas, coke and raw material temperature and mass flow rates and gas concentration profiles inside the cupola.

Figure 10 shows a plot of the dimensionless mole flows of the gas components

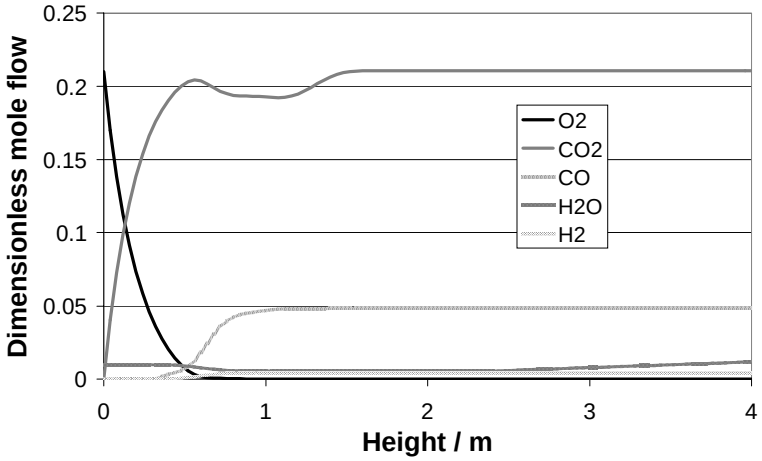

Figure 10. Dimensionless mole flows of the gas species except N_2.

predicted by the model. The flow rates have been made dimensionless with the total gas mole flow rate of air through the tuyeres. The plot in figure 10 shows that oxygen is consumed during the first 600mm. Its reaction with coke forms the net product CO_2 since CO is rapidly oxidised in the gas phase when oxygen is present. When the oxygen is consumed CO and H_2 are formed while CO_2 and H_2O are consumed until the temperature has decreased sufficiently such that the gasification reactions virtually have stopped. At a point the CO_2 concentration increases again when the limestone decomposes, and the H_2O concentration increases as the coke and rocks are dried.

Figure 11 shows the temperature profiles of gas, coke and rocks predicted by the model. At the tuyeres the gas is 500^oC while coke and raw materials enter at the top at ambient temperature. The inlet air is heated by the combustion of CO in the gas phase to a maximum of 2200^oC at 300mm above the tuyeres. After that, heat from the hot gas is transferred to the countercurrently flowing raw materials and the coke. At a point the raw materials starts to melt, but this is not visible on the temperature profile because the heat of fusion is so low. This differs from foundry cupolas where the heat of fusion of the scrap iron and pig iron is so large that the temperature is almost constant during the melting. At the bottom the melt is cooled a bit by the colder blast air entering the cupola.

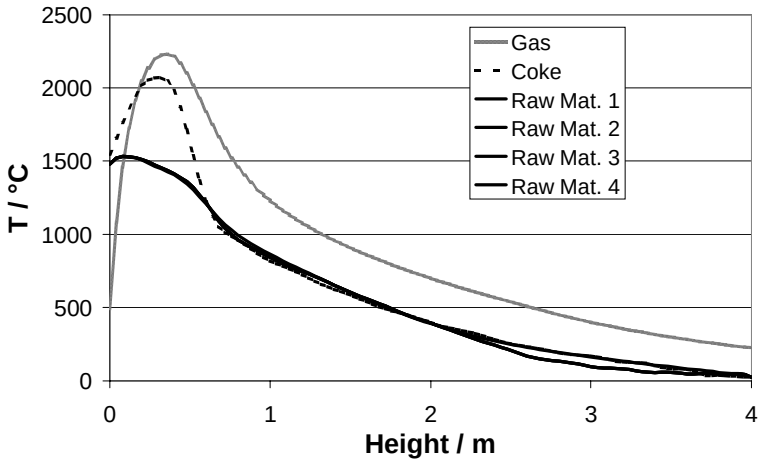

Figure 11. Temperature of the gas, coke and four raw materials.

Calibration

The cupola model developed contains a number of parameters of which some are better known than others. The less known parameters will be adjusted to obtain good agreement with full scale observations. This section describes how the model is calibrated to experimental values.

The data that will be used for the calibration of the model are the measured input and output data (T_m, T_{flue}, $C_{CO,flue}$, $q_{CoolWater}$). The other experimental data from the probe measurements and the quenching experiment will be used for validating the model in the next section.

Parameters

The developed model of the cupola contains a number of parameters that can be determined independently of the cupola, such as properties of raw materials (51) and coke (25). Other model parameters are very difficult (or impossible) to measure, and these must be estimated using the full cupola model and experimental full scale cupola data.

The heat and mass transfer coefficients are modelled using general correlations for spherical particles in fixed beds. The coke and rocks charged into the cupola are not spherical; hence multiplicative surface area correction factors are used on the correlations, e.g. $h^*_{gc} = h_{gc} corr_{h,gc}$ where h^*_{gc} is used in equation 11 in

stead of h_{gc}. The parameter $corr_{h,gc}$ is then estimated with a value of 1 as initial guess.

The cupola model is 1-D, and thus the temperature is an average temperature over the cross section. Since the temperature at the wall is in reality lower the predicted radiation from the coke to the wall will be too high. To correct for this effect the radiation from coke to wall can be predicted using a lower coke temperature than the predicted average. A factor multiplied onto the coke temperature for the radiation evaluation is estimated. The factor can be interpreted as the ratio of the real temperature of the coke at the wall and the average temperature (see equation 18).

The melt looses energy in the melt bath. The melt bath is not included in the model, but if the melt temperature is to be compared with measured values, a heat loss in the melt bath must be taken into account. This is simply done by transferring an amount of energy to the cooling water given by a heat transfer coefficient in the melt bath to the cooling water and the temperature difference between the melt and the cooling water. The heat transfer coefficient is unknown and has to be estimated.

There is only little information available on the melt droplet size. The quenched cupola indicates that drops of 10mm diameter are present, but also much larger droplets are found caught on the coke. The average droplet size in the model determines how large a surface area is available for heat exchange. The droplet size must therefore be estimated in the cupola model.

The corrections to the mass and heat transfer correlations, the coke temperature ratio, melt droplet size and the heat transfer coefficient from the melt bath to the cooling water will be estimated as described in the following.

Residual Function

The residual function that is minimised with a Levenberg-Marquardt method is given by

$$F_{resid} = \sum_{i=1}^{N} \left[(k_{T_m}(T_{m,model,i} - T_{m,exp,i}))^2 + (k_{T_{flue}}(T_{flue,model,i} - T_{flue,exp,i}))^2 \right.$$
$$\left. + (k_{CO_{flue}}(CO_{flue,model,i} - CO_{flue,exp,i}))^2 + (k_{Q_{cw}}(Q_{cw,model,i} - Q_{cw,exp,i}))^2 \right]$$
$$+ \sum_{j}^{N_{PAR}} \left(w_{reg,j} \frac{\Theta_j - \Theta_{j,0}}{\Theta_{j,0}} \right)^2 \quad (43)$$

where T_m is the temperature of the melt, T_{flue} is the flue gas temperature, CO_{flue} is the CO concentration in the flue gas, and Q_{cw} is the cooling water loss. The constants, k_x, are chosen such that all four terms have the unit MW, i.e. the temperature deviation of the model compared to experimental data is converted to the difference in MW that the modelled and experimental values each represent in the cupola operation. Subscripts *model* and *exp* denote predicted and experimentally determined values respectively. Subscript i denotes the index number of the data set and corresponding model solution and N is the total number of data sets. The second summation is a regularisation contribution where $w_{reg,j}$ are weights for each parameter Θ_j, and $\Theta_{j,0}$ are the initial values of the parameters. Regularisation is a method used to trade off the parameter variance and model bias in the minimisation. The parameter variance is typically high when the model parameters are highly correlated. Here the selected term is a Ridge regression. The regularisation has earlier been used by (66) for a non-linear model and is described in general terms by e.g. (67; 68).

The four quantities in the residual function have been chosen because they represent the major energy streams out of the cupola.

Procedure

The tuning of the model to experimental data is divided into four steps:

1. Initial values for the parameters
2. Sensitivity analysis
3. Parameter estimation through minimisation of F_{resid}
4. Validation

The first three steps are described below and the validation is described in the next section.

Initial values for the parameters

The initial values for the correction factors to the heat and mass transfer correlations are unity assuming that the correlations directly apply. The $T_{c,w}/T_c$-ratio, $r_{T_{c,w}}$, is set to a factor between 0 and 1 that gives reasonably good results (a manual tuning shows that $r_{T_{c,w}} = 0.7$ gives good results), and the heat transfer coefficient in the melt bath is also initially manually tuned. The droplet size can

be partly estimated from the quenched cupola where some droplets are found in the visible cross section. However, this is highly uncertain since not all the droplets could be caught during the quenching, and those that where caught may be of a size that is not present during normal cupola operation.

Sensitivity analysis

The sensitivity for each parameter is calculated as

$$\Delta_j = \sum_i \left| k_i \frac{\partial y_i}{\partial \Theta_j} \cdot \overline{\Delta \Theta_j} \right| \tag{44}$$

where y_i are the output parameters of the model, k_i are weights to scale each term to the same unit (MW in this case) and $\overline{\Delta \Theta_j}$ is a reference change or uncertainty for parameter j. The calculated sensitivity is thus (roughly) the resulting influence on the energy balance from the change of the model parameter. The sensitivity analysis is performed to determine the necessity of estimating each of the parameters.

Parameter Estimation

The model parameters are estimated simultaneously using Levenberg-Marquardt's method (63; 65). The required Jacobian is obtained numerically. The solution to the parameters are found iteratively where the step for each iteration are found from

$$\left(\mathbf{J}^T\mathbf{J} + \lambda \mathbf{I}\right) \Delta \boldsymbol{\Theta}_{k+1} = -\mathbf{J}^T F_{resid}(\boldsymbol{\Theta}_k) \tag{45}$$

where $\boldsymbol{\Theta}_{k+1} = \boldsymbol{\Theta}_k + \Delta \boldsymbol{\Theta}_{k+1}$ and F_{resid} is defined in equation 43. $\mathbf{J}$ is the Jacobian and λ is set to a suitable value and reduced as the solution converges. For $\lambda = 0$ the method is identical to Newton-Raphson's method.

Evaluation of F_{resid} requires that the cupola model is solved for each data set, so the numerical evaluation of the Jacobian is expensive in terms of computing time. The problem can be formulated more efficiently where the solution of the model and the minimisation of the residual function are made in the same Levenberg-Marquardt iteration instead of the nested structure with one iteration algorithm inside another that is used here (69).

Calibration results

The parameter estimation is based on five sets of data from the same cupola. The parameter estimation reduces the error of each of the data sets to less than 5% of the total energy consumption, which is approximately 8-10MW. Some of the remaining error is due to the fact that the measured in- and output energy flows did not match, i.e. the experimentally determined energy balance could not be closed.

The correction factors were found to $corr_{h,gc} = 1.52$, $corr_{h,gr} = 1.24$, and $corr_{k,gc} = 1.13$, which is reasonable since deviation from spheric shape will increase the surface area and thus the heat and mass transfer. The coke temperature ratio was found to $r_{TcwTc} = 0.67$ indicating that the coke temperature near the cupola wall is lower than the average, which is expected. The melt droplet size was found to $r_d = 0.05$m and the heat transfer coefficient in the melt bath was estimated to $h_{meltbath} = 387$W/K.

The model can predict the output of the cupola based on the new parameters with the precision indicated in table 5, i.e. the melt temperature within of 45^oC, the gas temperature within of 25^oC, the CO content in the flue gas within of 4.5% (percentage point), and the cooling water loss within of 300kW, in a 95% confidence interval, i.e. approximately two standard deviations. Considering the uncertainties in the measurements this precision is fairly good. The precision is tested on the data sets that were used for the parameter estimation, which is not the optimal way to do it, but there is not a sufficient number of data sets available to leave some out of the parameter estimation and only use them as validation data.

Validation

The calibration described in the previous section only compares the model with output data for operating cupolas. Extrapolation from the experimental data used in the calibration must be done with caution. The model is based on a detailed description of the inside of the cupola, and in this section the concentration profiles, temperature profiles and mass flow profiles predicted by the model are compared to measurements for validation of the model.

True validation requires an infinite number of data sets since agreement between the model a finite number of data sets only proves that the model is valid for those exact data sets. The validation process is actually an attempt to falsify the model, i.e. show that the model can not describe the experimental data.

Table 5. The table shows measured and modelled melt temperature (^{o}C), flue gas temperature (^{o}C), CO content in flue gas (%) and cooling water loss (MW) for five different sets of cupola operation conditions. (Measured/Modelled). The last column contains standard deviations of the five simulations from the measured data.

	1	2	3	4	5	Std.Dev.
T_m / K	1501/1485	1487/1510	1481/1517	1501/1541	1485/1525	23.7
T_{flue} / K	165/176	158/154	176/154	195/193	175/160	12.7
CO_{flue} / %	6.4/5.4	9.6/6.4	10.9/6.9	6.5/7.9	6.6/6.8	2.27
CW / MW	1.64/1.63	1.34/1.59	1.52/1.56	1.78/1.70	1.61/1.50	0.14
Operation conditions						
Coke / %	13.5	16.1	17	15	14	
Cal. Val. / MJ/kg	28.465	31.194	31.194	30.721	30.721	
$V_{blast}/V_{blast,max}$	0.802	0.802	0.813	1	0.879	

Thus it can in reality never be concluded that a model is valid, but only that it is not falsified.

In this paper, however, the model will be concluded valid if it is not falsified. The validated model is more reliable when predicting cupola operation far away from the experimental data used for the calibration, because the validation indicates if the model has captured the essential phenomena of the process. It is possible that a model can be fitted to output data without having captured the essential phenomena in a process, and such a model is not likely to be predictive except near the operating conditions that were used in the calibration. The validation data was obtained through the experiments described earlier; the two types of probes and the quenching. The data obtained from the two types of probe experiments and the quenching experiment will be used for the validation.

Wall Probes

In this section model simulations are compared to concentration and temperature profiles obtained with the wall probes.

Figure 12 shows the measured CO concentration as function of vertical position at the wall, half way from the centre and at the centre, and a CO concentration profile obtained through simulation with the cupola model. The predicted CO profile can not be directly compared to any of the measured profiles, because the model is based on the 1-D assumption, but should be a weighted average of the measured, where the flow rate profile is used to determine the weights. This average profile depends on the gas velocity profile in the cupola, which is not

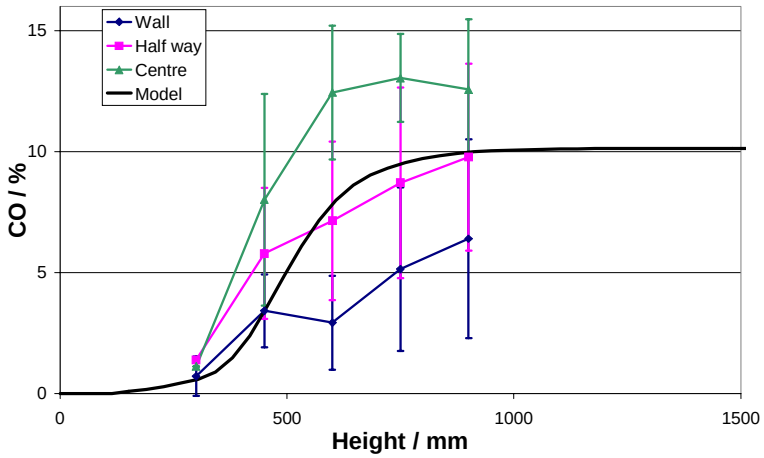

Figure 12. CO profile predicted and measured with the probes. (Vertical bars indicates the standard deviation of the measurement.)

known. CFD model simulations (11) show that the velocity profile is almost flat above 300mm above the tuyeres, hence the predicted profile should be close to the profile measured half way to the centre, and closer to the profile measured near the wall than the one measured at the centre. Figure 12 shows that the predicted CO concentration is very close to zero until 300mm above the tuyeres and then the concentration increases to approximately 10% at 900mm above the tuyeres. The modelled behaviour is very similar to the measured profiles, both when comparing the position in the cupola where the CO is formed and at the final level of the CO.

Figure 13 shows the measured temperature profiles and the predicted profiles of the gas, coke and rock temperatures. The IR-pyrometer was designed to measure the temperature of solid/liquid surfaces, so the temperature profile measured with the wall probes should be compared to either the temperature of the raw materials or the coke. Figure 13 shows that both the modelled raw material temperature and the modelled coke temperature are several hundred degrees lower than the measured values. Secondary air is injection of air 1.5m above the tuyeres to reduce the amount of CO in the flue gas, and the combustion of the CO heats the raw materials and coke. This is probably the reason that the measured profiles are higher than the modelled. The model does not include secondary combustion since it is only used on a few factories in ROCKWOOL®. In the future CO will instead be reduced in an afterburner, because the secondary combustion in the cupola is not very efficient.

The conclusion is that there is good agreement between the model predicted and the measured CO concentration profiles. The agreement for the temperatures

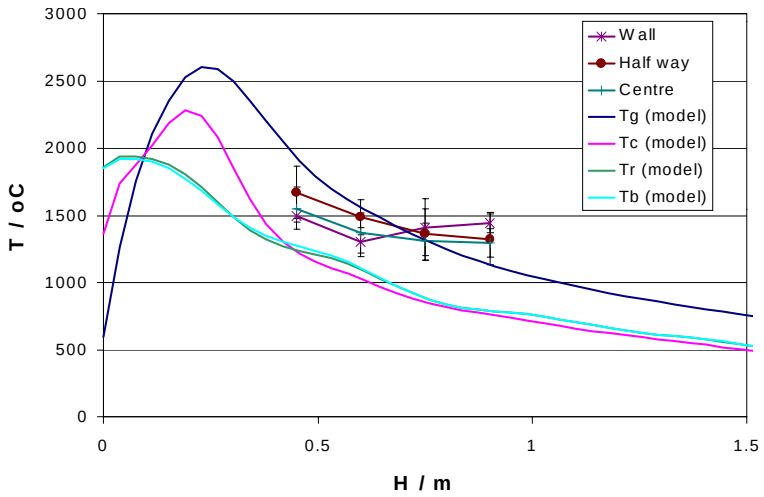

Figure 13. Temperature profile predicted and measured with the probes. (Vertical bars indicates the standard deviation of the measurement.)

in the cupola was not very good probably because of the secondary combustion.

Quenching a Cupola

The results of quenching of the cupola will be compared in qualitative terms using the obtained information about the position of the melting zone.

Figure 14 shows simulated mass flow profiles in the cupola. In the simulation two raw materials were included. At the top of the cupola both raw materials are solid. The raw materials starts to melt approximately 800mm above the tuyeres leading to a decreasing solid mass flow and an increasing liquid mass flow rate. Approximately 400mm above the tuyeres the raw materials are all melted and the solid mass flow rate is zero while the liquid mass flow rate is the same as the solid mass flow was at the top of the cupola. Coke is present at any vertical position.

In the quenched cupola there was evidence that the melting zone was located from 400mm to 750mm above the tuyeres. The simulated results thus agree qualitatively with the quenched cupola.

In the wall probe experiments, however, it was possible to collect melt in the melt sample probe 900mm above the tuyeres, which proves that the melting zone can extend to over 900mm above the tuyeres. However, these measurements were

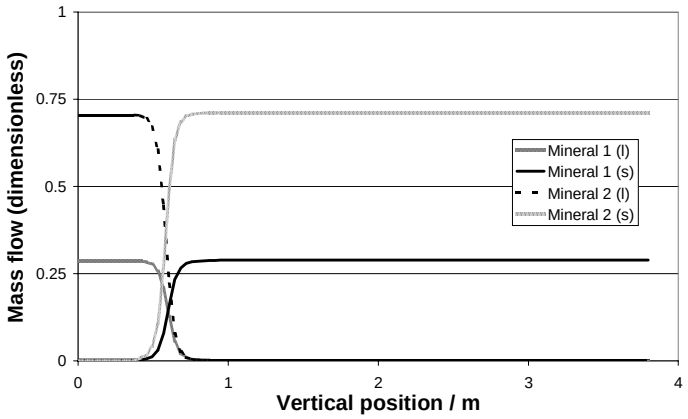

Figure 14. Dimensionless mass flow through the cupola of two raw materials in solid and/or liquid form.

made on a different cupola than the one that was quenched.

Top Probes

The predicted gas temperature profile is compared to the top probe measurements as shown in figure 15. The results show a very good prediction of the measurements of the gas profile marked 20.4., while the measurements made the day before is slightly colder at the top and slightly hotter 1.5m above the tuyeres. The reason for the difference between the two measurements is not clear, but the simulation apparently agrees well with measured gas temperature. The radial position of the top probes were 200-300mm from the wall.

Discussion of the Validity

From the validation made in this section it can be concluded that the model in general performs reasonably well compared to the measurements. This indicates that the model includes the most important phenomena in a sufficiently detailed way, and that the assumptions made are reasonable for the model to describe gas temperature, CO concentration and melt zone location. The good agreement with the melting zone location indicates that the temperature of the raw materials is also well predicted.

The model compares better with the temperatures measured with the top probes

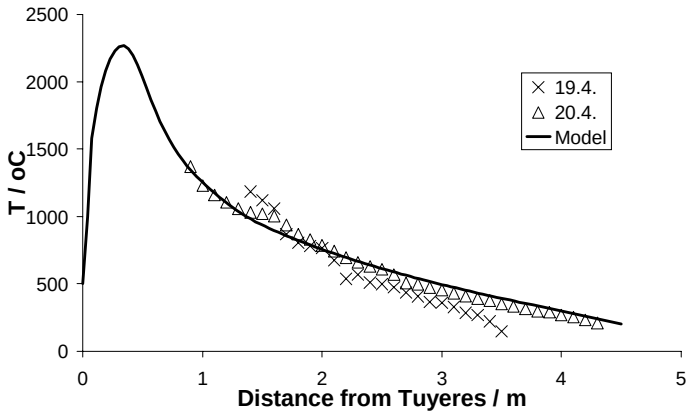

Figure 15. Model predicted gas temperature profile in the cupola and two gas temperature profiles measured with the top probes.

than those measured with the wall probes. The top probe results are more reliable since much less noise was detected.

Discussion

The four types of experiments described are all made on full scale operating cupolas. The results of the experiments have provided new insight about the conditions inside of the cupola. The interpretation of the results of measurements on full scale cupolas should be done with caution since it is difficult to determine what the exact conditions were during the measurements. Also the cupolas are not designed for measurement purposes but for production, so e.g. no effort has been made to prevent that air comes in through the charging system every time new raw materials and coke are charged, and this disturbs the flue gas measurements.

The model developed in this work has some limitations. Since the model is 1-D, it does not capture the effects indicated by the probe measurements that show significant differences between the CO concentration in the centre and at the wall. The chemical reactions can be described in more detail with e.g. reaction mechanisms accounting for gas phase radicals and with several reaction steps in stead of the lumped expression.

The mechanisms for iron reduction and calcination of the limestone are very simple. This may not matter much for the limestone, but the model is not able to give any reliable predictions of the amount of iron reduced in the cupola. So

the model can not be used to optimise the cupola operation to reduce the iron reduction.

The model was calibrated to experimental data that are known to be of low accuracy, and the precision of the model will of course be limited by this. The deviations of the predictions from measured data are thus not only caused by the assumptions that the model is based on, but also inaccuracy of the data. It is a weakness of the calibration that the experimentally determinated energy balances can not be closed. Data reconciliation would improve this.

Conclusion

In-situ measurements on full scale operating cupolas have been performed to investigate the inside conditions of an operating cupola. The measurements provide new insight, and are also used for calibrating and validating a mathematical cupola model. Four types of experiments have been made:

1. Gas concentration, solid/liquid phase temperature profiles and melt composition in the zone from the tuyeres and 1m up were measured by probing the cupola through the wall.
2. Gas temperature from 1m above the tuyeres and up was measured with a probe inserted from the top of the cupola.
3. Quenching the cupola provided insight into the state of the cupola charge and the location of melting zone.
4. Measurements of input/output streams from the cupola provided an energy balance that could be used for parameter estimation.

The experiments with the probes and the quenching provided new qualitative and quantitative knowledge about operating mineral melting cupolas. The measurements gave a good basis for calibrating and validating the cupola model.

A mathematical model of a mineral melting cupola furnace has been developed. The model is a static 1-D model where the one spatial dimension is the vertical position in the cupola. The model development is based on chemical engineering principles.

The model was calibrated against experimental data and is able predict the melt temperature with a precision of 45°C, the gas temperature with a precision of 25°C, the CO content in the flue gas with a precision of 4.5% (absolute), and

the cooling water loss with a precision of 3%. Considering the uncertainties on the measurements this precision is acceptable.

Comparison of the model and the probe measurements and the quenched cupola shows that the model description of the conditions inside of the cupola agrees with the measurements, which indicates that the relevant phenomena are included in the model and described sufficiently detailed.

Acknowledgement

This work is part of the research programme of ROCKWOOL® International A/S carried out in cooperation with CAPEC (Computer Aided Process Engineering Centre) and CHEC (Combustion and Harmful Emission Control) at the Department of Chemical Engineering, Technical University of Denmark. The project is funded by ROCKWOOL® and Erhvervsfremmestyrelsen (Danish Ministry of Business and Industry), and the industrial Ph.D. programme is administrated by the Academy of Technical Sciences.

References

[1] V. Stanek, B. Q. Li, and J. Szekely. Mathematical model of a cupola furnace - part i: Formulation and an algorithm to solve the model. *AFS Transactions*, 100:425, 1992.

[2] V. Stanek, J. Szekely, S. Katz, and C. Landefeld. Mathematical model of a cupola furnace - part ii: Computed profiles and discussion of intrinsic parameters. *AFS Transactions*, 100:439, 1992.

[3] V. Stanek, J. Szekely, S. Katz, and C. Landefeld. Mathematical model of a cupola furnace - part iii: Effect of operating conditions on cupola performance. *AFS Transactions*, 100:447, 1992.

[4] V. Stanek, J. Szekely, V. Sahajwalla, R. Pehlke, S. Katz, and C. Landefeld. Mathematical model of a cupola furnace - part iv: Carbon pickup, metal charge oxidation. *AFS Transactions*, 100:459, 1992.

[5] V. Stanek, S. Katz, C. Landefeld, and A. Schoene. Mathematical model of a cupola furnace - part v: New mode of the model with variable melting rate. *AFS Transactions*, 101:825, 1993.

[6] V. Stanek, S. Katz, R. Pehlke C. Landefeld, and V. Sahajwalla. Mathematical model of a cupola furnace - part vi: Role of holdup of liquid metal in the coke bed of the shaft. *AFS Transactions*, 101:833, 1993.

[7] V. Stanek, S. Katz, and C. Landefeld. Mathematical model of a cupola furnace - part vii: Effect of humidity of the blast on the cupola performance. *AFS Transactions*, 101:839, 1993.

[8] V. Stanek, S. Katz, C. Landefeld, R. Pehlke, and V. Sahajwalla. Mathematical model of a cupola furnace - part viii: Distribution of sulfur in the cupola. *AFS Transactions*, 101:847, 1993.

[9] V. Stanek, S. Katz, and C. Landefeld. Mathematical model of a cupola furnace - part ix: Role of carbon pickup under the tuyeres. *AFS Transactions*, 103:803, 1995.

[10] V. Stanek, S. Katz, and C. Landefeld. Mathematical model of a cupola furnace - part x: Role of carbon monoxide evolving in the well. *AFS Transactions*, 103:809, 1995.

[11] N. N. Viswanathan, M. N. Srinivasanand, and A. K. Lahiri. Steady state three-dimensional matehematical model for cupola. *Ironmaking and Steelmaking*, 24(6):476 – 483, 1997.

[12] H. Saxén. Blast furnace on-line simulation model. *Metallurgical Transactions B*, 21B:913 – 923, 1990.

[13] H. Saxén and R. Östermark. State realization with exogenous variables - a test on blast furnace data. *European Journal of Operational Research*, 89:34 – 52, 1996.

[14] *Neural-Network Based Model of Blast Furnace Slag Viscosity*, volume 2, 1997.

[15] H. Saxén and L. Karilainen. A prototype expert system for diagnosis of blast furnace conditions. *Proceedings, IASTED International Symposium, AINN*, pages 263 – 266, 1990.

[16] E. Piwowarsky. Matematishes modell des kupolofenprozesses. *Giessereiforschunng*, 2:1, 1973.

[17] H. Saxén. Interpretation of probe temperature in the blast furnace using polynomial approximation. *Steel Research*, 3:73 – 78, 1996.

[18] M. L. Hobbs, P. T. Radulovic, and L. D. Smoot. Combustion and gasification of coals in fixed-beds. *Prog. Energy Combustion Science*, 19:505 – 586, 1994.

[19] B. Sarma, A. W. Cramb, and R. J. Fruehan. Reduction of FeO in smelting slags by solid carbon: Experimental results. *Metallurgical and Materials Transactions B*, 27B:717 – 730, 1996.

[20] M. Sheikhshab Bafghi, M. Fukuda, Y. Ito, S. Yamada, and M. Sano. Effect of CO gas formation on reduction rate of iron oxide in molten slag by graphite. *ISIJ*, 33 (11):1125 – 1130, 1993.

[21] R. K. Paramguru, R. K. Galgali, and H. S. Ray. Influence on slag and foam characteristics on reduction of feo-containing slags by solid carbon. *Metallurgical and Materials Transactions B*, 28B:805 – 810, 1997.

[22] N. Siddiqi, B. Bhoi, R. K. Paramgura, V. Sahajwalla, and O. Ostrovski. Slag-grafite wettability and reaction kinetics, part 1: Kinetics and mechanism of molten FeO reduction reaction. *Ironmaking and Steelmaking*, 27 (5):367 – 372, 2000.

[23] D.-J. Min and R. J. Fruehan. Rate of reduction of FeO in slag by Fe-C drops. *Metallurgical and Materials Transactions B*, 23B:29 – 37, 1992.

[24] Y. Sasaki and T. Soma. Reduction mechanism of molten iron oxide by solid carbon. *Metallurgical and Materials Transactions B*, 8B:189 – 190, 1977.

[25] R. Leth-Miller, J. Jensen, A. D. Jensen, P. Glarborg, S. B. Jørgensen, L.M. Jensen, and P.B. Hansen. Comparative study of coke reactivity towards CO_2. *Ironmaking and Steelmaking (submitted)*, 2002.

[26] W. L. McCabe, J. C. Smith, and P. Harriot. *Unit Operations of Chemical Engineering (international ed.)*. McGraw Hill, 5th ed. edition, 1993.

[27] V. Stanek, S. Katz, C. Landefeld, and L. Smiley. Application of the AFS/DoE cupola model. *AFS Transactions*, 202:1223 – 1232, 1996.

[28] B. Bird, R. W. E. Steward, and E. N. Lightfoot. *Transport Phenomena*. John Wiley, New York, 1960.

[29] S. R. Turns. *An Introduction to Combustion*. McGraw Hill, 1996.

[30] P. W. Atkins. *Physical Chemistry*. Oxford University Press, 5th ed. edition, 1994.

[31] T. B. Reed, J. P. Diebold, and R. Desrosiers. Proc. of specialists workshop on fast pyrolysis of biomass, 1980. p. 7.

[32] C. G. von Fredersdorff and M. A. Elliott. Chemistry of coal utilization, supplementary volume, 1963. Chap. 20, p. 892.

[33] T. W. Hoffman and L. L. Ross. A theoretical investigation of the effect of mass transfer on heat transfer to an evaporating droplet. *International Journal of Heat and Mass Transfer*, 15:599 – 617, 1972.

[34] S. Hadvig. *Fyringsteknik, del 1 (in Danish)*. Akademisk forlag, København, Denmark, 1964.

[35] H. Jüntgen. Coal characterization in relation to coal combustion, part 1: Structural aspects and combustion. *Erdl und Kohle - Erdgas - Petrochemie vereinigt mit Brennstoff-Chemie*, 40:153, 1987.

[36] D. D. Eley, P. W. Selwood, and P. B. Weisz. *Advances in Catalysis*. Academic Press Inc., New York, 1959.

[37] R. H. Essenheigh. Proc. combustion institute, 1977. 16:372.

[38] M. A. Elliott. *Chemistry of Coal Utilization, Second Supplementary Volume*. John Wiley, New York, 1981.

[39] N. M. Laurendeau. Heterogeneous kinetics of coal char gasification and combustion. *Progress in Energy and Combustion Science*, 4:221–270, 1978.

[40] I. W. Smith. Proc. combustion institute, 1982. 19:1045.

[41] L. D. Smoot and D. P. Pratt. *Pulverized Coal Combustion and Gasification*. Plenum, New York, 1979.

[42] W. Bartok and A. Sarofim. *Fossil Fuel Combustion: A Source Book*. Wiley-Interscience, New York, 1991.

[43] R. W. Froberg and R. Essenhigh. Proc. combustion institute, 1978. 17:179.

[44] R. H. Hafner. *Cupola Handbook*. American Foundrymen's Society, 5th ed. edition, 1984.

[45] T. V. Vilienskii and D. M. Hezmalian. Dynamics of the combustion of pulverized fuel (in russian). *Energia, Moscow*, page 246, 1978.

[46] W. Gerhartz. *Ullmann's Encyclopedia of Industrial Chemitry*, volume A.15. VCH verlagsgesellschaft mbH, 1986.

[47] D. Merrick. Mathematical models of the thermal decomposition of coal. *Fuel*, 62:540 – 546, 1983.

[48] H. Scott Fogler. *Elements of chemical Reaction Engineering*. Prentice Hall, 2nd ed. edition, 1992.

[49] R. Wagner, W. Wanzl, and K. H. van Heek. Influence of transport effects on pyrolysis reaction of coal at high heating rates. *Fuel*, 62:540 – 546, 1985.

[50] A. H. Abdel-Hafez. Simplified overall rate expression for shrinking-core bituminus char combustion. *Chemical Engineering Science*, 43 (4):839 – 845, 1988.

[51] R. Leth-Miller, A. D. Jensen, P. Glarborg, S. B. Jørgensen, L.M. Jensen, and P.B. Hansen. Experimental investigation and modelling of heat capacity, heat of fusion and melting interval of rocks. *Thermochemica Acta (submitted)*, 2002.

[52] G. W. H. Höhne, W. Hemminger, and H.-J. Flammersheim. *Differential Scanning Calorimetry, An Introduction to Practioneres*. Springer Verlag, 1996.

[53] H. D. Nathan and C. K. van Kirk. A model of magmatic crystallisation. *Journal of Petrology*, 19:66 – 94, 1978.

[54] Deer, Howie, and Zussmann. *An Introduction to the Rockforming Minerals.* Longman group limited, Essex, Eng., 14th ed. edition, 1983.

[55] J. F. Steppins, I. S. E. Carmichael, and L. K. Moret. Heat capacities and entropies of silicate liquids and glasses. *Contributions to Mineralogy and Petrology*, pages 131 – 148, 1984.

[56] J. Konnerup-Madsen. *Energi-behovet ved opsmeltning af mineraler og bjergarter (Energy Requirements for Melting of Minerals and Rocks, in Danish).* Institut for Petrologi, Københavns Universitet, 1982.

[57] M. G. Best. *Igneous and Metamorphic Petrology.* W.H. Freeman and Company, 1982.

[58] R. A. Howie, B. S. Hemmingway, and J. R. Fisher. *Thermodynamic Properties of Minerals and Related Substances at* $298.15K$ *and 1bar (*10^5 *Pascals) Pressure and at Higher Temperatures.* United States Government Printing Office, Washington, 1978.

[59] H. Bach and D. Krause. *Analysis of the Composition and Structure of Glass and Glass Ceramics.* Springer-Verlag, 1999.

[60] L. B. Pankratz, J. M. Stuve, and N. A. Gocken. *Thermodynamic Data for Mineral Technology, Bulletin 677.* United States Department for the Interior, Bureau of Mines, 1984.

[61] J. M. Smith, H. C. van Ness, and M. M. Abbott. *Introduction to Chemical Engineering Thermodynamics.* McGraw Hill, 5th ed. edition, 1996.

[62] J. Villadsen and M. L. Michelsen. *Solution of Differential Equation Models by Polynomial Approximation.* Prentice Hall, 1978.

[63] J. E. Dennis and R. B. Schnabel. *Numerical Methods for Unconstrained Optimisation on Nonlinear Equations.* Prentice-Hall Inc., 1983.

[64] Rice and Do. *Applied Mathematical Modelling for Chemical Engineers.* John Wiley and sons Inc., 1995.

[65] W. H. Press, S. A. Teukolsky, W. T. Vetterling, and B. P. Flannery. *Numerical Recipes in FORTRAN.* Cambridge University Press, 1992.

[66] F. Lei and S. B. Jørgensen. Estimation of kinetic parameters in a structured yeast model using regularisation. *Journal of Biotechnology*, 88:223 – 237, 2001.

[67] P. C. Hansen. *Rank-Deficient and Discrete Ill-Posed Problems: Numerical Aspects of Linear Inversion (Siam Monographs on Mathematical Modelling and Computation).* Society for Industrial and Applied Mathematics, 1998.

[68] T. Hastie, R. Tibshirani, and J. Friedman. *The Elements of Statistical Learning; Data Mining, Inference, and Prediction.* Springer Verlag, New York, 2001.

[69] K. W. Hansen and S. B. Jørgensen. Dynamic modelling of a gas phase catalytic fixed-bed reactor - i. *Chemical Engineering Science*, 31:579 – 586, 1976.

Article IV

Application of a Mathematical Model of a Mineral Melting Cupola

R. Leth-Miller[†‡*], A.D. Jensen[‡], P. Glarborg[‡], S. B. Jørgensen[‡], L.M. Jensen[†], P.B. Hansen[†]

[†]ROCKWOOL® International A/S, Denmark
[‡]Department of Chemical Engineering, Technical University of Denmark
May 14, 2002

Abstract

A mathematical model of a mineral melting cupola furnace is used to illustrate how different process parameters affect the operation. The parameters studied include oxygen enrichment in the blast air, the influence of coke reactivity and coke size and the influence of raw materials melting point temperature and heat capacity.

The model is further compared to experimental data and rules of thumb for cupola operation at stone wool factories. The comparison with the rules of thumb indicates that the model has captured the essential phenomena in the process and describes gas concentrations, temperatures and flow rates inside the cupola well.

Introduction

The cupola furnace is the main technology used for melting raw materials (e.g. rocks and briquettes) in stone wool production and has been so for more than 70 years. In this period the cupola and its operation have been improved continuously. The improvements of cupola operation have mainly been achieved

*Corresponding author, e-mail: rasmus.leth.miller@rockwool.com

through trial and error in ROCKWOOL® and also in the foundry industry development Viswanathan et al. (1997)). However, further development is becoming more and more difficult, since the most obvious improvements have already been made.

A mathematical model of a mineral melting cupola based on extensive experimental investigation on operating cupolas have been developed Leth-Miller et al. (2002a) to increase the knowledge about the cupola and facilitate new improvements in a systematic way. In this paper the model performance is compared to rules of thumb for cupola operation used in the stone wool industry. Furthermore the model is briefly described and simulations with the model are presented to illustrate its capabilities.

Process Description

A cupola furnace is a vertical shaft furnace, $4-6$m tall, with a diameter of $1-2.5$m (cupolas in the foundry industry are often larger), see figure 1. Preheated air is blasted through a number of tuyeres (4 to 20) at the bottom of the furnace and coke and raw materials are fed from the top. The furnace is made of steel and is cooled with water in a cooling jacket to prohibit the steel from melting. In the cupola the downwards flow of coke and rocks are heated by the upwards flow of air and combustion products.

The coke burns in the bottom part of the furnace, and the combustion proceeds till the oxygen is consumed approximately 0.5m above the tuyeres. In the zone $0.5-1$m above the tuyeres the hot gas from the combustion melts the rocks, and the upper part of the furnace acts as a simple preheater of the raw materials. Below the tuyeres is the melt bath, from where the melt is maintained at a certain level by a simple siphon.

The zone in the bottom where the oxygen is present is referred to as the combustion zone. Above the combustion zone is the reduction zone where CO is formed from gasification of the coke with CO_2 and H_2O. The reduction zone extends upwards until the temperature has decreased sufficiently for the chemical reactions to virtually have stopped. The gasification is undesired since the reaction is endothermic and consume coke and the CO formed must be removed from the flue gas, typically by the use of an afterburner. The zone where the raw materials melt is referred to as the melting zone. The melting zone overlaps the combustion zone or the reduction zone or both.

The melt temperature (i.e. the temperature of the melt leaving the cupola) is a key parameter in the production since it determines the viscosity of the melt when it reaches the spinning machines, and thereby influences the quality of the

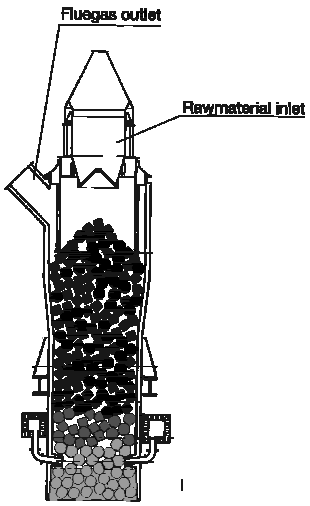

Figure 1. Cupola furnace.

wool. The cupola operation is mainly controlled to adjust the melt temperature and the capacity. The control actuaters are mainly the coke percentage (i.e. the mass fraction of coke in the charge) and the blast air flow rate.

Model

The model of the mineral melting cupola furnace is a steady state 1-D mathematical model, see Leth-Miller et al. (2002a) for details. The spatial dimension is the vertical position. The model consists of mass and energy balances for the gas species, four different types of raw materials and coke. It accounts for mass and heat transfer between coke, gas and four raw material phases and heat loss to the water cooled wall. The model includes seven chemical reactions: combustion of the coke, CO and H_2, gasification of the coke with CO_2 and H_2O, calcination of lime and reduction of iron oxides. It accounts for mass and energy balances of the gas phase, coke and four different raw material phases. Mass transfer between the gas and the coke is modelled using a mass transfer coefficient to particles in a fixed bed. Heat transfer includes both convection and radiation.

The model is discretised using orthogonal collocation Villadsen and Michelsen (1978) and the system of equations is solved with the Levenberg-Marquardt method Dennis and Schnabel (1983) and Newton-Raphson, Rice and Do (1995).

The model predicts the output of the cupola for a given input, i.e. the coke percentage, coke type, raw material types, charge composition and blast air temperature, flow rate and composition is specified and then the model predicts melt capacity, flue gas composition and temperature, melt temperature, and mass flows, temperatures and gas concentrations inside the cupola.

Comparison with Rules of Thumb

During the more than 70 years that the cupola has been used in ROCKWOOL® a number of rules of thumb for the operation has developed. In this section the cupola model is compared to some of these rules as a test of the model and to further investigate whether the model has captured the essential phenomena in the process.

One of the rules of thumb used is that adding 1% coke to the charge will increases the melt temperature with 20 ± 20^oC. The rule is not very precise because different cupolas have been observed to behave very differently and the rules of thumb are averages of all these observations. Table 1 shows the results of some simulations. It can be shown that the melt temperature decreases 16^oC when the coke percentage is decreased from 13% to 12%, and that the melt temperature increases 15^oC when the coke percentage increased from 13% to 14%. The results of the model is in good agreement with the rule of thumb.

Another rule of thumb is that if the blast air temperature is increased 100^oC it is possible to save 0.7% coke and sustain the same melt temperature. In table 2 results of three simulations are shown in terms of coke percentage as function of blast air temperature. The table shows that the model predicts that 1% of coke can be saved for each 100^oC the blast air temperature is increased. This is also in good agreement with the rule of thumb.

Table 1. Simulation results compared to the rules of thumb (RoT) that are used in ROCKWOOL®. RoT say that increase of 1% coke increases the melt temperature with 20 ± 20^oC.

Coke	Melt temperature	
percentage	RoT	Model
12	1465	1469
13	1485	1485
14	1505	1500

Table 2. Simulation results compared to the rules of thumb (RoT) that are used in ROCKWOOL®. RoT says that an increase of 100°C of the blast air temperature saves 0.7% coke.

$T_{\text{Blast air}}$	Coke percentage	
	RoT	Model
600	11.5	11.5
700	10.8	10.5
800	10.1	9.5

Table 3. Simulation results compared to the rules of thumb (RoT) that are used in ROCKWOOL®. RoT says that a decrease from full capacity to 70% capacity costs 1% extra coke.

$V_{\text{Blast air}}$	Coke percentage	
	RoT	Model
Max.	13.0	13.0
70% of max.	14.0	13.9

The last rule of thumb says that a decrease in blast air amount from the upper capacity limit to 70% of the capacity limit costs 1% of coke to sustain the same melt temperature. Table 3 shows results of two simulations in terms of coke percentage. The simulations show that 0.9% extra coke is needed when the production of the cupola is decreased from maximum capacity to 70% of the full capacity and still sustain the same melt temperature. Again good agreement is obtained.

The comparison of the model to the three rules of thumb shows good agreement indicating that the model reliably predicts the static behaviour of an operating cupola furnace.

Parametric Study

In this section examples of the model capabilities are given. There is some empirical knowledge about how changes in operating conditions affect the outputs of the cupola. However the knowledge is in general limited to the direction that the output changes when one parameter is changed. With the present knowledge it is difficult to say much about the effect of changes of several parameters simultaneously. An overview of this can be obtained with the model as illustrated with the following examples.

Oxygen Enrichment

On some production lines the blast air is enriched with oxygen. There has been discussion in the stone wool industry whether this improves the energy efficiency of the cupola or not. There is no doubt that oxygen enrichment can increase the capacity of a cupola, since the limiting factor is the amount of blast air. If oxygen is added to the blast air more coke can be burned and thus the capacity is increased. With respect to the efficiency improvement it has been observed that coke can be saved on some lines while the impact on other lines has been very modest when the blast air is enriched with oxygen.

The cupola model has been used to simulate different scenarios to investigate what coke percentage was needed to sustain a certain melt temperature as function of oxygen content in the blast air.

Figure 2 shows the required coke percentage to maintain a certain melt temperature as function of the oxygen content in the blast air. Simulations have been made for two different blast air temperatures of 500^{o}C and 800^{o}C. The plots show that at low oxygen content (18% for 500^{o}C and 15% for 800^{o}C) the curve is steep, which means that relative more coke can be saved when the blast air is enriched with oxygen. The possible efficiency improvement of oxygen enrichment depends on other operation conditions.

The results have been more closely examined to explain to the observations. Increase of the blast air temperature and increase in oxygen content in the blast air have similar effects on the temperature profiles as illustrated in figure 3. When either of the two parameters is increased the temperature in the combustion zone becomes higher and the peak more narrow. The more narrow temperature peak decreases both the CO formation and the cooling water loss, and the higher temperature ensures that the melt is still heated to the desired temperature. Since the influence on the temperature profiles is similar for the two changes in operation conditions the combined effect of both changes at the same time can not be obtained.

Whether or not the blast air should be enriched is a question of whether the money that can be saved by reducing coke is sufficient to pay for the oxygen enrichment. This depends on the location of the factory, i.e. the local coke, oxygen and transportation costs.

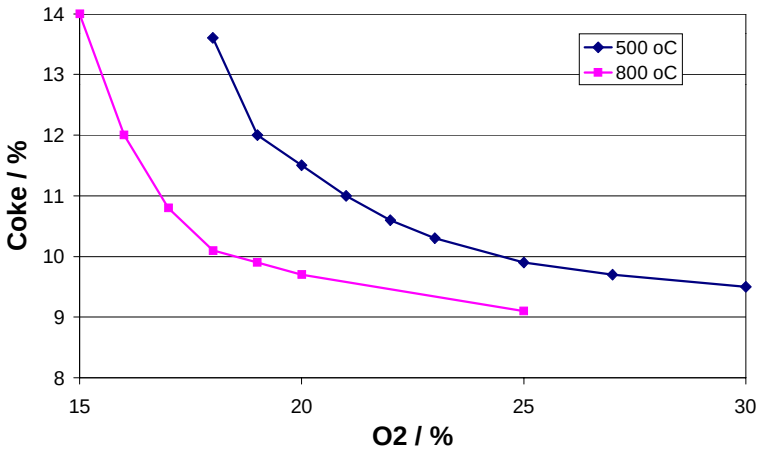

Figure 2. Coke consumption as function of oxygen concentration in the blast air predicted by the cupola model.

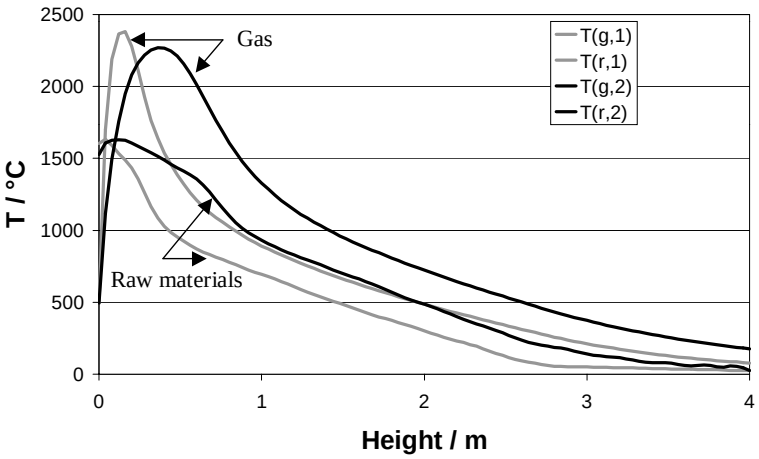

Figure 3. Temperature profiles of gas (g) and raw material/melt (r) from two simulations. $H = 0$ is at tuyere level, and $H = 4$m is the top of the cupola. The base situation is marked with *2* while the profiles marked *1* illustrated either oxygen enrichment or higher blast air temperature.

Coke Size

Traditionally foundry coke (large coke, ø ≈ 200mm Hafner (1984)) has been used also in mineral melting cupolas. Recent development on the coke market has made it interesting to consider metallurgical coke (small coke, ø ≈ 50mm Hafner (1984)) because the foundry coke from China has been taxed in EU leading to a general price increase of foundry coke in Europe. In this section the dependence of the coke size is investigated through simulations with the cupola model.

Figure 4 shows results of a number of simulations. The coke consumption to sustain a given melt temperature is plotted against the coke size for two blast air temperatures. The plot shows that for both blast air temperatures less coke is needed as the coke size increases. However, the sensitivity is largest for the low blast air temperature (500^oC). The case with the high blast air temperature (800^oC) is less sensitive because the temperature is lower in the most of the cupola, as illustrated in figure 3, and the CO formation is thus lower. The reason that more CO is formed in the cupola and thus more coke is consumed by gasification reactions and energy is lost when using smaller coke is that they have a larger surface area per mass.

The relative price difference on the large and small coke is the main influence on the decision of which coke to use. However, the simulations show that cupolas running on 800^oC blast air are more likely to benefit from smaller coke than cupolas running on 500^oC blast air.

Coke Reactivity

Several types of coke are used for stone wool production. The coke types differ by reactivity as well as other characteristics of the coke Leth-Miller et al. (2002c). The coke reactivity is expected to influence the cupola operation in several ways. The reactivity towards oxygen can have an influence on the combustion and the reactivity towards CO_2 can have an influence on both the combustion and the CO formation in the reduction zone. The reactivity towards CO_2 affects the combustion because the CO_2 also reacts with the coke in presence of oxygen, but the CO formed is immediately combusted in the gas phase as long as oxygen is present. CO_2 acts in this way as a carrier of carbon from the coke to the gas phase in the combustion zone. The general perception in the stone wool industry has been that low reactivity coke was desired to minimise CO formation thereby energy loss.

The impact of different coke reactivities were investigated with the cupola

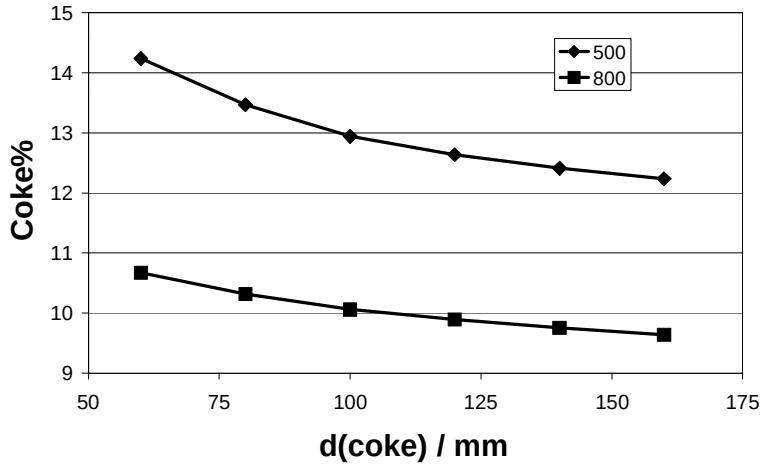

Figure 4. Coke consumption as function of coke size predicted by the model. The coke consumption is adjusted to sustain a given melt temperature.

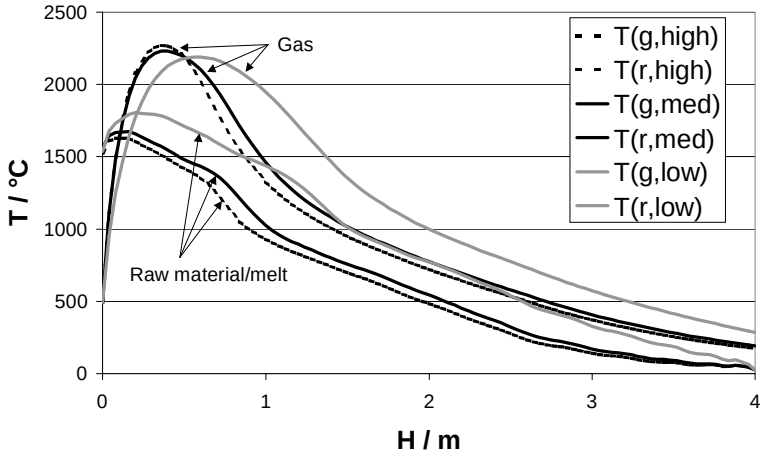

Figure 5. Gas and raw material temperature profiles from three different simulations with varying coke types. Profiles marked with *high* is the standard coke. The *med* coke has half the reactivity towards CO_2 of the standard coke. The *low* coke has half the reactivity towards O_2 and CO_2 of the standard coke

model. Figure 5 shows temperature profiles from three simulations. Three simulations have been made with cokes of varying reactivity. The most reactive coke is marked *high*. The medium reactive coke, marked *med*, has half the reactivity towards CO_2 as the most reactive coke. The least reactive coke has half the reactivity towards both O_2 and CO_2 than the most reactive coke. In the case of the least reactive coke the coke percentage was increased from 13.5% to 17% to maintain the same melt temperature.

Figure 5 shows that the temperature profiles of the high and medium reactive cokes are very similar. The most reactive coke has a little higher peak temperature and a slightly more narrow peak than the medium reactive coke. The temperature of the melt leaving the cupola (i.e. at $H = 0$) in the case of the medium reactive coke is slightly higher. The simulation indicates that coke with lower reactivity towards CO_2 forms less CO in the reduction zone and therefore releases more heat in the combustion zone resulting in a higher melt temperature, thus providing a higher thermal efficiency of the cupola.

Figure 5 shows that the temperature profiles of the least reactive coke is different from the other cokes. The least reactive coke has a much broader peak and a lower peak temperature located further up in the cupola than in the other two cases. More coke is needed because of the lower peak temperature and the position and width of the peak.

The choice of coke depends on several other parameters apart from reactivity, such as ash content, heating value, size (as illustrated above), mechanical strength and of course price. These simulations can help make the choice on a rational basis in terms of furnace performance.

Raw Material Properties

Several different raw materials are used in stone wool production. In this section the influence of changes in melting point temperature and changes in heat requirements on the coke percentage is investigated. The coke percentage is determined to maintain a certain melt temperature.

Four simulations have been made with raw materials with different heat capacities. The heat capacities are related so that $c_{p,i} = (1 + 0.1 \cdot i)c_{p,0}$ where i denotes the number of the raw material and raw material 0 is the base. The enthalpy is evaluated as $H_{1500} = \int_{298\mathrm{K}}^{1773\mathrm{K}} c_p dT$. For each raw material the coke percentage for maintaining a certain melt temperature is found. The enthalpy range selected for the simulations cover the range that has been found in measurements of raw material enthalpies and the heat of fusion was set to zero Leth-Miller

et al. (2002b). The results are plotted in figure 6. The figure shows that the coke percentage and enthalpy are almost linearly proportional.

Simulations of cupola operation with raw materials with different melting points have been made. The coke percentage needed to maintain a certain melt temperature is found. Figure 7 shows the coke percentage plotted against the melting point of the raw materials. The melting point temperature range covers the range found in measurements by Leth-Miller et al. (2002b). The figure shows that there is a minimum on the curve. Below the minimum the slope is very steep indicating that even a little decrease of the melting point temperature below the minimum is expensive, while the influence above is not as pronounced. The reason that more coke is needed when the melting point temperature is lowered is that the residence time of the raw material is short after it has melted and hence the temperature must be higher in the combustion zone to assure that the melt formed at low temperature is heated sufficiently. Higher melting point temperature of the raw materials require more coke because raw materials will be present in the combustion zone resulting in smaller coke surface area in the combustion zone and thus lowering the temperature in the combustion zone.

Hydrogen Enrichment

In this section simulations with hydrogen enrichment of the blast air are described. The hydrogen enrichment is made to simulate fuel supplied through the tuyeres. Figure 8 shows the coke percentage necessary to maintain a certain melt temperature. The coke percentage decreases from 13% at 0% H_2 in the blast air to 9.1% at 12% hydrogen in the blast air. The slope is steeper at low hydrogen concentrations than at high concentrations. Hydrogen enrichment has a similar impact on the temperature profiles as oxygen enrichment. The temperature peak becomes more narrow and the peak temperature higher. The hydrogen enrichment also shifts the peak downwards because the combustion of the hydrogen occurs very close to the tuyeres and only 100mm above the tuyeres the hydrogen concentration has dropped to zero.

Figure 9 shows the energy distribution between coke and hydrogen per mass produced melt plotted against the hydrogen concentration along with a summation of the two. The summation in figure 9 has a minimum at a hydrogen concentration of 10%. The minimum indicate the operation point where the cupola is most energy efficient. This is, however, not necessarily the operating point where the production is most profitable, because this depends on the fuel (coke, natural gas, etc.) prices.

Hydrogen is too expensive to be a realistic fuel, but it is used in the simulations

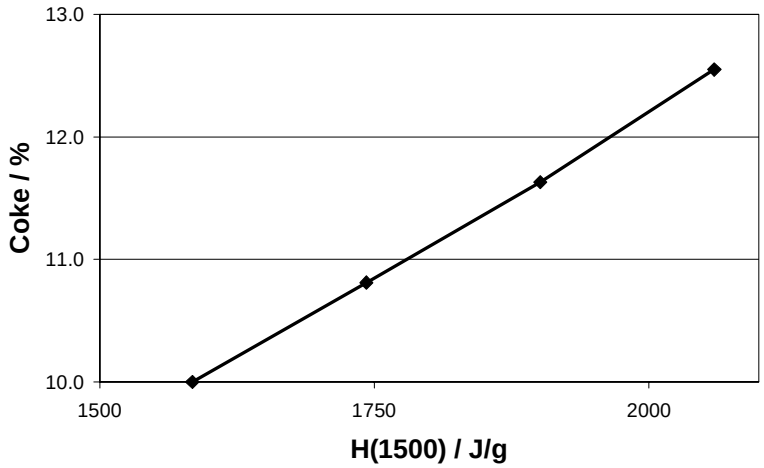

Figure 6. Coke percentage plotted against raw materials enthalpy, H_{1500}. The coke percentage is determined to maintain a certain melt temperature. H_{1500} is the heat needed to heat, melt and superheat the raw material from 25^{o}C to 1500^{o}C.

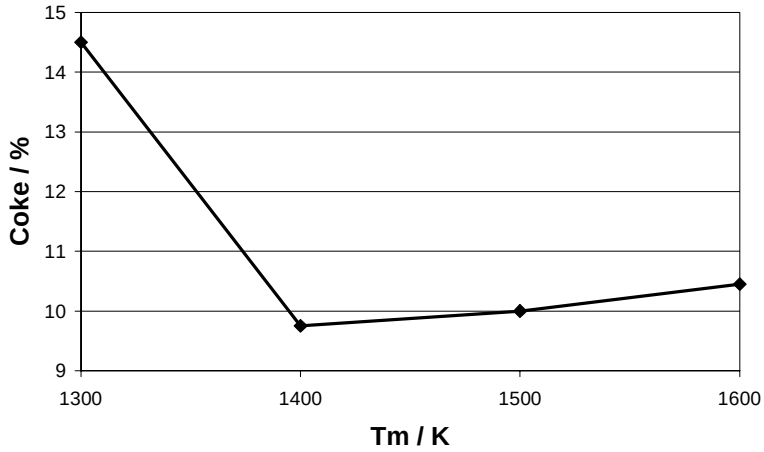

Figure 7. Coke percentage plotted against the melting point temperature of the raw material. The coke percentage is determined to maintain a certain melt temperature.

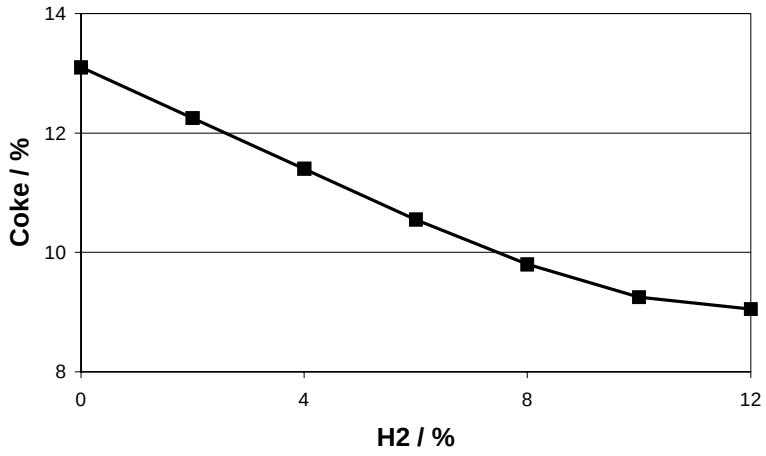

Figure 8. Coke percentage necessary to maintain a certain melt temperature as function of hydrogen concentration in the blast air.

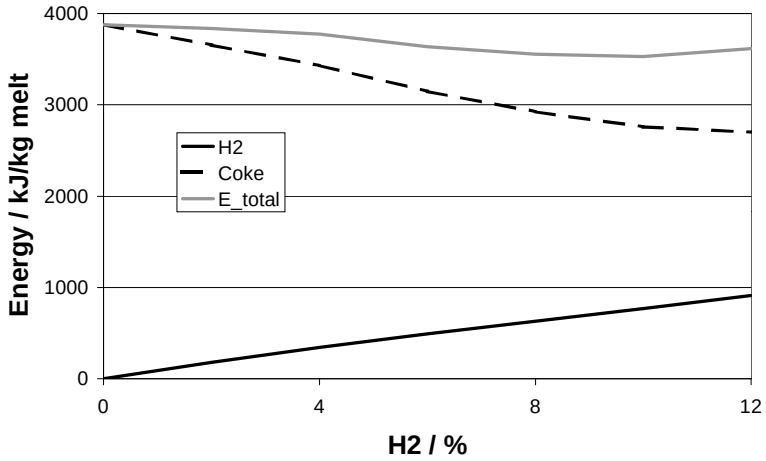

Figure 9. Energy supplied to the cupola per mass of melt produced plotted against hydrogen concentration in the blast air. Curves of energy in the hydrogen and in the coke supplied and a summation of the two are included.

because the model does not handle more realistic fuels such as coal or natural gas. The choice of fuel affects the gasification reactions since it changes the ratio of H_2O and CO_2 in the gas leaving the combustion zone.

Raw Material Diameter

In this section the influence of the raw material diameter on cupola operation is investigated. Figure 10 shows the coke percentage needed to maintain a certain melt temperature plotted against the raw material size. The necessary coke percentage increases as the raw material diameter increases. The sensitivity of the coke percentage towards the raw material diameter is largest at small diameters (the slope is steeper). The results reflect that smaller raw materials have a larger surface area and are therefore more easily heated. Changes in raw material size has little effect on width of the peak on the temperature profile and the peak temperature. The difference is that the flue gas temperature is higher when large raw materials are used, i.e. more energy is lost in the flue gas.

Interpretation of the simulations using different raw material sizes should be made with caution since the raw material diameter may affect the bulk porosity of the cupola, which influences the counter pressure in the cupola. This is not included in the model which assumes a constant porosity. Small raw materials will plug the cupola and reduce the maximum production rate which requires extra coke (see table 3).

Conclusion

A model of a mineral melting cupola furnace used for stone wool production developed by Leth-Miller et al. (2002a) has been compared to rules of thumb for cupola operation to test the qualitative capabilities of the model. Applications of the model have been illustrated with studies of influence of oxygen enrichment in the blast air, of the influence of coke reactivity and coke size and of the influence of raw materials melting point temperature and heat capacity.

The rules of thumb have evolved over the years in ROCKWOOL® and include the coke percentage on melt temperature, blast air temperature on necessary coke percentage and blast air flow on necessary coke percentage. In general the model predicts similar changes as the rules of thumb.

The simulations with the model further showed that the influence of a change

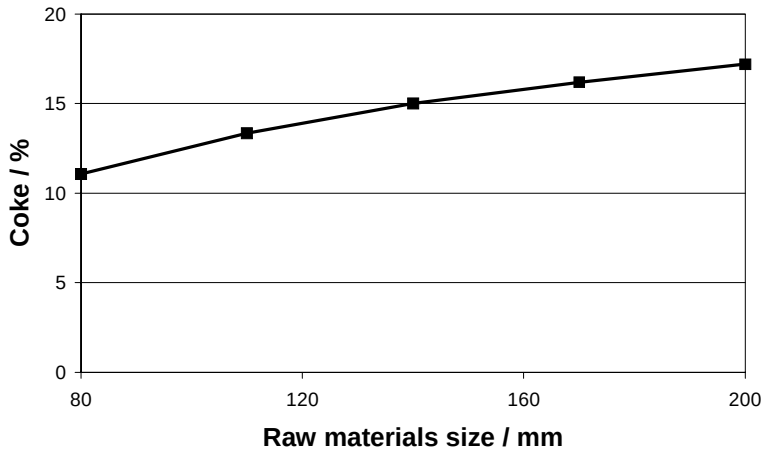

Figure 10. Coke percentage needed to maintain a certain melt temperature plotted against raw material diameter.

in an input dependence on the initial conditions. For example more coke can be saved by enriching the blast air with oxygen if the blast air temperature is 500^{o}C than if it is 800^{o}C. The simulations explain why operators of cupola furnaces have observed different effects of changes in operating conditions.

Acknowledgement

This work is part of the research programme of ROCKWOOL® International A/S carried out in cooperation with CAPEC (Computer Aided Process Engineering Centre) and CHEC (Combustion and Harmful Emission Control) at the Department of Chemical Engineering, Technical University of Denmark. The project is funded by ROCKWOOL® and Erhvervsfremmestyrelsen (Danish Ministry of Business and Industry), and the industral Ph.D. programme is adminestrated by the Academy of Technical Sciences.

References

J.E. Dennis and R.B. Schnabel. *Numerical Methods for Unconstrained Optimisation an Nonlinear Equations*. Prentice-Hall Inc., 1983.

R.H. Hafner. *Cupola Handbook*. American Foundrymen's Society, 5th ed. edition, 1984.

R. Leth-Miller, A. Jensen, P. Glarborg, S. B. Jørgensen, L.M. Jensen, and P.B. Hansen. Experimental investigation and mathematical modelling of a mineral melting cupola furnace. *Industrial and Engineering Chemistry Research (submitted)*, 2002a.

R. Leth-Miller, A.D. Jensen, P. Glarborg, S. B. Jørgensen, L.M. Jensen, and P.B. Hansen. Experimental investigation and modelling of heat capacity, heat of fusion and melting interval of rocks. *Thermochemica Acta (submitted)*, 2002b.

R. Leth-Miller, J. Jensen, A.D. Jensen, P. Glarborg, S. B. Jørgensen, L.M. Jensen, and P.B. Hansen. Compartive study of coke reactivity towards co_2. *Ironmaking and Steelmaking (submitted)*, 2002c.

Rice and Do. *Applied Mathematical Modelling for Chemical Engineers*. John Wiley and sons Inc., 1995.

J. Villadsen and M.L. Michelsen. *Solution of Differential Equation Models by Polynomial Approximation*. Prentice Hall, 1978.

N.N. Viswanathan, M.N. Srinivasanand, and A.K. Lahiri. Steady state three-dimensional mathematical model for cupola. *Ironmaking and Steelmaking*, 24 (6):476 – 483, 1997.